Investigations of Laser Ablation and Laser-Induced-Plasma Ignition of Cyclotrimethylenetrinitramine (RDX)

by

Huijiao Sun

A dissertation submitted to the Graduate Faculty of
Auburn University
in partial fulfillment of the
requirements for the Degree of
Doctor of Philosophy

Auburn, Alabama
May 9, 2011

Approved by

Rik Blumenthal, Chair, Associate Professor of Chemistry and Biochemistry
German Mills, Associate Professor of Chemistry and Biochemistry
Curtis Shannon, Professor of Chemistry and Biochemistry
W. Charles Neely, Professor of Chemistry and Biochemistry
Andreas Illies, Professor of Chemistry and Biochemistry

Abstract

Performance and sensitivity are two factors almost equally weighed when an explosive is considered in application. With a superb combination of high detonation power and low sensitivity to external stimuli, secondary explosives, instead of primary explosives, have been mainly used as a charge in military and mining field. One of the main objectives of this dissertation is to study the mechanism of one of the most common secondary explosives, cyclotrimethylenetrinitramine (RDX), under 266nm UV-laser ablation both in air and argon environments. Preliminary investigations on laser-induced plasma initiation on RDX have been carried out.

Chapter 1 presents a comprehensive literature review on explosives, laser ablation on explosive and plasma initiation. Detailed information was provided of background knowledge and recent advances of explosive initiation.

In chapter 2, the products of the ultraviolet (UV) laser ablation of RDX in air havebeen investigated using infrared (IR) spectroscopy. The total carbon and nitrogen content of the observed gas phase species account for less than 10% of the material removed by the ablation process. The low fraction is explained by an ablation process specific to molecular solids, where a large fraction of the RDX is removed in the ablation process, > 83% in this case, is simply sublimed from the surface only to deposit on the walls of the container without reaction. The chemical products observed by IR include HCN, N_2O, CO, CO_2, NO_2.

Chapter 3 presents a comparative study of the products obtained under an argon environment vs. in air as in the previous chapter. The IR detection of gas products showed all

previously detected compounds (HCN, NO_2, N_2O, CO, CO_2) with addition of a new peak, NO. The understanding of the dependence of plasma formation on the laser fluence provides insight into the chemical mechanism of each direct gas product. Comparison of the anticipated line shape of gas distribution over laser fluence with the experimental data implies the following possible mechanisms under Argon environment: a) HCN, N_2O and NO are formed via multi-photon process; b) NO_2 may be a single photon product; c) CO and CO_2 are formed via thermal process of plasma chemistry. Further comparison of gas distribution over laser fluence under air and Ar indicates that the above-mentioned direct products may be formed in air following the same mechanism, except the reactive species O_2 in air reacts secondarily with some direct products, such as NO, alternated the line shapes to some degree.

Chapter 4 presents a preliminary investigation on laser-induced-plasma initiation of RDX. A thin polycarbonate (PC) film has been used as the plasma generating source. A sample of PC film spin-coated on top of RDX has been exposed to laser pulse irradiation. The laser –induced plasma initiation has been probed and proved through a variety of approaches, namely, gas products pressure detection, observation of reflected light, witness board experiment and dynamic pressure measurement. All approaches provided evidence for an initiation of RDX films by a laser-induced-plasma.

Acknowledgments

First of all, I would like to express my deep and sincere gratitude to my advisor Dr. Rik Blumenthal, for his support and guidance throughout this study. His wide knowledge and persistence have been of great value and inspiration for me. I am also grateful to the helpful discussions and insightful suggestions from my committee members: Dr. German Mills, Dr. Andreas Illies, Dr. Curtis Shannon and Dr. Charles Neely. I especially want to thank Dr. Mills for his detailed and constructive comments on the revision of this manuscript. I would also like to thank my outside reader of this dissertation, Dr. Dean Hoffman, for his time, interest and helpful comments. I wish to thank Mr. Tom Carrington, for his suggestion and help with gas detection experiments, and Dr. Yonnie Wu, for his help with mass spectroscopy detection. Special thanks are due to my group members Dr. Tatiana Bormotova, Rodney Valliere and Artem Dyachenko. It was a pleasure to share research studies and life with them. I wish to extend my warmest thanks to all my friends and colleagues in the Department of Chemistry and Biochemistry at Auburn.

Finally, I wish to take this opportunity to express my gratitude to my family members, to my parents, for their constant support and encouragement in all my pursuits, and to my loving husband, Michael, for his understanding and standing there with me.

Table of Contents

List of Tables

List of Figures

Chapter 1

Introduction and Background

1.1 Review of explosives

An explosive is a substance which stores a great amount of energy and can be initiated to undergo rapid decomposition, usually accompanied with generation of pressure, heat or light. The first application of explosives in human's history could be dated back to the invention of black powder in 9th century in China. The invention of nitroglycerine, dynamite and gelignite in the 19th century marked a breakthrough in the explosive field, due to the greater power and the improved safety of those materials. Since World War II, two new explosives, RDX and HMX, have been extensively applied in both the military and industry.

Based on the rate of reaction, explosives have been classified into two main categories: low explosive (LE) and high explosive (HE). Low explosives deflagrate, reacting and expanding at a subsonic speed, propagating through thermal conductivity. High explosives detonate where materials expand faster than the speed of sound by the mean of shock wave propagation. Before introducing explosives in more detail, several concepts relating to explosion need to be clarified: combustion, deflagration and detonation. Combustion is the process in which a substance reacts with oxygen, usually accompanied by a flame. Deflagration is a rapid and more violent form of combustion, accompanied by not only a flame or sparks, but also a hissing sound. For example, when a log in a fireplace is ignited, it deflagrates. Detonation is the fastest form of explosive reaction, accompanied by loud, sharp bang and sometimes by fire.

According to the sensitivity of substance, high explosives again have been divided into two branches: primary and secondary explosives. Primary explosives (PE) are extremely sensitive to stimuli and require small amount of energy to initiate a reaction, whereas secondary explosives are much less sensitive to initiation and consequently safer to handle. Another important difference is in detonation velocity. Secondary explosives (SE) normally have much higher detonation velocity than primary explosives. Normally, the value of SE detonation velocity is in the range of 6000-9000 m/s, whereas the value of PE detonation velocity is in the range of 3500-5000 m/s. For practical application, primary explosives have been used as an initiating source for the main charge, which are secondary explosives. The schematic categorization and representation of explosives are showed in figure 1.1.

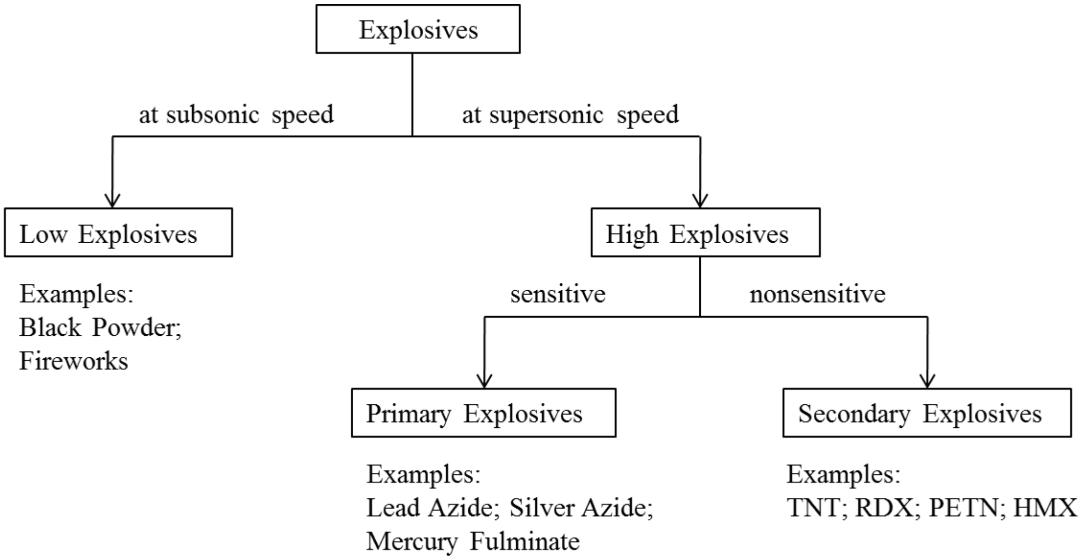

Figure 1.1: Scheme of categorization and representation of explosives

1.1.1 Basic Explosive Compounds:

The most important class of primary explosives includes inorganic azides, such as lead azide and silver azide etc. Due to their sensitivity, primary explosives are used in small quantities, with main functions limited to initiation of the main reactor: secondary explosives. Therefore, the following pages will give emphasis to secondary explosives.

The structure of secondary explosives has generally been characterized by a NO_2 group in an organic molecule, with divisions as $C\text{-}NO_2$ in nitro compounds, e.g. TNT (2,4,6-Trinitrotolune TNT; $C\text{-}O\text{-}NO_2$ in nitrate esters, e.g. PETN (Pentaerythritol Tetranitrate); and $C\text{-}N\text{-}NO_2$ in nitroamines, e.g. RDX (Cyclotrimethylenetrinitramine) and HMX (Cyclotetramethylenetetranitramine). Among them, nitroamine based explosives have demonstrated to have the best combination of power and low sensitivity, which is a required characteristic of an ideal explosive. Therefore, these nitroamine explosives, represented by RDX and HMX, have been used most widely in military and industry during the past decades.

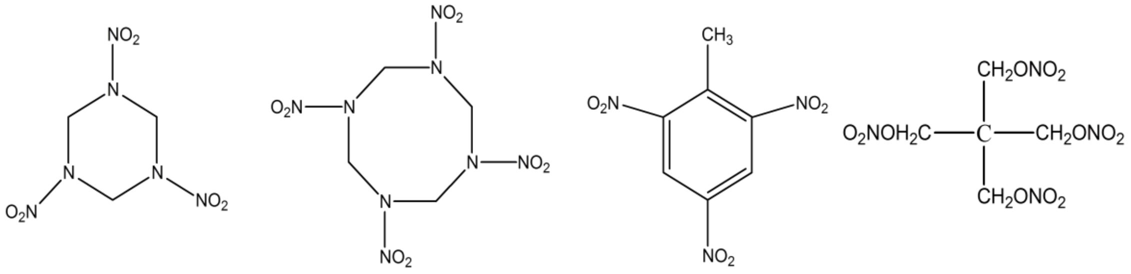

RDX HMX TNT PETN

Figure 1.2 Structures of several important secondary explosives: RDX, HMX, TNT and PETN

Efforts to synthesize new types of explosives have been made in strained or caged polynitro organic molecules.[1] For example, Eaton and coworkers synthesized 1,4 Dinitrocubane[2]. Polynitro derivatives of pentacyclo undecane $[5.4.0.0^{2,6}.0^{3,10}.0^{5,9}]$ have been synthesized and investigated by Marchand etc.[3,4] Figure 1.3 shows the structure of these two molecules. The motive for these new energetic materials lies in the fact that the relief of the molecular strain and the higher density, resulted from the lack of molecular motion, can release great energy. For example, octanitrocubane is theoretically predicted to have a heat of formation of 142 kcal/mole[5], about 10 times greater than heat of formation of RDX, 14kcal/mol[6]. The complex synthesis procedures with this group of explosives, however, have limited their wide application as explosives and propellants.

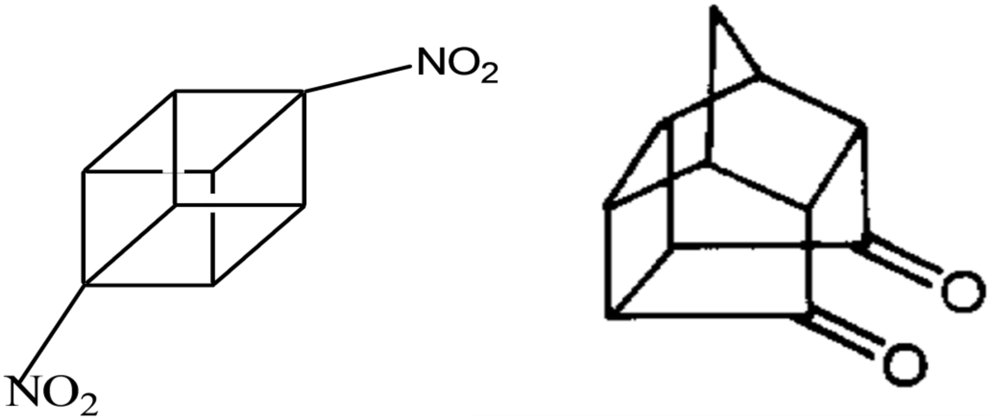

1, 4 dinitrocubane

Pentacyclo undecane $[5.4.0.0^{2,6}.0^{3,10}.0^{5,9}]$

Figure 1.3 The structure of 1, 4 dinitrocubane and Pentacyclo undecane $[5.4.0.0^{2,6}.0^{3,10}.0^{5,9}]$

1.1.2 Physical Factors of Secondary Explosives

Some physical properties in secondary explosives directly determine their performance as energetic materials, which include the number of moles of products per unit molecule; the oxygen balance, the density and the heat of formation. It is easy to understand that the more moles of products per unit explosive molecule produced, the greater work potential will be achieved from these gas products of certain volume. Oxygen balance (OB) is a parameter reflecting the sufficiency of oxygen in a molecule for complete oxidation of its fuel elements, like carbon and hydrogen. When the OB value in one explosive is close to zero, it is expected to be more powerful and with non-toxic complete oxidation products like CO_2 and H_2O etc. Oxygen balance is important in designing the mixtures of secondary explosive materials, called formulations. Density is a very important parameter for explosives in order to achieve great power, since density is directly related with the detonation velocity and detonation pressure. Table 1.1 shows the dependence of the detonation velocity of four commonly used secondary explosives on their density. This table demonstrates that the greater the density, the higher the detonation velocity.

It is important to note that the density used here is the density of solids without air spaces. In real applications, loading density, instead of absolute density, is often considered. Loading density is defined as the ratio between the weight of the powder and the space into which the material is loaded. For a given secondary explosive, the detonation velocity also increases with increasing loading density. Therefore in order to ensure the strongest detonation effect, it is essential to attain the maximum loading density by casting or pressing methods. The detonation pressure was calculated to be linearly proportional to the density of the explosives.[7]

It is critically important to build the association between physical parameters mentioned above with the performance of the explosive material. Based on those parameters, the performance of a newly-designed explosive can be predicted by theoretically calculation prior to synthesis.[6] This capability is highly desirable to scientists and to the explosives industry since elimination of poor candidates will significantly reduce unnecessary energy expenditure, and potential toxicity in a synthesis process.

Table 1.1 Dependence of detonation velocity of explosives on their density. Density and velocity of detonation are summarized based on reference 7

	Density	Velocity of Detonation
TNT	1.654 g/cm^3	~6900 m/s
PETN	1.70 g/cm^3	~8400 m/
RDX	1.82 g/cm^3	~8750 m/s
HMX	1.90 g/cm^3	~9110m/s

1.2 Initiation Methods

The stimuli for initiation of explosives, both primary and secondary, include heat, friction, impact, shock, light and electric charge. A stimulus can initiate a detonation in a purposeful or an accidental way, which involves with a critical parameter of SE: sensitivity. The following section will discuss the sensitivity and several initiation methods of secondary explosives.

1.2.1 Sensitivity

From a chemical point of view, the sensitivity of a SE material to a stimulus can be understood as determined by the following three factors: (a) the probability with which a small reaction will initiate in the explosive; (b) the tendency of this initial reaction to grow into a greater scale; (c) the easy with which a detonation can be established in the system. Therefore, sensitivity is a very complex problem. In assessing sensitivities, impact and shock sensitivity are the most well-known and well-characterized, since detonation caused by accidental impact or shock is more likely to happen than by other stimuli. The shock sensitivity is often measured in a variety of gap tests, such as the small scale gap test at Naval Surface Warfare Center (NSWC) and large scale gap test at Los-Alamos National Laboratory (LANL)[8]. The gap test usually consists of an explosive charge (donor), which generates an input pressure, a barrier (gap), a container holding the test SE material (acceptor) and a witness plate. Physical damage to the witness board provides evidence of go/no-go in testing results. Shock sensitivity is denoted by the pressure at which an explosive explode 50% of the time when it is pressed into 90%, 95%, and 98% of its theoretical packing density. For instance, P_{98} stands for the initiation pressure threshold for an explosive with 98% of their theoretical packing density. The impact sensitivity is commonly measured in hammer-drop test and indicated by the height H_{50} in centimeter, which stands for the distance at which the probability of explosion initiated by the impact of a 2.5 kg weight dropping object is 50%. [9] Kamlet and Adolph proposed that impact sensitivity is directly correlated with oxygen balance (OB) through the equation:

$$\text{Log } h_{50} = a_1 + a_2 \text{ OB\%} \qquad (1.1)$$

where a_1 and a_2 are positive and negative constants, respectively, for various classes of explosives.[10] According to this equation, the higher OB indicates a higher sensitivity with an explosive.

Electric sparks have also been studied as an accidental initiation source for explosives since electric sparks can occur in many handling situations. The Explosives Division of the U.S. Bureau of Mines started to investigate this area as early as in the 1940's.[11] The common electric spark sensitivity test is carried out in a needle-to-plate electrode design, as showed in figure 1.4. A needle electrode connected to a high voltage is firstly positioned away from base electrode, and then gradually moved towards the sample and the base electrode on the bottom until to a distance at which a spontaneous breakdown of the SE sample occurs. During the 1970's, U.S. Army Picatinny Arsenal used needle electrode apparatus to screen and distinguish primary and secondary explosives.[11] They positioned the needled electrode at a certain distance from the base electrode so that the energy exerted on explosives samples as 0.02 J. Explosives which ignited at this energy were put into sensitive primary explosive category and the rest into the non-sensitive secondary explosives category.

1.2.2 Thermal Initiation

When explosives are heated to a temperature which reaches the decomposition temperature, an explosion may occur. It is important to study thermal initiation of SEs, because it provides guidance toward storage of a SE in term of thermal sensitivity. Studies of thermal initiation

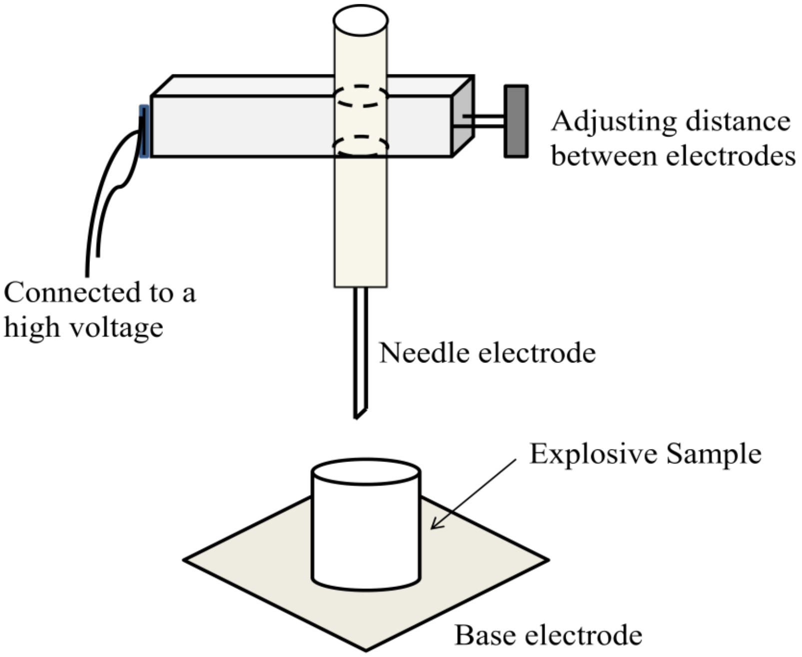

Figure 1. 4 Schematic of the Needle-to-plate electrode testing apparatus for electric sparks sensitivity

have been done in two heating rate ranges: slow cook off and fast heating rate. In slow cook-off, programmed heating can take over minutes or hours to attain a certain temperature. Heating times in the microsecond scale to a chosen temperature are considered initiations occurring at fast heating rates, which can be achieved through the voltage-induced temperature-jump (T-jump) method[12] or irradiation by an IR-laser.[13] Depending on the temperature and the heating rate, different reactions and sets of products may take place. At low temperature, the initial reaction with lower activation energy which proceed exothermically are favored. On the other hand, an endothermic reaction or a reaction with higher activation energy will dominate at high temperature. For instance, Zeman concluded that the thermal decomposition of RDX follows two different mechanisms: homolysis of $N-NO_2$ bond under low temperatures (<600K); ring cleavage into three $H_2C=N-NO_2$ under high temperatures (>600K).[14] A striking feature that is commonly displayed in thermal initiation of explosives is an induction period proceeding ignition, during which there is little or no observable change. For example, figure 1.2 showed a generalized profile of heat released by liquid TNT over time at elevated temperature.[15] The heat released was obtained using isothermal differential scanning calorimetry. The induction phase represents the length of time between the point when the thermal energy starts accumulating and the onset of an acceleration phase. The acceleration phase corresponds to the time when exothermic reactions normally take place and more heat is released to eventually reach a detonation point. The decay phase is the time when the productive gas plume expands and cools down. Tarver et al. has developed a heat transfer computer code to predict the time to explosion in thermal decomposition of SEs, such as PETN and HMX, showing a good accuracy compared with experimental results.[16,17]

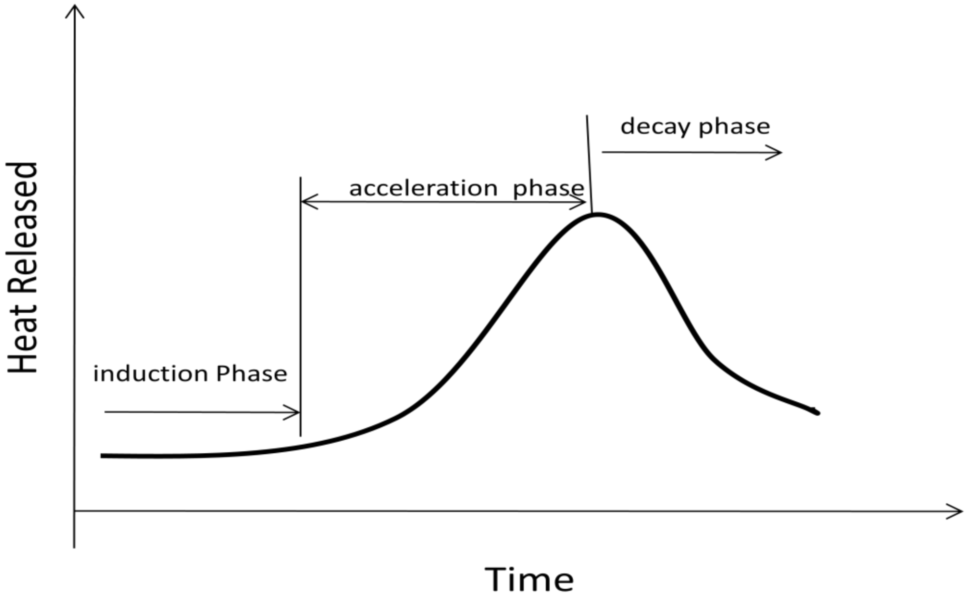

Figure 1.5 Generalized energy release trace for liquid TNT thermal chemical process. Redrawn from the digram in Ref 12.

1.2.3 Shock Initiation

A considerable amount of research has been done on the shock initiation of explosives. According to the strength of the shocks, those studies can be broadly divided into two groups: initiated by a fast velocity shock (FVS) and low velocity shock (LVS). When the shock wave is in the order of 100 kbar, an explosive could be induced to explosion because the energy exerted through the shock can raise the equilibrium temperature of a bulk sample sufficiently to pass the thermal initiation temperature. This is believed to be the initiation mechanism with laser driven flyer plates.

1.2.3.1 Fast Velocity Shock (FVS)--Laser Driven Flyer Plates

Study of FVS has been carried out in a number of groups on the initiation of energetic materials using laser driven flyer plates.[18,19,20,21] A schematic description of this process is shown in figure 1.3. A high fluence laser pulse is focused at the interface between a substrate and a metal film. The substrate should be transparent to the laser wavelength and the energy from the laser excites the metal film into vaporization, forming a region of plasma. The rapid expansion of the hot plasma launches the un-ablated film as a flyer plate. Aluminum has commonly been used as flyer plate material for its relative high melting point and low molecular weight.[22]

Laser driven flyer plates are typically few microns thick and in order of 1 mm in diameter.[23] Watson and Field found that the thickness of the flyer plate can be adjusted by changing laser pulse energy, since the ablation depth in the original metal film is dependent on the laser pulse energy.[24] Flyer plates typically achieve supersonic velocities of a few kilometers per second.[25] Ignoring the resistance of the air, the velocity of flyer plates is governed by the following equations:

$$V_t = \int a\,(t)dt \qquad (1.2)$$

$$a_{(t)} = \frac{S * P_{(t)}}{m} \qquad (1.3)$$

where V_t is the velocity of the flyer at time t; a(t) is the acceleration at time t; S is the area of the plate exposed to plasma force; P(t) is the pressure from the expanding plasma; m is the mass of the flyer plate. It is clear that a higher velocity can be achieved by using a thin flyer plate and high laser pulse power, which was demonstrated in the examination done by Goveas et al.[25]. VISAR measurements of velocity of flyer plates demonstrated a relatively good reproducibility at a given thickness.[26] High speed streak photography has also been used to record and measure the detonation event.[27] It was found that rate of successful initiation by flyer plates is dependent on the packing density and the particle size of the SE materials.[27] In a group of experiments on a SE material, hexanitrostilbene (HNS), SE column with 70% of theoretical maximum density (TMD) showed much greater initiation rate than with 65 % TMD. It was also found that fine grained HNS (sub-micron particle size) would detonate, while conventional HNS (particle size ≈ 25 μm) could not be detonated.[27]

In an alternative design, the driving plasma is not formed from part of the metal film, but in a separate layer, such as carbon layer.[28] The metal flyer is attached to the substrate and will be driven to launch by the carbon plasma when the carbon layer is exposed to a laser pulse. One advantage of this design is that the thickness of flyer plates is easy to control. One of challenges with the laser driven flyer plate method is that the uneven intensity distribution in a typical laser pulse introduces a velocity gradient across the flyer, resulting in a shear force and consequently breaking up the flyer before impacting a target.[29] A top hat beam profile of laser pulses was used to generate a desirable flat planar flyer.[25]

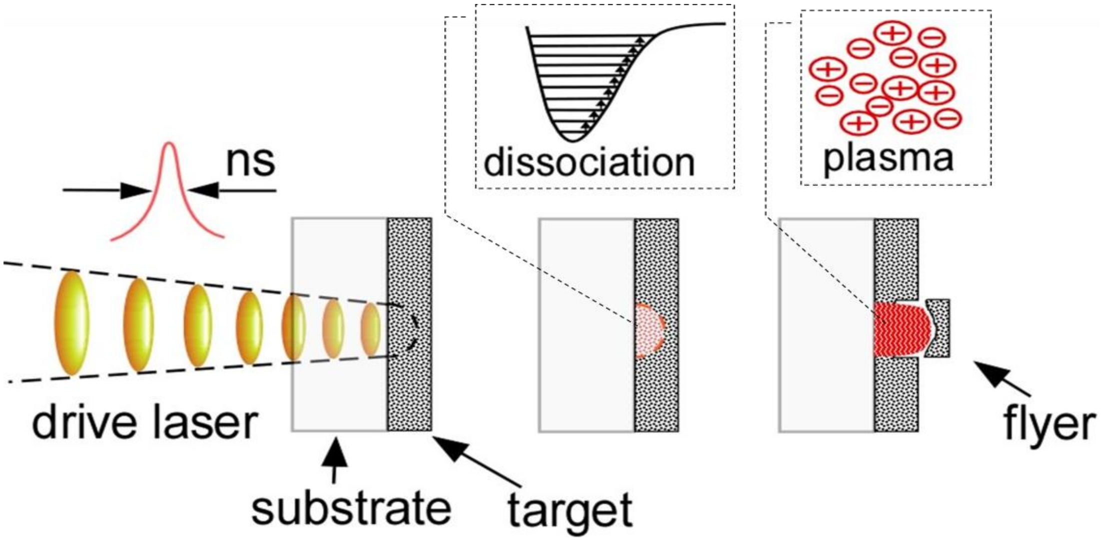

Fig 1.6: schematic description of the formation of a laser driven flyer plate

1.2.3.2 Low Velocity Shock (LVS)

LVS (e.g. pressure of only few kbars) would fail to raise the temperature enough to initiate thermal detonation,[30] but they have been observed to successfully initiate explosions.[31] There are several theories have been proposed to account for this phenomenon.

(i) Adiabatic collapse of gas pockets

When an idea gas is compressed, the temperature will start rising and the final temperature can be calculated by the following equation:[32]

$$T_2 = T_1 \left(\frac{V_1}{V_2}\right)^{\gamma} \tag{1.4}$$

where T_2, T_1 and V_2, V_1 are the final and initial temperature and final and initial volume respectively, γ is the ratio of the specific heats C_p/C_v.

For example, an ideal gas bubble at room temperature compressed to 1/60 of its original volume by a shock wave, its final temperature will reach 1533K. The photographic studies showed that the initiation takes place within 1 μs when the gas bubble reaches its minimum volume.[33] It also demonstrated that smaller bubbles initiate explosion faster since it takes shorter time to reach their minimum volume due to relatively smaller rebound.[33]

(ii) Multi-Phonon Up-Pumping

Multi-phonon up-pumping mechanism has been proposed, based on the results of experiment[34] and simulation,[35] to explain LVS initiation. Under a low velocity impact, modes of intermolecular vibration will be excited, generating a multitude of phonons. The up-pumping of multi phonons can accumulate energy to break a chemical bond through two patterns: a), continuously slow pumping until the energy level of weakest chemical bond is reached; b), an intense burst of coherent phonons pump energy directly into a higher chemical bond level, which will most strongly couple with those phonons. The latter way is different from the conventional slow thermal method and a bond-selective initiation can be expected from this mechanism. Even though the up-pumping of multi-phonons behind a shock front have been undoubtedly observed experimentally, the pumping patterns still remain unclear.

(iii) Microcracks and Fracture Mechanism

The final theory to explain a LVS initiation might be termed as microcracks and fracture mechanism, proposed by Dienes et al.[36] Under a LVS, the gases in voids of a SE sample will be compressed by a much greater factor than the solid crystals. As a result, an ensemble of micro shear cracks is formed inside the sample. Those cracks grind and generate frictional heat, inducing a local ignition point. The burned gases created a high-pressure zone, accelerating formation of hot spots in adjoining cracks. And eventually, microcracks coalesce and when the percolation threshold is exceeded, an explosion starts to take place.

1.2.4 Optical Initiation

Optical initiation can be divided into two categories based on the source of light: the one from a laser and from a lamp. Laser light consists of a single wavelength, high power photon beam (in the order of GW/cm^2 for SE's initiation), whereas a lamp irradiates light of multiple wavelength and less power, over a large surface area. Among these two optical sources, lasers have been more commonly employed to study the optical initiation of SE materials.

1.2.4.1 Optical initiation by a laser

Optical initiation with a laser beam offers the following potential advantages:

a. Safety would be greatly improved since SE is immune to accidental initiations from electrostatic discharge, mechanical shock or a heat source.

b. Precisely timed release.

c. Multi-point simultaneity can be easily achieved

d. Great versatility in initiating explosives of varied sensitivity, since the output energy and the power of the laser can be easily adjusted.

e. Because the availability of power control, a less sensitive explosive can be deployed with laser initiation at higher power than the conventional ignition methods would allow.

The wavelengths employed can encompass the infrared and ultraviolet range, which will be discussed separately in the following paragraphs.

- Initiation with IR laser beams

At a long wavelength, the initiation is considered to follow a thermal mechanism, where hot-spots are created by successive absorption of many photons. In order for initiation to occur, hot-spots must surpass certain thresholds such as dimension greater than 0.1 μm; a temperature 700K or greater and a minimum duration time of 10 μs.[37] Infared lasers have frequently been used as a source in study of thermal decomposition of SEs. Wight and Botcher carried out experiments in which a pulsed CO_2 laser (wavelength 944 cm^{-1}, pulse length 35 μs) was used to dissociate condensed-phase RDX.[38,39] The FTIR spectra of the products showed the presence of N_2O_4, a NO_2 dimer molecule. Therefore, they proposed N-N bond fission is the initial reaction step. They also suggested no ring scission mechanism took place, since there was no evidence of depolymerization products. Earlier work done on molecular gas-phase RDX exposed to CO_2 laser pulses were carried out by Zuckermann and Zhao et al.[40,41]. Zuckermann et al. used a CO_2 laser to dissociate RDX and HMX in seeded supersonic nozzle beams. The results from laser-induced fluorescence experiments showed the existence of OH radicals.[40] Studies from Zhao et al. suggested that the N-N bond rupture and ring scission are two competing reaction pathways with the later one being the primary channel, based on the results from time-of-flight and angle-resolved Mass Spectroscopy[41]. The different results from these two studies may be resulted from the effect of SE's phase. However, the question is not settled as to how the phase influences the decomposition channel of SE under IR laser irradiation.

- Initiation with UV laser beams

In a UV-laser pulse initiation process, the mechanism should be different than energy pumping-up in vibrational manifolds of the ground state as happened with IR-laser, since the energy of a photon with ultraviolet wavelengths can be sufficient to excite electrons into excited states. Unfortunately, there is no clear understanding regarding this fundamental difference in mechanisms of laser initiation of SE with laser beams at IR or UV wavelength regions. There are few works done on UV laser induced decomposition of SEs. Capellos et al. studied the decomposition of molecular gas phase RDX induced by an unfocused KrF excimer laser beam.[42] The gas phase RDX is generated by heating RDX crystals to 460 K. Electronically excited NO_2 and OH were observed in the emission spectra and were postulated to derive from N-N bond rupture and a loss of HONO group, respectively. More recently, Bernstein's group has carried out a series of studies on UV-laser induced decomposition of isolated gas-phase RDX, which is produced from combination of matrix assisted laser desorption (MALD) and supersonic molecular beam techniques. [43, 44, 45, 46] In their work, NO was observed as an initial product of the isolated gas phase RDX molecules dissociated by a 225 nm photon source[43]. The possibility of NO_2 being an intermediate in the production of NO was eliminated by femtosecond laser pump-probe experiments in the UV wavelength range.[45] Laser-induced fluorescence spectroscopy detected the generation of NO in this system, but not of OH, despite that the transition intensity of OH is calculated to be 1.5 times that of NO. Therefore, the HONO intermediate reaction pathway was concluded as not of importance in this system.[44] Based on experimental observations and theoretical calculations of the potential energy surface from both SE system and non-energetic model systems, a new nitro-nitrite isomerization mechanism was suggested[46]. In the nitro-nitrite isomerization mechanism, NO can be explained as the initial product from group NONO, converted from original NNO_2 group in the molecule. In these works, it was emphasized by the authors that MALD and supersonic jet expansion generate cold RDX isolated molecules. In Capellos's work, the molecular RDX should be in vibrationally excited states at 460K. This difference in original states of RDX molecules may be one of the factors accounting for the different experimental observations.

1.2.4.2 Optical initiation by lamp light

During the 1990's, a medium pressure Xenon lamp and high pressure Hg lamp were used to study photo-decomposition of RDX.[47,48] The study with Xenon lamp, which irradiates light of multiple wavelengths, showed the photodecomposition process took a long time (≈40min).[47] Compared to the Xenon lamp, the high pressure Hg lamp usually has a power in the range of several hundred watts, which decompose RDX crystals more rapidly.[48] More recently, an interesting work was done with an output power in the milliwatt range.[49] In this study, PETN, with commercially available single-walled carbon nanotubes (SWNTs) on its top, was initiated using a conventional flashbulb which has a power output only 17 W/cm^2. Figure 1.7 is a photograph of the burning phenomenon that resulted when 10 mg SWNT placed on top of the same amount of PETN was irradiated using a common camera flashlight. In a larger scale test,

Figure 1.7 Photograph of Burning of a 10mg sample of SWNT placed on top of 10mg of PETN upon irradiation with a common flashlight. Samples were placed 3 cm from the light source. Ref 49

a flashbulb irradiated a column containing 30 g of the SE material covered with 0.02 g SWNT, resulting in detonation speed of 6.8 km/s. Ignition was understood as resulting from the formation of hot spots when the SWNT were ignited by the light source.[50] Another important factor is the high thermal conductivity of SWNT, which facilitates the reaction propagation and initiation of SE material.

1.2.5 Plasma Initiation

The main implementation of plasma initiation is in Electrothermal-Chemical (ETC) guns, where an electrical pulse is passed through a chemical material to generate a high-energy density plasma, inducing the ignition of energetic materials. Figure 1.8 shows a schematic of an ETC system, using plastic tubing as a plasma generation source. As mentioned in several reviews about the ETC initiation technique, this plasma initiation system has been demonstrated to have several advantages over the conventional chemical initiation: (1) reduced delay time; (2) improved reproducibility; (3) temperature compensation.[51, 52, 53]

The irreproducible time delay of conventional ignition, using a primary explosive to ignite secondary explosives, becomes an important issue in gun propulsion systems when the target is moving. ETC initiation has exhibited promising performances with time delay in the order of < 0.2 ms, comparing with 6-8 ms delay showed in conventional ignition tests. Another practical factor influencing the muzzle performance is temperature, which can change dramatically from place to place and from season to season. The temperature compensation is control of muzzle energy performance (reflected and measured by breech pressure) by adjusting electrical energy and when it is constant, reproducible performance has been demonstrated at different temperatures.

Figure 1.9 shows a comparison of test results using conventional ignition (on the top) and

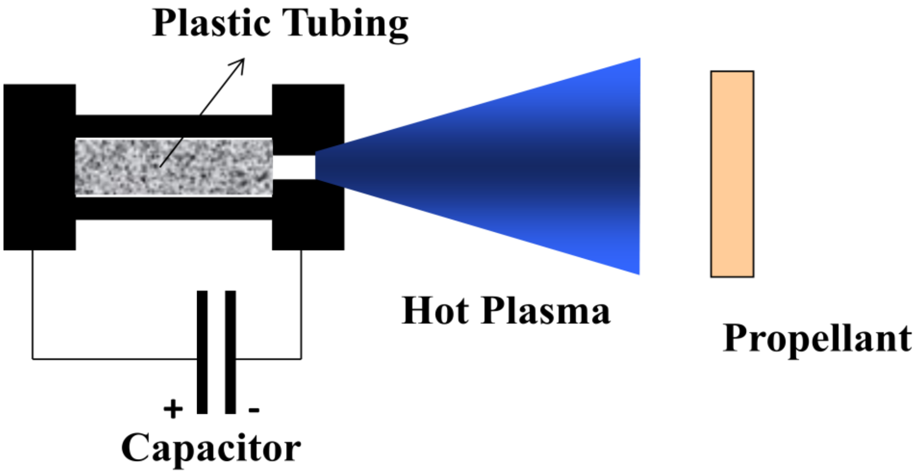

Figure 1.8 A schematic of ETC system

ETC ignition (on the bottom), in which a breech pressure was plotted versus time after the starting point of initiation. In the plot obtained from conventional ignition, the muzzle performance revealed a 36% decrease in peak pressure from ambient temperature 25 ºC to -59 Cº. Consequently, firing velocity dropped at low temperatures and response time increases. In ETC ignition, the test has been done at three temperatures, 68 ºC, 25 ºC and -59 ºC, as showed in three lines on the right plot in figure 1.9. Muzzle performance resulting from ETC ignition exhibited a satisfying reproducibility of all three above-mentioned factors, breech pressure, firing velocity and response time, as temperature was varied by more than 100 ºC.[51]

There has been considerable experimental and theoretical research carried out to investigate this plasma-propellant interaction (PPI) process. Plasmas can interact with propellants through three main mechanisms: (1) radiation from a hot plasma body covers a wide range of wavelengths, which may induce photochemical changes within propellants; (2) high densities of ions and electrons can strike propellant molecules and induce chemical reactions; (3) convective heat transfer through plasma.

Travelling at the speed of light, the radiation from the hot plasma was initially proposed to be the source accounting for the shorter response time in ETC as compared with conventional ignition. Beyer's group studied the response of several propellants to plasma radiation by isolating the propellant sample from non-radiation components.[54] They proposed that radiation would increase the surface area of the propellant samples, which serve as an activation for the decomposition reaction. Further study was conducted on opaque propellant, such as RDX, which did not show the surface area enhancement to the radiation as the transparent and semi-transparent one did[55].

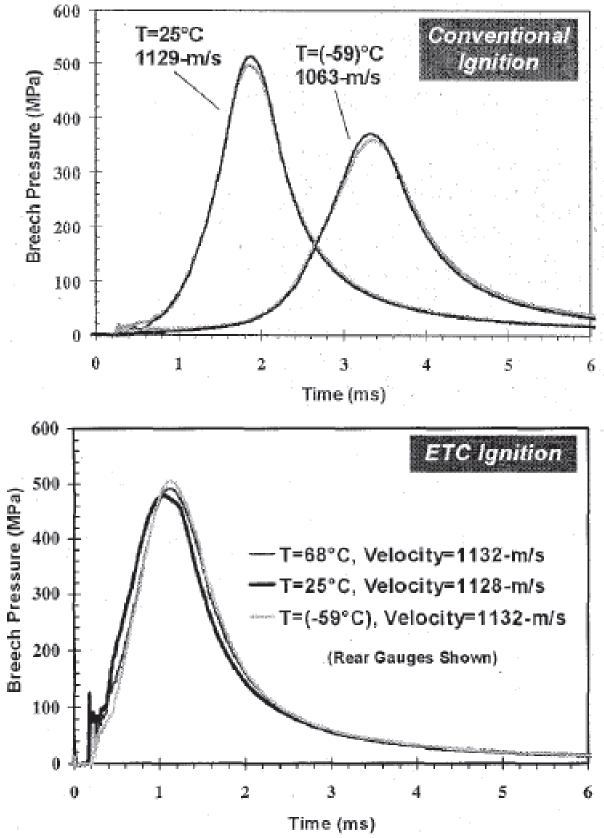

Fig. 1.9 Test results using conventional ignition and ETC ignition. In the conventional ignition plot (at top), the black and grey line is measured result from frond gauge and rear gauge respectively. In ETC ignition (at bottom) results from only rear gauge are plotted. Ref 51

With respect to the radiation theory, many questions still remain to be answered; one of them would be the dependence of wavelength of radiation absorption on the propellant molecules.

The PPI process occurs in an environment of extremely high temperatures and high pressures, which makes the study of this process very difficult. As a result, experimental modeling has been adopted to understand the mechanism in PPI. In one experimental modeling study of the ETC process, plasma was generated from electron cyclotron resonance (ECR) using microwave plasma source. The interaction of individual components of plasma was investigated separately and in combination. Strong synergistic effects between ions and reactive Hydrogen atoms were proposed to be the source for the erosion rate enhancement.[56] It should be noted that in this study both electron impact and exposure to light showed no noticeable contribution to the propellant film erosion.

A laser-induced-plasma interaction with propellant, which will be introduced in later chapter, was designed as a new experimental modeling of PPI process. This model bears the following promising features: (1) by using same plasma generating materials as used in ETC system, such as polycarbonate, a laser-induced-plasma will resemble the plasma generated from an ETC pulse; (2) highly tunable parameters with a laser pulse indicates a possible precise control of the generated plasma, optimizing propellant performance; (3) replacement of a bulky capacitor as power supply in a traditional ETC system with a laser, which is the size of a computer case.

1.3 Laser Ablation

Laser ablation is a process which removes materials from a surface by irradiation with laser light. In laser ablation, a laser typically operates in pulsed mode, which provides much higher power density. Several parameters of a laser pulse are very important in laser ablation: wavelength, pulse energy (in joules), pulse energy density (in J/cm^2 or mJ/cm^2) and pulse fluence (in W/cm^2) and duration of laser pulse. A laser pulse is considered to be consisted of continuous short photon pulses and the temporal profile of intensity of these successive pulses typically shows a Gaussian distribution,[57] see figure 1.10. The length of the whole pulse is commonly characterized by full width at half-maximum (FWHM), which is the temporal width of the pulse evaluated at the intensity of half peak intensity. In laser ablation, as shown in figure 1.10, an overall laser pulse interacts with the surface of the ablating material as a series of successive short pulses. Therefore the length of the laser is critically important since the concentration of absorbed photons must exceed a threshold within a short time scale in order for ablation to occur. More detailed discussion about ablation threshold will be presented in section "laser ablation of polymers".

High pulse fluence is achieved using short duration laser pulses, such as with a nanosecond, femto-second and picoseconds laser. A laser pulse of 6 ns in FWHM with an energy of 50 mJ and the beam size 0.01cm^2, has a pulse fluence $8.3*10^8$ W/cm^2. It is worth mentioning that at powers greater than $5*10^{10}$ W/cm^2, a vacuum environment may be required since air breakdown at room temperature at this power is possible.[37]

The absorption of a laser pulse by a material at a moderate intensity is directly related to the wavelength of the laser pulse and the ablating coefficient of this material at this wavelength, as given by the Beer-Lambert Law:

$$I = I_0 \exp(-\alpha x) \qquad (1.\ 5)$$

where I is the intensity at a distance x into the target, I_0 is the original intensity, α is the ablation coefficient and x is the penetration depth. A moderate intensity is emphasized here because plasma process will dominate at high intensities[58]. Absorption saturation may occur if the number of transition from ground state into excited state renders a depleted ground state[58].

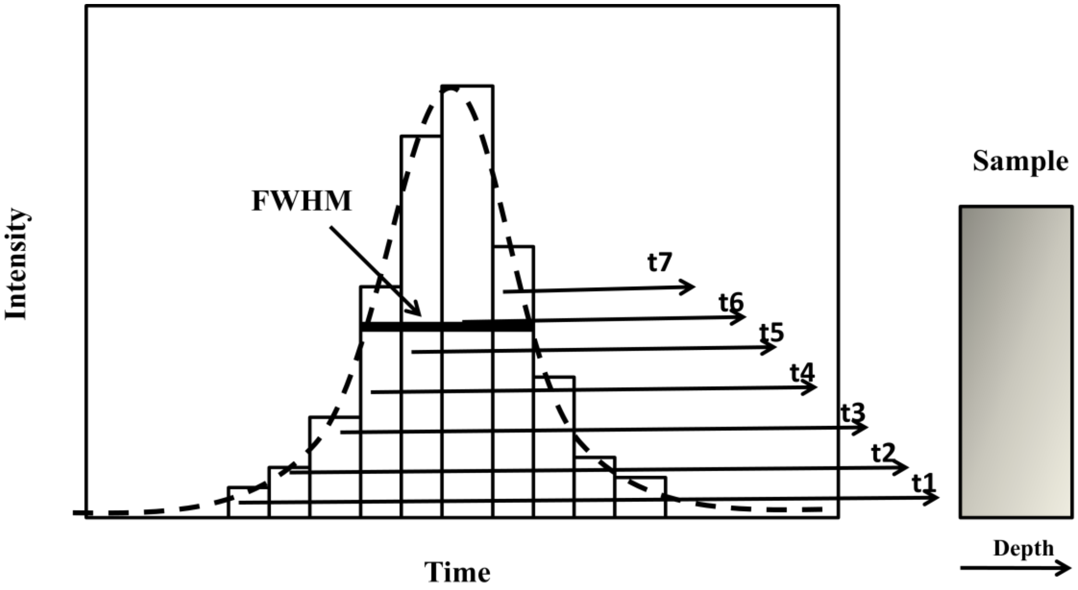

Figure 1. 10 Schematic of a laser pulse temporal profile during laser ablation. Redrawn from Reference 57

1.3.1 Laser Ablation Mechanism:

According to the literature, the most prevalent discussion in laser ablation process focuses on two mechanisms : the photothermal and the photochemical mechanism. Photothermal model dominates the ablation processes with long wavelength, such as infrared, where rapid thermalization takes place and decomposition of heated material follows the Arrhenius law. The photochemical model, on the other hand, occurs in ablation processes with short wavelengths, such as the ultraviolet range, where direct bond breaking happens in an excited state induced by an incoming photon pulse. An illustration of the energy diagram of a molecule after being stimulated by laser pulses at two different wavelength ranges is shown in figure 1.11.

The process with a UV-laser pulse, however, cannot be always treated as following a pure photochemical mechanism. The photothermal model will also contribute depending on the situation. Considering the scenario of part b in figure 1.11, the step after this excited state can take two possible ways: (1) a direct bond-breaking dissociation in this state, or (2) an internal conversion leaning back into ground state S_0, but with high vibration energy. In the latter situation, a bond breaking from ground state will compete with vibrational relaxation. The energy pathways present in ultraviolet processing of polymers in figure 1.12, concluded by Ball and Sauerbrey, can be taken as a schematic description of this process in general.[58]

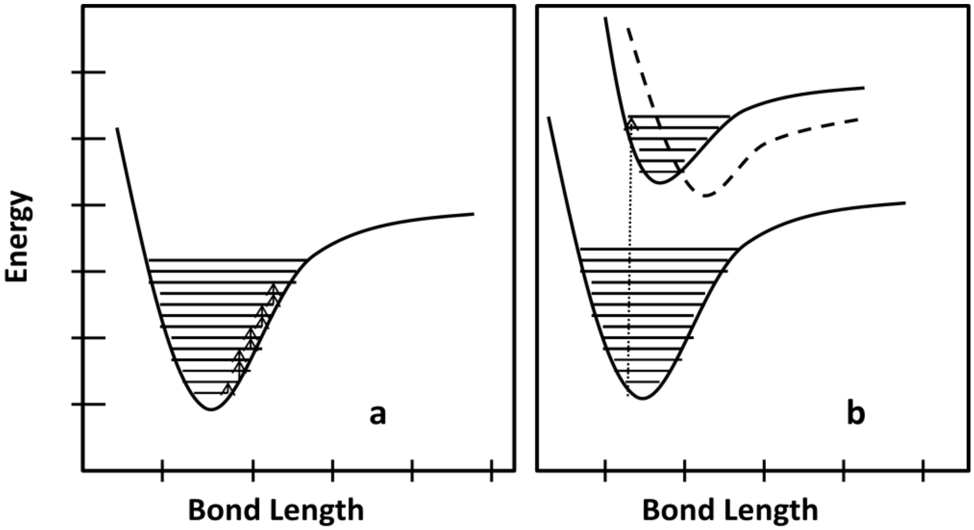

Figure 1.11: Illustration of excitation processes of long wavelength (a) and short wavelength light (b). In (a), absorption of IR photons induces thermal pumping in the vibrational manifold. In (b), absorption of photons excite molecules into their electronic excited state from ground state ($S_0 \rightarrow S_1$) The dashed line in (b) is the triplet state of the excited state.

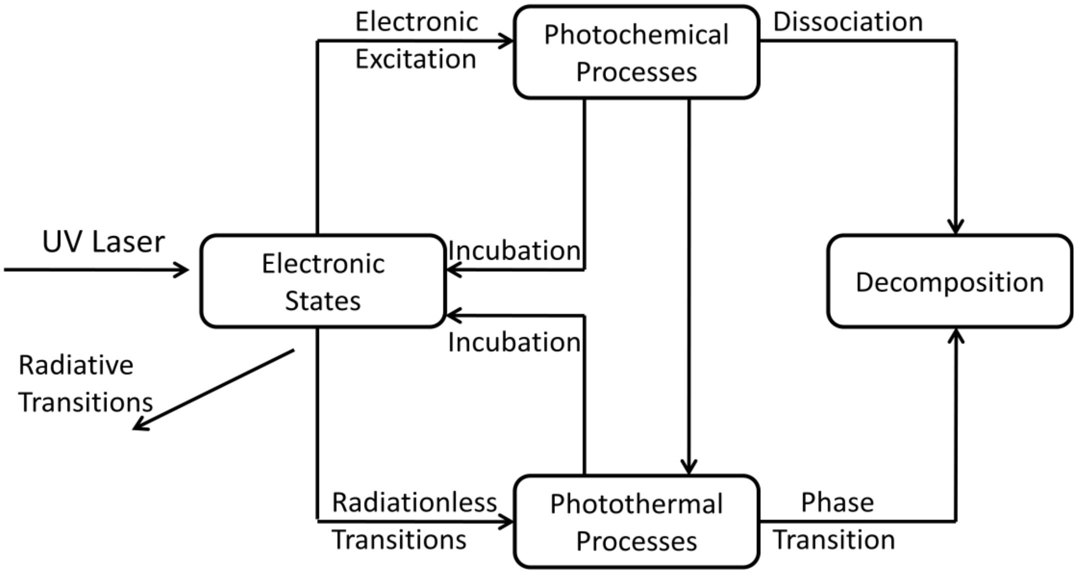

Figure 1.12 Diagram showing various energy pathways during ultraviolet processing of polymers. Redrawn from reference 57

1.3.2 Plume Formation and Expansion

In laser ablation, the plume is the cloud of volatile products that is expelled from the irradiated surface by a laser pulse. The understanding of laser-induced-plume not only has importance as a fundamental physical process, but also in applications of various techniques, such as laser-induced breakdown spectroscopy (LIBS), [59, 60] and pulsed laser deposition (PLD).[61,62] A great amount of theoretically modeling work on laser ablated plume has been carried out and reviewed by Dwivedi.[63]

Regardless of the details of the process, it is well accepted that upon formation of a plume: (1) a shock wave is generated that expands into the environment; (2) the ambient gas between the shock wave front and plume frontier is compressed and heated, as shown in figure 1.13. When the shock wave is strong enough to raise the compressed gas to a high temperature, the gas, which initially was transparent to the laser radiation, will start to absorb the energy from the laser pulse and become ionized, thus generating a laser-supported plasma.[64] The pressure behind the shock wave is decreasing from the maximum at shock front to certain value at the surface of the ablation. The material density drops from the maximum at the shock front to plume front and the density inside of the plume is higher than the heated ambient gas and keeps increasing as it gets closer to the ablation surface. A plume can expand 2 -3 mm and the whole expansion process usually takes place in a time scale of about 100 ns.[65]

The motion of the shock front R in a spherical expansion follows the following relationship

$$R = \xi_0 (E/\rho)^{1/5} t^{2/5} \qquad (1.\ 6)$$

where ξ_0 is a constant which depends on γ, the specific heat capacity of the ambient gas, ρ is the density of the ambient gas, E is the absorbed laser energy, and t is the travelling time.[66] This

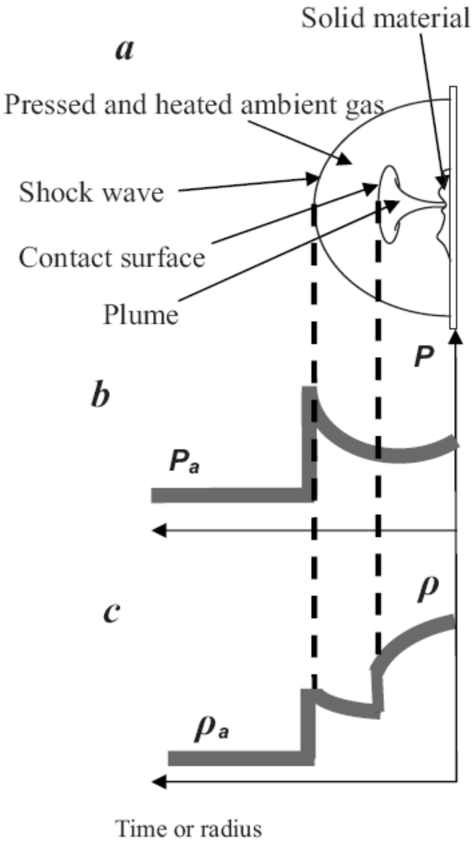

Figure 1.13: Sketches of the ablation process (a) and the corresponding pressure (b) and density (c) distributions.

equation has two limiting conditions: (1) when the ambient pressure P_0 is very low, the plasma plume takes form of a free expansion; (2)when P_0 is very high, almost equal to the pressure driving the shock front, a different equation will govern the expansion distance R_2 :

$$R_2 = (E/P_0)^{1/3} \qquad (1.\ 7)$$

In general, a flame extends farther from the surface at low pressure than at high pressure. But the thermal profile of the plume gives a higher surface temperature at high pressure than at low pressure.[67]

The expansion of a plume shows a different directional dependence in the UV and IR laser pulse regimes. In a recent study of laser ablation of an organic sample, nylon 6,6, shadowgraph photography showed shockwave expands in spherical wave in the UV (266nm) regime, whereas a clear anisotropic expansion was showed in the IR (1064nm) regime.[68] This was explained as the result of a tailing part of an IR laser pulse feeding energy into the expanding plume. The absorption of the later part of the incident laser energy by a plasma plume (formed during a laser pulse), is commonly referred as plasma shielding. The study of the conditions at which a plasma shielding arises and the extent of shielding are of considerable interest for controlling the laser ablation process.

The influence of the surrounding gas composition and pressure on the plasma plume shielding process has been studied by several groups.[69,70,71] Russo et al compared ablation of copper in Argon and Helium with varied pressure and at both picosecond and nanosecond pulse regimes.[69] In the picosecond regime, Argon, as being with a smaller ionization potential 15.8 eV vs. Helium 24.6 eV, showed more plasma shielding than He. They also proposed that a higher degree of plasma shielding arises when the pressure increased beyond 10 Torr in Ar and 100 Torr in He, due to enhanced collisions between high-energy electrons and gas atoms at higher pressure. On the contrary, plasma shielding with nanosecond laser pulse showed independence of the gas environment and pressure. A hypothesis was proposed that the vapor plume is mainly composed of copper ions in nanosecond interaction, whereas plume from a picosecond laser ablation involve Ar or He ions as well, due to collision between high-energy electrons and gas atoms. The high-energy electrons, generated initially from attenuation of a high electric field of the light on the target, can only be feasible in picosecond pulse.

The independence of plasma shielding on the gas environment with nanosecond laser pulses was later discovered to be disputable. Boudreau et al. found that laser fluence influences the extent of plasma shielding greatly, as plasma shieldings in Ar and He behave similarly until the laser pulse irradiance exceeds 2.5 GW/cm^2. Beyond this fluence, there appears to be significant plasma shielding in Ar, whereas little shielding exists in He[71].

1.3.3 Multi-photon Ionization (MPI)

Multi-photon ionization involves the simultaneous absorption of more than more photon by a molecule or an atom to go through an ionization process, as showed in the reaction:

$$M + m\,h\nu = M^+ + e^- \qquad (1.\,8)$$

In this equation, hν refers to the energy of one photon. m is the number of photons absorbed simultaneously by molecule M. If ϵ is the ionization potential, the number of photons required for MPI to take place has to be greater than the integer part of ($\epsilon/h\nu + 1$). Clearly, for an ionization of a certain molecule, it will take more photons with longer wavelengths than with short wavelengths. Hence, MPI is more important in the case of UV laser ablation. Clearly, the MPI process is dependent on laser fluence. For example, the diatomic products from a 248 nm UV-laser ablation of a polyimide film have been shown to possess a translational energy of approximately 5eV.[72] For a one photon (less than 5eV) absorption is inadequate to generate a product of such velocity, a multi-photon ionization process must dictate the reaction.[72]

Since the overall project in this work involve both laser ablation of polymers and laser ablation of RDX, the following introduction on laser ablation will be divided into these two areas.

1.3.4 Laser Ablation of Polymers

Since the first reports on laser ablation of polymers in 1982,[73,74] there are numbers of review articles in this subject that have been published.[75,76,77,78] A polymer is a large molecule, consisting of repeating smaller molecular units (monomer) with basic elements as carbon, hydrogen, oxygen and sometimes also nitrogen. The commonly studied polymers which are also commercially available, include polyimide (PI), polymethylmethacrylate (PMMA), and polycarbonate (PC). A new type of designed triazene polymer (TP) has also been intensively studied. Their chemical structures are shown in figure 1.14.

In a study of laser ablation on polyimide film, based on the chemical analysis of the ablation products, Srinivasan found that the reaction occurred via a thermal process upon exposure to IR laser pulses of nanosecond duration and also to UV laser pulses of long duration (> 10 µs). But nanosecond UV laser pulses showed fundamentally different reaction routs.[79] This finding suggested that a photochemical process may dominate the nanosecond UV- laser ablation process. Nanosecond surface interferometry measurement has been used as an effective tool to distinguish the two mechanisms in the ablation event, since a photothermal ablation is often related with surface swelling and a delayed material ejection, whereas a photochemical ablation

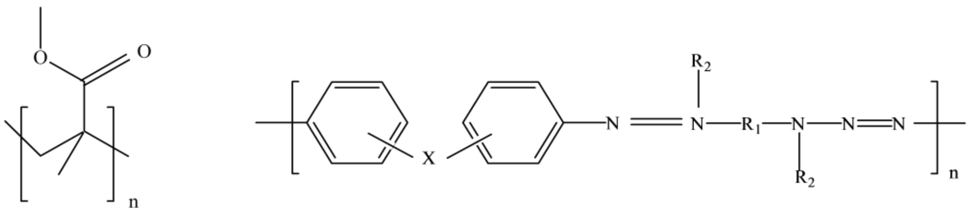

polymethylmethacrylate (PMMA)

Triazene Polymers (TP)_

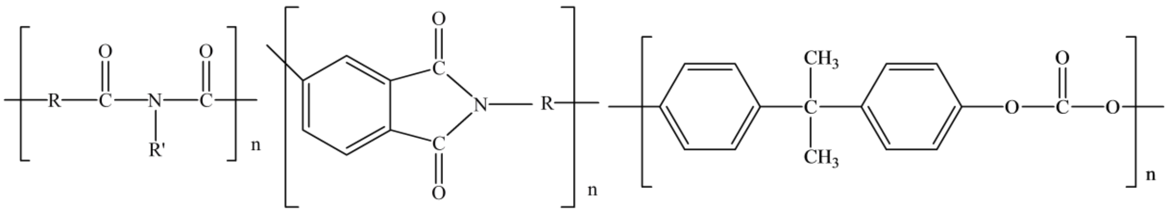

Polyimide (linear and acromatic)

Polycarbonate (PC)

Figure 1.14 Chemical structures of the commonly studied polymers in laser ablation

only occurs during the laser pulse and no sample swelling taking place.[80,81,82] The two mechanisms are differentiated for polyimide ablation at 248 nm and 351 nm wavelength, based on the morphological dynamics from nanosecond interferometry.[83] Lippert et al studied the 308nm laser ablation characteristics of three kinds of polymers: polymers containing triazene groups; ester groups and imide groups. They found that triazene polymers exhibit the lowest threshold (25 mJ cm^{-2}) and highest ablation rate. Polyimide showed the highest ablation threshold and lowest ablation rate. This was explained by the possible different ablation mechanisms, where a photonthermal model applies for polyimides and a photonchemical model predominates for triazene polymers. Moreover, the results from nanosecond interferometry and shadowgraphy supported the photonchemical model for triazene polymers by showing that ablation starts and ends within the laser pulse.[84]

The ablation depth induced by a single laser pulse follows a Lamber-Beer law in a corrected form:

$$h_e = \begin{cases} 0, & if\ F < F_{th} \\ \frac{1}{\alpha} log\left[\frac{F}{F_{th}}\right], & if\ F \geq F_{th} \end{cases} \qquad (1.\ 9)$$

here h_e is the ablation depth per pulse, α is absorption coefficient, F is the laser fluence, and F_{th} is the threshold fluence. Photoacoustic measurements demonstrated that below the polymer ablation threshold, only a sinusoidal stress pulse was produced, indicating that the UV laser pulse merely heated the polymer. Whereas above the threshold, a strong positive signal was generated and it increases with increasing fluence.[85,86] It is well established that the value of α can be modified after ablation takes place.[87] However, this modification cannot alone explain the deviation of α value obtained from fitting the kinetic curve to experimental data from the theoretical value of α. Screening of the ablated plume can also limit the ablation rates, especially at high fluences.[30, 35]

It is found that the existence of a threshold fluence is not solely a UV phenomenon but occurs through a broad range of wavelengths.[88] This can be understood from both photonthermal and photonchemical points of view. In photon-thermal model, as noted before, the reaction follows Arrhenius law:

$$k = A \exp [-E_A/RT] \qquad (1.\ 10)$$

here k is reaction rate, A is a exponential factor; E_A is activation energy and T is reaction temperature. If k has a critical value for a measurable ablation depth, a temperature threshold arises. Moreover, the heat loss through conduction into the bulk underlying polymer works against heat accumulation. In photochemical model, the threshold fluence is explained using the idea that ablation starts only when the density of broken bonds at the surface reaches a critical value. In another words, when a long polymer chain was broken into short segments, products will leave the surface and ablation depth appears. In comparison, the threshold fluence is always more significant with UV-laser ablation than IR-laser ablation. An abrupt rise is a typical characteristic of a profile of ablation-depth -per-pulse vs. log fluence in UV-laser ablation of polymer[32].

In conclusion, there are several main characteristics of UV-laser ablation of polymers:

1 A threshold fluence exists for laser ablation to take place and threshold phenomenon is more significant for ablation with UV photons than using IR wavelengths.

2 Ablation depth per laser pulse increases with increasing laser fluence. Typically, the ablation depth is a fraction of a micron for intense absorbers to many tens of microns for weekly absorbing polymers at one wavelength.

3 In general, the ablation depth increases with increasing laser wavelength and laser fluence.[77]

1.4 Conclusion

This chapter has attempted to introduce explosive materials according to different categorizations. Secondary explosives (SE) are a group of explosives which combine two critical properties of high energetic materials: high power and low sensitivity. In contrast, primary explosives (PE) are easy to be ignited and also have less power. Several important SEs include Hexahydro-1,3,5-trinitro-1,3,5-triazine (RDX), cyclotetraethylene tetranitramine (HMX), 2, 4, 6-Trinitrotoluene (TNT) and Pentaerythritol Tetranitrate (PETN), which are widely used in military and industrial applications.

Several methods of initiation (thermal, shock, impact, light and electric field) have been discussed. Laser initiation shows promising advantages because its intrinsic properties of being versatile, fast acting, immune to accidental firing and powerful to meet the initiation threshold of insensitive secondary explosives. There have been studies on decomposition of SEs initiated by Infrared (IR) lasers, which is utilized as a versatile heating source. In comparison, fewer investigations have been performed on the decomposition of SEs by Ultraviolet (UV) laser. Several studies that used UV photons were performed with molecular gas-phase RDX utilizing a molecular beam technique. In reality, however, the SEs exist as a solid material when they are to be initiated. One of the objectives of the following chapters is to address the products and possible mechanism of UV-laser induced decomposition of solid-phase RDX.

Plasma initiation has been investigated as an alternative to conventional primary initiation in Electrothermal-Chemical (ETC) guns, exhibiting advantages of reduced delay-time, improved reproducibility and temperature compensation. One of the hurdles to real application of this system is the bulky size of the capacitor in ETC system. A laser-induced-plasma initiation has been proposed and investigated in the fourth chapter. In this design, a polymer material as used in ETC, in this case polycarbonate, is the source material to be converted into localized plasma by a UV-laser pulse. This plasma, which resembles the one generated from ETC pulse in many ways, as discussed in section 1.2.5, is expected to initiate the main charge. In addition, laser ablation of polymers has been discussed in terms of mechanisms and plasma plume formation.

1.5 References

---

1 Agrawal J.P.; Hudgson R.D. *Organic Chemistry of Explosives,* John Wiley&Sons, Ltd, West Sussen, England, **2007.**

2 Eaton P.E. and Wicks G. E., *J. Org. Chem*., **1988,** 53, 5353.

3 Arney Jr B. E.; Dave P. R.; Marchand A. P. *J. Org. Chem*., **1988**, 53, 443.

4 Chander Suri S. and Marchand A. P. *J. Org. Chem.*, **1984**, 49, 2041.

5 Astakhov A. M; Babushkin A. Y. ; Stepanov R. S. *Combustion, Explosion and Shock Waves,* **1998**, 34, 85.

6 Muthurajan H.; Sivabalan R.; Talawar B.; Anniyappan M.; Venugopalan S. *Journal of Hazardous Materials* **2006**, A133, 30.

7 Meyer, R. Explosives, Weinheim, New York, **1977.**

8 Keshaarz, M. H.; Motamedoshariati, H.; Pouretedal, H. R.; Tehrani, M. K.; Semnani, A. *J. Hazardrous Materials.* **2007**, 145, 109.

9 Keshavarz, M. H.; Poureteda, H. R. *J. Hazardous Materials*. **2005**, A124, 27.

10 Kamlet, M. J.; Adolph, H. G. *Propellants Explos*. **1979**, 4, 30.

11 Skinner, D.; Olson, D.; Block-Bolten, A. *Propellants., Explosives, Pyrotechnics*. **1997**, 23, 34.

12 Brill, T. B.; Kenneth, J. J. *Chem. Rev*. **1993**, 93, 2667.

13 Liau, Y.-C.; Kim, E. S.; Yang, V. *Combustion Flame*, **2001**, 126, 1680.

14 Zeman, S. *Struct Bond* **2007**, 125, 195.

15 Shackelford, S. A.; Beckmann, J. W. Wilkes, J. S. *J. Org. Chem*. 42, **1977**, 4201.

16 Tarver, C. M.; Tran, T. D.; Whipple, R. E. *Propellants. Explosives, Pyrotechnics* **2003**, 28 (4), 189.

---

17 Tarver, C. M.; Tran, T. D. *Conbust. Flame* **2004**, 137, 50.

18 Watson, S.; Gifford, M. J.; Field, J. E. *J. Appl. Phys.* **2000**, 88, 65.

19 Gu, Z. W.; Sun, C. W.; Zhao, J. H.; Zhang, N. *J. Appl. Phys.* **2004**, 96, 344.

20 Schmidt, S. C.; Dick, R. D.; Forbes, J. W.; Tasker, D. G. Shock Compression of Condensed Matter, Elsevier: Amsterdam, **1991;** p 829.

21 Cogan, S.; Shirman, E.; Haas, Y. *J. Appl. Phys*. **2005**, 97, 113508/1.

22 Fu, S.; Gu, Y.; Huang, X.; Wu, J.; He, J.; Ma, M.; Luo, P.; Zhang, Y. *Physics. Plasmas* **2002**, 9, 3201.

23 Schmidt, S. C.; Johnson, J. N.; Davidson, L. W. Shock Compression of Condensed Matter, Elsevier: Amsterdam, **1989;** pp. 733.

24 Watson, S.; Field, J. E. *J. Phys. D: Appl. Phys.* **2000**, 33, 170.

25 Greenaway, M. W.; Proud, W. G.; Field, J. E.; Goveas, S. G. Intern. *J. Impact Engineering* **2003**, 29, 317.

26 de Resseguier, T.; He, H.; Perberretche, P. Intern. *J. Impact Engineering* **2005**, 31, 945.

27 Greenaway, M. W.; Gifford, M. J.; Proud, W. G.; Field, J. E.; Goveas, S. G. Shock an Investigation into the Initiation of Hexanitrostilbene by Laser-Driven Flyer Plates, In *Shock Compression of Condensed Matter*, Furnish, M. D.; Thadhani, N. N.; Horie, Y. Eds.; **2002**Elsevier: Amsterdam, pp 1035-1038.

28 Swift, D. C.; Niemczura, J. G.; Paisley, D. L.; Johnson, R. P.; Luo, S. Tierney, T. E. IV. *Review of Scientific Instruments* **2005**, 76, 09307.

29 Watson, S.; Field, J. E. *J. Appl. Phys.* **2000**, 88 (7) 3859.

30 McNesby, M. L.; Coffey, C. S. *J. Phys. Chem*. **1997**, B101, 3097.

---

31 Idar, D. J.; Straight, J. W.; Osborn, M. A.; Coulter, W. L.; Skidmore, C. B.; Phillips, D. S.; DeCroix, M. E.; Buntain, G. A.; Howe, P. M. 704(JANNAF 19th Propulsion Systems Hazards Subcommittee Meeting, **2000**, Vol. 1, 233.

32 Fair, H. D.; Walker, R. F. (Ed) Energ. Materials V. 1, Plenum, New York, **1977,** Chapter 8

33 Bowden, F. P; Chaudhri, M. M. *Nature* **1968**, 220, 690

34 Lee, I-Y. S.; Hill, J. R; Suzuki, H.; Bare, B. J.; Chronister, E. L.; Dlott, D. D. *J. Chem. Phys.* **1995**,103, 8313

35 Fried, L. E.; Tarver, C. M. *AIP Conf. Proc.* **1996**, 370, 179

36 Dienes, J. K., Zuo, Q. H.; Kershner, J. D. *J. Mech. Phys. Solids* **2006**, 54, 1237.

37 Bourne, N. K. *Proc. R. Soc. London*, **2000**, A457: 1401

38 Botcher, T. R.; Wight, C. A. *J. Phys. Chem*. **1993**, 97, 9149.

39 Botcher, T. R.; Wight, C. A. *J. Phys. Chem***. 1994**, 97, 5441.

40 Zuckermann, H.; Greenblatt, G. D.; Hass, Y. *J. Phys. Chem*. **1987**, 91, 5159.

41 Zhao, X.; Hintsa, E. J.; Lee, Y. T. *J. Chem. Phys*. **1988**, 88, 801.

42 Capellos, C.; Papagiannakopoulos, O.; Liang, Y. L. *Chem. Phys. Lett*. **1989**, 164, 533.

43 Im, H. S.; Bernstein, E. R. *J. Chem. Phys.* **2000**, 113, 7911.

44 Guo, Y. Q.; Greenfield, M.; Bernstein, E. R. *J. Chem. Phys.* **2005**, 122 (24), 244310/1.

45 Greenfield, M. Guo, Y. Q. Bernstein, E. R. *Chem. Phys. Lett***. 2006**, 430, 277.

46 Guo, Y. Q.; Greenfield, M.; Bhattacharya, A.; Bernstein, E. R. *J. Chem. Phys*. **2007**, 127, 154301/1.

47 Alix, J.; Collins, S. *Can. J. Chem.* **1991**, 69, 1535.

48 Choi, M.; Kim, H. Chung, C. *J. Phys. Chem.* **1995**, 99, 15785.

---

49 Manaa, M. R.; Mitchell, A. R.; Garza, R. G.; Pagoria, P. F.; Watkins, B. E. *J. Am. Chem. Soc.* **2005**, 127, 13786.

50 Ajayan, P. M.; Terrones, M.; de la Guardia, A.; Huc, V.; Grobert, N.;Wei, B. Q.; Lezec, H.; Ramanath, G.; Ebbesen, T. W. *Science* **2002**, 296, 705.

51 Chaboki, S.; Zelenak, B. Isle. *IEEE Trans. Mag.* **1997**, 33. 284.

52 Porwitzky, A. J.; Keidar, M.; Boyd, I. D. *IEEE Trans. Mag.* **2009**, 45. 412.

53 Dyvik, J.; Juleigh, H; Appleton, R.; O'Reilly, J.; Shin, J. *IEEE Trans. Mag.* **2007**, 43. 303.

54 Beyer, R. A.; Pesce-Rodriguez, R. A. The Response of Propellants to Plasma Radiation ARL TR-3189

55 Pesce-Rodriguez, R. A.; Beyer, R. A. A Theory of Plasma-Propellant Interactions ARL-TR-3286

56 Valliere, R.; Blumenthal, R. *J. Appl. Phys*. **2006**, 100, 084904/1.

57 Srinivasan, R. *Science*, **1986**, 234 (4776), 559.

58 Ball, Z.; Sauerbrey, R. Surface Modification with Lasers. In *Laser Ablation and Desorption*, Miller, J. C.; Haglund, R. F. Eds.; Academic, San Diego, **1998**; pp 333-373.

59 Michel, A. P. M. *Spectrochim. Acta, part B: Atomic Spectroscopy* **2010**, 65 B, 185.

60 Galbacs, G.; Jedlinszki, N.; Herrera, K.; Omenetto, N.; Smith, B. W.; Winefordner, J. D. *Appl. Spectrosc*. **2010**, 161.

61 Norton, D. P.; Park, C.; Budai, J. D.; Pennycook, S. J.; Prouteau, C. *Appl. Phys. Lett*. **1999**, 74, 2134.

62 Perez-Tijerina, E.; Machorro, R.; Bohigas, J. *Review of Scientif.Instrum.* **2004**, 75, 455.

63 Dwivedi, A. *Surf. Rev. Lett*. **2007**, 14, 57.

---

64 Laser Induced Plasmas and Applications, Radziemski, L. J.; Cremers, D. A. Ed. Marcel Dekker Inc, New York, **1989**, p71.

65 Yalcin, S.; Tsui, Y, Y,; Fedosejevs, R. *IEEE Trans Plasma Sci.* **2005,** 33, 482.

66 Dyer, P. E.; Sidhu, J. *J. Appl. Phys.* **1988**, 64, 4657.

67 Beckstead, M. W. *Pure Appl. Chem.* **1993**, 65, 297.

68 Boueri, M.; Baudelet, M.; Yu, J.; Mao, X.; Mao, S. S.; Russo, R. *Appl. Surf. Sci.* **2009**, 255, 9566

69 Mao, C., L.; Chan, W. T.; Shannon, M. A.; Russo, R. E. *J. Appl. Phys.* **1993**, 74, 4915

70 Sdorra, W.; Kiemax, K. *Mikrochim. Atca* **1992**, 107, 319

71 Gravel, J.-F. Y., Boudreau, D. *Spectrochimica Acta Part B* **2009**, 64, 56

72 Srinivasan, R.; Braren, B.; Dreyfus, R. W. *J. Appl. Phys.* **1987**, 61, 372

73 Kawamura, Y.; Toyoda, K.; Namba, S. *Appl. Phys. Lett*. **1982**, 40, 374

74 Srinivasan, R.; Manye-Banton, S. *Appl. Phys. Lett.* **1982**, 41, 576

75 Lippert, T.; Dicknson, J. T. *Chem. Rev.* **2003**, 103, 453.

76 Bityurin, N.; Lukyanchuk, B. S.; Hong, M. H.; Chong, T. C. *Chem. Rev*. **2003**, 103, 519.

77 Srinivasan, R.; Braren, B. *Chem. Rev*. **1989**, 89, 1303.

78 Lippert, T., Kunz, T., Hahn, C., Wokaun, A. *Recent Res. Devel. Macromol. Res*. **1997**, 2, 121.

79 Srinivasan, R. *Appl. Phys. A* **1993**, 56, 417.

80 Furutani, H.; Fukumura, H.; Masuhara, H. *J Phys. Chem.* **1996,** 100, 6871.

81 Furatani, H.; Fukumura, H.; Masuhara, H. *Appl. Phys. Lett.* **1994**, 65, 3413.

82 Furatani, H.; Fukumura, H.; Masuhara, H.; Lippert, T.; Yabe, A. *J. Phys. Chem. A* **1997**, 101, 5742.

---

83 Masubuchi, T.; Tada, T.; Nomura, E.; Hatanaka, K.; Fukumura, H.; Masuhara, H. *J. Phys. Chem. A* **2002**,106, 2180.

84 Lippert, T.; Hauer, M.; Phipps, C. R.; Wokaun, A. *Appl. Phys. A: Mater. Sci. & Proc.* 2003, 77, 259.

85 Dyer, P. E.; Srinivasan, R. *Appl. Phys. Lett.* **1986**, 48, 445.

86 Gorodetsky, G.; Kazyaka, T. G.; Melcher, R. L.; Srinivasan, R. *Appl. Phys. Lett*. **1985**, 46, 828.

87 Schmidt, H.; Ihlemann, J.; Wolff-Rottke, B; Luther, K.; Troe, J. *J. Appl. Phys.* **1998**, 83, 5458.

88 Dyer, P. E. *Appl. Phys. A* **2003**, A 77, 167.

Chapter 2

Study of Products of 266nm UV-Laser Ablation of RDX in Air

2.1. Introduction

Due to its very nature as an energetic material, RDX (Hexahydro-1,3,5-trinitro-1,3,5-triazine) undergoes extremely rapid decomposition. Its rapid rate of decomposition and its shock insensitivity have both led to its ubiquitous use as a military propellant. In a scientific sense, the rapid rate of decomposition has made the investigation of the process simultaneously difficult and fascinating. Few experimental methods are capable of probing chemical processes with the time resolution necessary to observe the formation of reaction intermediates. One technique which has demonstrated adequate time resolution is laser induced fluorescence (LIF).[1] However, even LIF becomes hampered by the fact that the intermediates of interest exists only near the solid surface which advances through focal space of the detector at velocities of up to 7000 m/s. In such experiments, the first millimeter above the surface would pass through a 1.0 mm imaging field in only 0.14 microseconds, severely limiting the time available for signal integration and thus, limiting the signal to noise ratio that is possible.

Over the past two decades, advances in computational power have made possible to use molecular dynamics calculations as an atomic-scale microscope of extremely fast processes. These calculations have proved highly effective in providing an understanding of the atomic scale processes that underlie secondary ion mass spectrometry[2] and laser ablation,[3] providing details that no experimental probe could provide. The key to their success is an empirical potential energy force field which is readily solved mathematically, thus allowing the calculation to follow a large number of molecules over the physically and chemically important time scale of the process. The critical word in the last sentence is empirical. For molecular dynamics calculations to have significance to the real world, their results must correlate with experimental observables. For the ablation of energetic materials, little experimental evidence exists to which the results of the calculations can be compared. In this study, the products of the UV laser ablation of RDX are reported. The chemical products and their dependence on the laser fluence should serve as a valuable reference for the evaluation of the empircal potential used in molecular dynamics calculations and also as tests of proposed mechanisms of the UV photodecomposition of solid RDX.

Before proceeding, it is critical to emphasize that the UV laser ablation of RDX is not a linear optical process, nor is it a simple multi-photonic process. Previous investigations on laser ablation of RDX using 266 nm illumination[4] indicated no removal of material below a sharp threshold laser fluence. In this work, the laser fluence was varied by adjusting the distance between the sample and a 110 mm laser focusing lens. At sample-lens separations of less than 90 mm, maximum removal of material was observed just above that threshold, and further increases in photon flux resulted in decreasing amounts of material removed. The observation of a threshold is strong evidence of a non-linear (multi-photonic) process. The decrease in the total amount removed above the threshold is the result of a combination of the reduced area of illumination and the adsorption and reflection of the laser fluence above the threshold by a plasma plume formed by the threshold fluence.

The photodecomposition of RDX has not been as heavily studied as the thermal decomposition. The majority of the investigations have relied on the use of infrared lasers, resulting in what often amounts to a fast version of thermal decomposition. A few reports on the photodecomposition of RDX induced by ultraviolet lasers are found in the literature.[5,6,7,8,9,10] In one study, photodecomposition of RDX vapor by 248 nm light from a KrF laser resulted in the observation of excited state NO_2 and OH in the emission spectra. The existence of both species was explained by a two reaction channel model incorporating both N-N bond scission and HONO elimination.[5] In a series of studies on isolated molecular RDX[6,7,8,9] generated by matrix assisted laser desorption (MALD) and molecular beam technique, Bernstein observed 1) rotationally hot NO using laser-induced fluorescence spectroscopy, 2) a lack of evidence of OH, despite the fact that the transition intensity of OH was calculated to be 1.5 times of that NO, and 3) a lack of NO_2 signals in femptosecond laser pump-probe experiments at three wavelengths (230nm, 228nm, and 226nm). The absence of OH ruled out the possibility of HONO as the intermediate responsible for the formation of NO molecules, while the femptosecond laser experiments ruled out NO_2 as the source of NO. As a result, a completely new mechanism of the ultraviolet photodissociation of isolated RDX molecules was proposed based on a nitro-nitrite isomerization that simultaneously explained the lack of traditional intermediates and the high vibrational but low rotational temperatures of the observed NO molecules.

In contrast to photodecomposition, the thermal decomposition of RDX has been heavily studied. Despite years of experimental and theoretical study, no single model for the thermal decomposition of RDX has achieved universal acceptance. Very early in the study of the thermal decomposition mechanism of RDX, it was recognized that the N-N bond was the weakest bond in the RDX molecule.[11] This fact lead to a thermal decomposition mechanism where the process begins with the loss of NO_2, followed by the breaking the weakened C-N bond in the ring.[12] The distinguishing characteristic of this mechanism is that the final products (HCN, N_2O, H_2O, NO and CH_2O) do not necessarily retain the C-N connectivity of the RDX ring.[11] Another frequently cited thermal decomposition mechanism views the RDX molecule as a ring formed from three $H_2C{=}N{-}NO_2$ units. In this mechanism, the molecule initially fragments into the $H_2C{=}N{-}NO_2$ which is subsequently converted into HCN, H_2CO, HONO (or HNO_2) and N_2O.[13] More recently, Zeman united these two mechanisms by suggesting the former as the high-temperature (above 600K) decomposition channel and the later as the low-temperature (below 600K) channel.[14] A third reaction mechanism has been proposed by Goddard.[15] This mechanism begins with the elimination of HONO from the dissociation of a five-member ring transition state formed by the attack of an NO_2 oxygen on a neighboring hydrogen atom. Following loss of three HONO units, the remaining tiazene ring dissociates into three HCN molecules.

The concentrations of the chemical products produced by the ultraviolet laser ablation of RDX are reported in air and as a function of laser fluence in an effort to probe the chemical mechanism. Ablation produced the products: HCN, NO_2, N_2O, CO_2 and CO. All of the observed products have been reported previously as decomposition products of RDX. To further probe the process, the product distributions were measured over a range of laser fluencies or focal distances from the lens. Due to the fact that ablation is a non-linear phenomenon, the ablation area is not a simple linear function of the focal distance, resulting in an initial laser plume with a diameter that is not a linear function of the focal distance. To further complicate things the shape of the plume evolves in time resulting in final concentrations of species being a complex convolution of photo-dissociation reactions of the solid, reactions within the bulk of the plume, and reactions at the contact surface. Hence, only general conclusions about mechanisms may be drawn from the fluence dependent measurements.

2.2. Experimental

2.2.1 RDX film preparation

RDX films were sprayed from 1.0 mg/ml standard solutions of RDX in acetonitrile obtained from Cerilliant or from 1.0 mg/ml solutions prepared in our laboratory. The spray deposition sprayer method (shown in bottom sketch of figure 2.1), was designed in a similar way as a nebulizer in electro-spray ionization mass spectroscopy. RDX solution is driven through a capillary by a syringe pump and the fast moving, dry, sheath nitrogen gas desiccates the droplets that emerge from the capillary end, carrying them to deposit on the substrate. The detailed construction has been described previously.[16] Small glass substrates (9 mm x 9 mm) were cut from standard VWR micro slides, in order to fit in the modified cuvette cell described in detail below. Glass substrates were cleaned with water and acetonitrile solution. Ten of them were attached to the rotating sample holder, which allows for the deposition of multiple identical samples on a substrate. A position kit was designed and used in this set up, as showed in the top picture of figure 2.1, which serves two functions: (1) to finely adjust and control the distance between capillary tube and substrate plate and (2) to ensure that the sample holder plate is perpendicular to the capillary to achieve uniformity of deposition. Using this deposition method, the factors which influence the size and the thickness of the sprayed RDX film include the sheath gas pressure, the solution flow rate and the distance between the end of the capillary tube and the sample holder. Using 25psi, 1.5 ml/h and 4.6 mm respectively, it has been found that ten reproducible RDX spots with an approximate diameter 8.5mm and thickness 8.0 µm for each is formed.

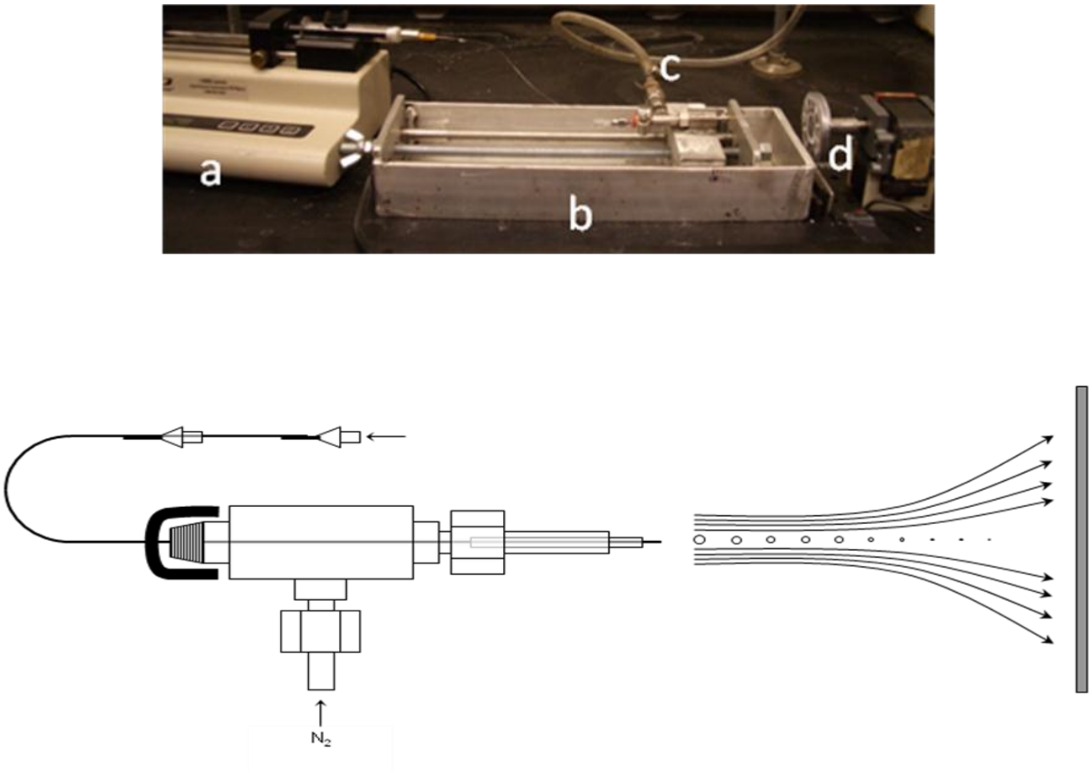

Figure 2.1, On the top: Photograph of the nebulizing spray setup a: syringe pump; b: positioning kit; c: nebulizing gas (dry, fast moving nitrogen gas) inlet; d: the rotating sample holder with ten spherically placed glass slides as substrate. On the bottom: Detailed schematic of nebulizing sprayer.

2.2.2 Instrumentation

Laser ablation was stimulated using a Continuum Electro-Optics, Inc. Inlite III-10 Neodymium doped Yttrium Aluminum Garnet (Nd: YAG) laser operated in the fourth harmonic mode (266 nm) with an output of 50 mJ / pulse, a pulse width of ~6 ns (achieved in Q-switch mode), and operated at a frequency of 10 Hz. The laser fluence was varied by changing the distance between the 200 mm focusing lens and RDX spot, as showed in figure 2.2.

For a Gaussian laser beam profile, the diameter of the laser beam at the sample distance can be written as

$$r = \frac{\lambda * f}{\pi * d} \tag{2. 1}$$

where λ is the wavelength of the laser, f is the focus distance of the focus lens, d and r are the diameters of the laser beam before the focusing lens and at a certain distance away from the lens respectively. Since a profile of a laser beam will not be converted into zero area in reality, the minimum beam size on the sample appears before the theoretical focusing point.

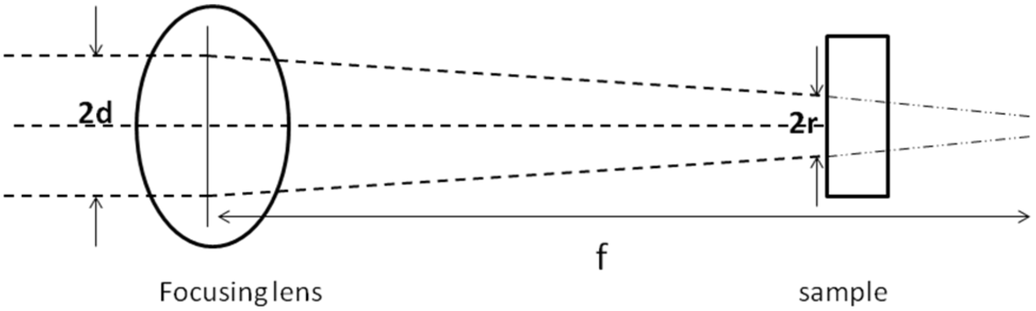

Figure 2.2 Dependence of the diameter of the laser beam at the sample surface on the separation distance between the two.

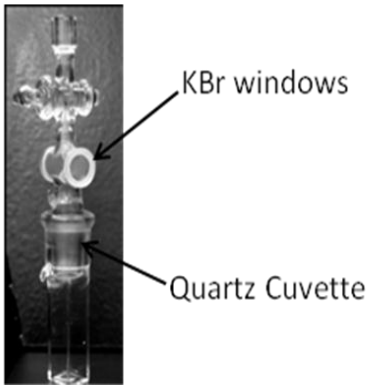

Figure 2.3: Photograph of the cuvette cell

IR spectra were obtained on a Shimadzu IR Prestige-21 FT-IR spectrometer averaging 32 scans and resolution of 1 cm^{-1}. In order to remove atmospheric CO_2 in the sample chamber, it is purged with nitrogen gas for 10 minutes prior to the measurement, as the IR spectra of the atmospheric gas was monitored since the starting of the purging gas and it showed a constant negative peak after 10 min at CO_2 region. It was noticed that a small amount of CO_2 was introduced into the chamber during sample loading. Therefore, a cautious handling was taken to ensure the removal of incoming CO_2 from loading the sample, so that the CO_2 peak in the spectra will be able represent the real level of CO_2 in the product. A quartz cuvette on the bottom, transparent to 266 nm light, with a cylinder-shaped cap on the top, which consists of a pair of KCl windows, was used as the sealed cell for containing the RDX sample and collecting the gas products from laser ablation. A photograph of the cell is shown in figure 2.3. The volume of the cell was determined to be 7.95 ml, where the measurement was made by filling the cell with hexanes, since the KCl windows are invulnerable to this solvent.

A RDX sample sprayed on a piece of glass slide (0.9 mm x 0.9 mm), as described above, was attached to the inside of the cuvette with a small piece of tape. The cuvette was moved around in the focal plane until all of the RDX was removed from the glass slide. The air-tightness of the IR cell was tested by monitoring the spectra of a sample of N_2O in the cell over 20 minutes and observing no measurable loss of signal. To demonstrate that none of the adsorption signals of interest are the result of irradiation of the cuvette, the IR spectra of an air filled cuvette after irradiated by the laser for one minute at 10 Hz is shown as the dashed line in figure 2.7.

2.2.3 Quantification of Gaseous Products

To establish the experimental sensitivity of our apparatus, N_2O was repeatedly injected in 0.01 ml increments into a cell initially filled with 1 atmosphere of argon and the IR spectrum was taken at each step. The integrated intensity of the 2223.5 cm^{-1} band was plotted as a function of N_2O concentration, and a slope as 1306.8 cm^{-2} atm^{-1} was obtained, see figure 2.4. This result compared well with previously reported result[17], which was 1421 cm^{-2} atm^{-1}.

The partial pressure of each gas species was calculated based on the equation:

$$n = \frac{\int \ln(\frac{I}{I_0})dw}{l * A} \qquad (2.\ 2)$$

where n is the partial pressure of the gas, l and A are the light pathlength and band strength, $\int \ln(\frac{I}{I_0})dw$ is the peak integral as measured in our spectrum in absorbance mode. The band strengths used here for calculation (in table 1) are from the data Brill assembled[18], with introduction of a correction factor 1.087 as obtained from the N_2O P-branch calibration mentioned above.

Because of spectral overlap of the R-branch of the N_2O signal with the P-branch of CO signal, only the intensity of P-branch of the N_2O adsorption, which accounted for 43% of the total band intensity, and the R-branch of the CO, which accounted for 52% of the total band intensity, were used in the calculations. The carbon and nitrogen fractions are calculated based on the sum of the total number of carbon and nitrogen atoms in the observed gases compared to the numbers in the original RDX spot.

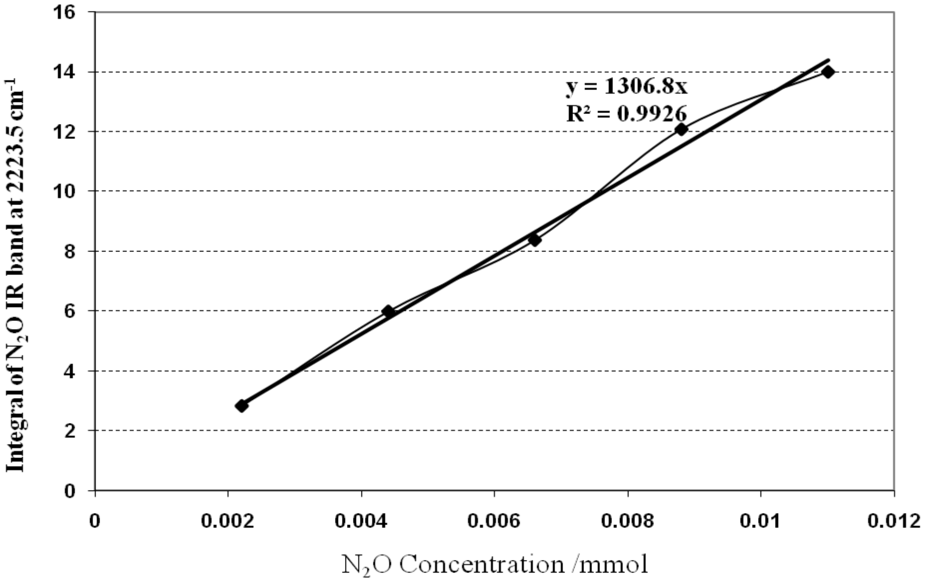

Figure 2.4: The dependence of the integral of N_2O IR band at 2223.5 cm^{-1} on the N_2O concentration, N_2O gas was injected into the IR chamber continuously with 0.01 mL increment; the integral was read from IResolution software

Table 2.1 Infrared band strength of Several Gaseous Products, ref 16

Gaseous Product	Band Frequency (cm^{-1})	Band Strength (cm^{-2} atm^{-1})
CO_2	2349	2580
N_2O	2224	1421
NO_2	1621	1419
CO	2143	268
HCN	713	260
NO	1876	133

2.3 Results

2.3.1 Preliminary observation on laser ablation pits on RDX

Photographs of the ablation pits formed on RDX at several different focal distances are presented in figure 2.5. As one might expect, the size of the ablation hole produced increases as the RDX sample is moved from the focal point of the lens. The ablation area as a function of the distance between lens and sample is shown in figure 2.6. The ablation areas were determined from digital analysis of the photographs of the pits, where the dark areas represented complete penetration of the film. In a linear photochemical process, based on equation (2. 1), the area of the ablation pits should show an inversely squared dependence on the lens-sample separation distance. The observed near linear dependence of the area on the distance is taken as further evidence of the non-linear nature of the ablation process. The last two pictures on the right showing an irregularly rough edge at the ablation pits even after many pulses. This may be a further indication of the non-linear characteristic of this ablation process, assuming that the laser light profile is not very uniform.

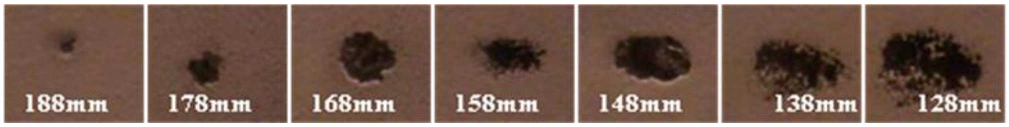

Figure 2.5: Photographic images of th ablation pits formed as a function of the distance between the RDX spot and the focusing lens, as indicated on the pictures. The area of each picture is 1.85mm by 1.60mm.

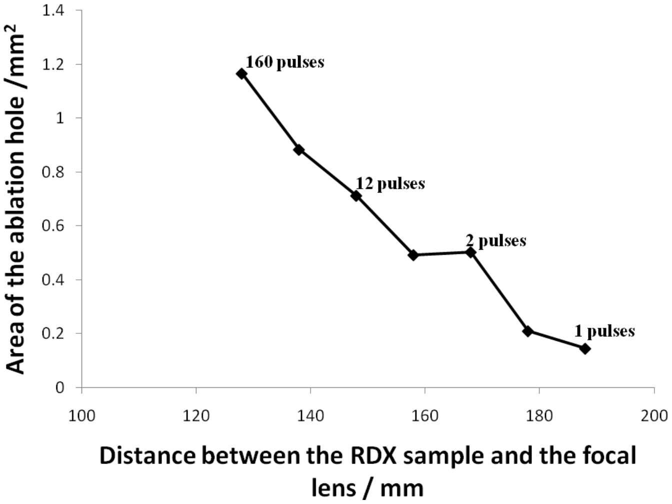

Figure 2.6: The dependence the area of the laser ablation pits (as shown in figure 2.5) vs. the distance between sample and focal lens; the data labels above indicate the number of laser pulses that took to make that ablation pits.

2.3.2 Ablation Gas Products Analysis

The IR spectrum of gas products from laser ablation of 2.7 mg of RDX in air is shown in figure 2.7. Five groups of peaks in the spectra revealed the production of the following molecules: HCN (double peak center at around 3300 cm^{-1}); CO_2 (double peak at around 2350 cm^{-1}); the overlapping two groups of double peaks of N_2O and CO, (centered at around 2218 cm^{-1} and 2139 cm^{-1} respectively) and NO_2 (double peak centered at 1615 cm^{-1}). All peak assignments and shapes are consistent with those reported by Brill[24] and also with the IR spectra obtained for available gases in our apparatus. The peaks around 3300cm^{-1} and 2139cm^{-1} showed detailed rotational structure. The rotational constants calculated for each were 4.335 x 10^{10} Hz and 5.7865 x 10^{10} Hz, respectively; confirming assignments as HCN[19] and CO.[20] In addition, HCN was generated in the cuvette by combining sulfuric acid solution with sodium cyanide aqueous solution. The IR absorption peaks from this generated HCN gas further confirmed the assignation of the HCN. A single peak, located at 1390 cm^{-1}, is tentatively assigned as the RDX vapor.[18] However, further understanding needs to be sought after since this peak is not always very conspicuous and other vibration modes of RDX were not noticed in this spectrum. The multiple small absorption lines observed from 3550 cm^{-1} to 4000 cm^{-1} and from 1400 cm^{-1} to 1800 cm^{-1} are attributed to the presence of H_2O.

The images shown in figure 2.5 provide clear evidence that both the area and the depth of the ablated RDX pits dependent the laser focus or laser fluence, hence, it would seem prudent to investigate the influence of focus on the product distribution. Figure 2.7 is the infrared spectra of the gas products obtained from laser ablation of RDX at three different positions from the lens,

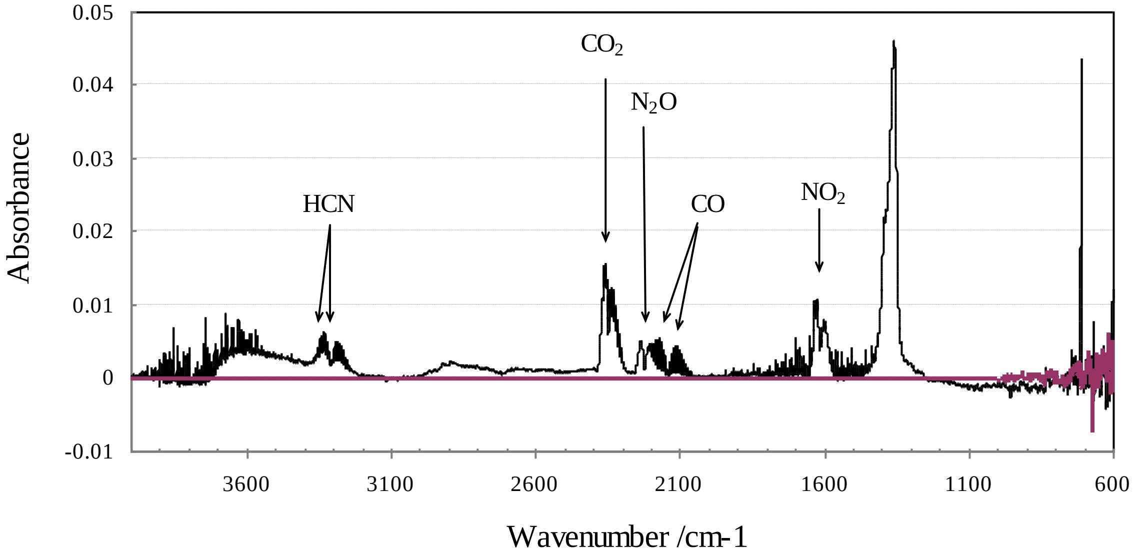

Figure 2.7: Infared Spectra of gas products after 2.7 mg RDX film ablated by 266 nm UV laser at focus distance of 168 mm in air.

specifically, 168.0 mm, 148.0 mm and 128.0 mm, labeled as a, b and c respectively. Curves b and c have been shifted vertically from zero absorbance for presentation purposes only. It is clear that the same gas products are generated at all three focus conditions, but not necessarily in the same relative amounts. The fractions of the ablated carbon and nitrogen contained in each gas product were calculated at eight various laser focus from 65 mm to 170 mm with increment as 15 mm, and the results are shown in table 2.2.

2.4 Discussion

Based on the calibrations described above, the species identified in the infrared spectra account for less than ten percent of the carbon in the ablated RDX spot, depending on laser focus. The small fraction of products that are observed may at first appear problematic, but it is readily explained as a natural consequence of the UV ablation of a molecular solid. In RDX solid, the individual molecules are bound by a combination of Van der Waals and dipole-dipole interactions. Although these interactions are strong enough to hold the solid together, they are an order of magnitude weaker than the covalent bonds which hold the atoms of the individual molecules together. The result is a molecular solid with a low but significant vapor pressure. Because of the large energy mismatch between the UV radiation and the weak non-covalent interactions, little or no molecular dissociation results from UV irradiation. Instead, it is the stronger covalent bonds, with electronic excitations energies closer to the energy of the UV photons, that directly adsorb the light. The initial result of direct UV light adsorption is the formation of a high pressure plasma, which then expands over next to form an ablation plume. [21]

For covalently bound solids, like polycarbonate and glass, the process essentially ends when plume reaches full expansion. However, for a molecular solid, the process of material removal

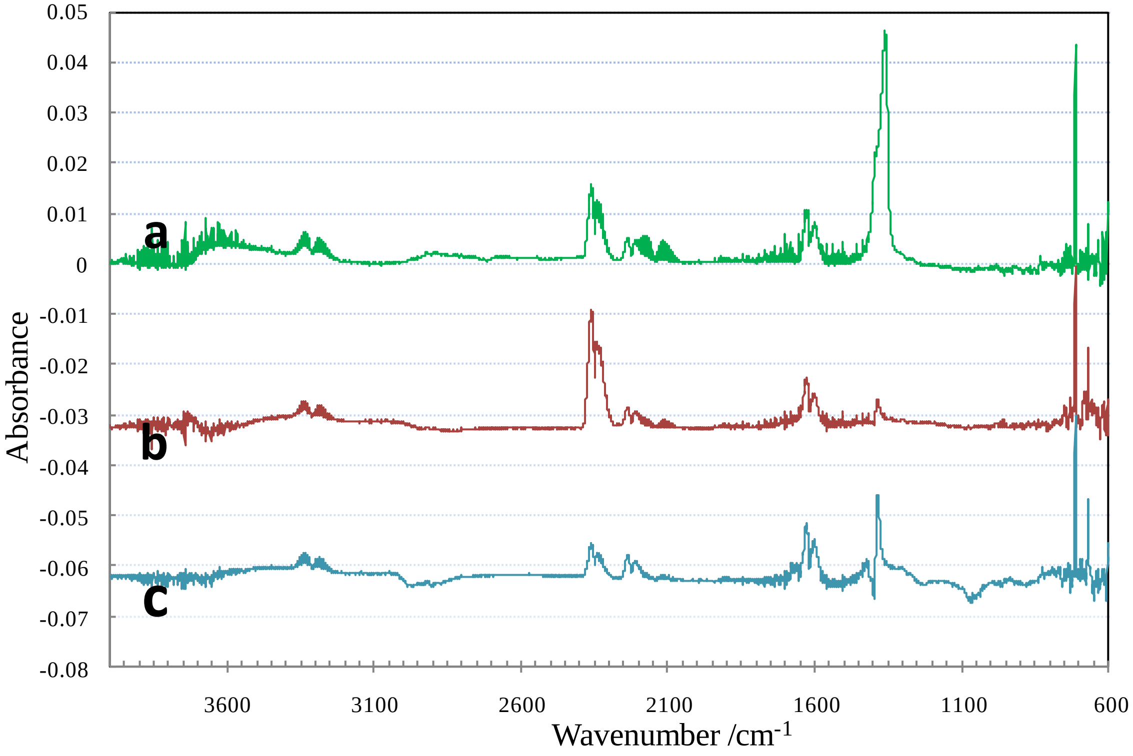

Figure 2.8 : Infared Spectra of gas products after 2.7 mg RDX film ablated by 266nm UV-laser in Air at laser fluences of a)168.0mm; b) 148.0mm; and c) 128.0mm

Table 2.2: Fractions of Carbon and Nitrogen following ablation in air (percent).

Carbon	170mm	155mm	140mm	125mm	110mm	95mm	80mm	65mm
HCN	3.50	4.43	3.21	1.98	1.23	0.59	1.15	0.23
N_2O	0	0	0	0	0	0	0	0
CO	4.80	4.16	1.54	0.53	0.24	0.041	0	0
NO_2	0	0	0	0	0	0	0	0
CO_2	1.06	1.93	1.48	0.57	0.60	0.32	0	0
Sum	9.36	10.52	6.23	3.08	2.07	0.95	1.15	0.23
Nitrogen	170mm	155mm	140mm	125mm	110mm	95mm	80mm	65mm
HCN	5.25	6.64	4.82	2.98	1.84	0.89	1.73	0.35
N_2O	1.11	1.55	1.24	0.90	0.81	0.17	0.04	0.10
CO	0	0	0	0	0	0	0	0
NO_2	2.21	3.01	2.35	1.91	1.35	1.17	1.47	0.46
CO_2	0	0	0	0	0	0	0	0
Sum	8.57	11.20	8.41	5.79	4.00	2.23	3.24	0.91

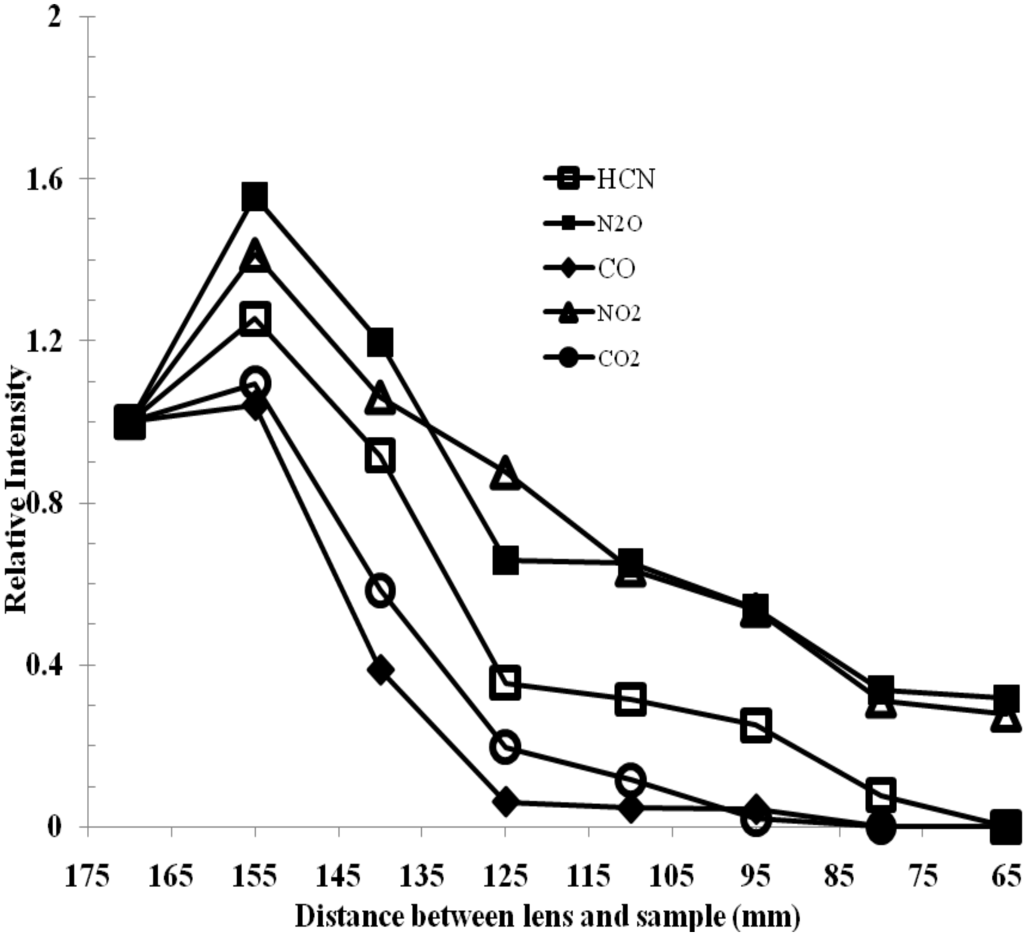

Figure 2.9: The relative intensity of five products in air, HCN, N_2O, CO, NO_2 and CO_2, at various focus

may continue as molecular species are sublimed from the exposed surface as the result of infrared irradiation emanating from the ablation plume. Evidence of this process can be found in the fourth photodeflection signal observed during UV ablation of RDX, that reaches the detector laser ~2 µs after the plume.[22] No such signal is detected when borosilate glass or polycarbonate are exposed to the laser beam. In a similar process, sublimation at the burning surface of RDX has been observed previously with the mass fraction of RDX vapor estimated to be ~ 40%.[23] The presence of large amounts of RDX vapor has been confirmed through observation of RDX deposits on the walls of the cell by comparing the signals of a solution made from dissolving a freshly prepared RDX spots in acetonitrile and a solution prepared by washing the cell with an equal volume of acetonitrile, as showed in figure 2.9. Four characteristic peaks from RDX are showed in this figure: NO_2 asymmetric stretch at 1587-1592 cm^{-1}; N-N asymmetric stretch at 1320 cm^{-1}, NO_2 symmetric stretch at 1267 cm^{-1} and NO_2 deformation peak at 917 cm^{-1}.[24] Since the RDX characteristic strong absorption peak at 1590 cm^{-1} was proved before to be suitable for purpose of quantitative measurement,[25] the peak heights from both solutions were compared and it shows that > 83 % of the RDX originally present in the spot ends up as RDX on the walls. The calculation on two other RDX peaks at 1320 cm^{-1} and 1267 cm^{-1} give similar results, with maximum of 0.6% deviation. It should also be noted that there is no evidence of other non-volatile species in the rinse solution spectra. Sublimation of RDX following UV laser ablation also explains the difference in the depths of the ablation pits formed in RDX and polycarbonate films. Where the ablation pit formed in polycarbonate is 0.6 µm per laser shot, identical laser conditions result pits ~6 µm deep in the case of RDX. If the additional material removed from the RDX is sublimed molecular RDX, which irreversibly deposits on the room temperature cell

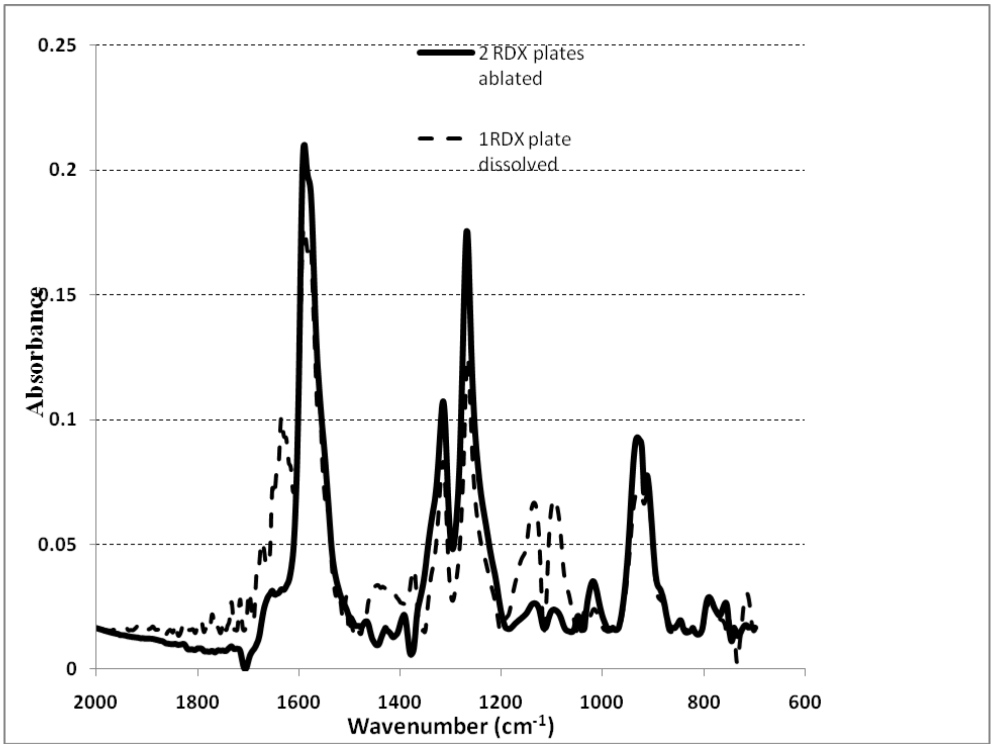

Figure 2.10: The comparion of Infared Spectrum of RDX before and after ablation; samples were prepared in dry acetonitrile. The solid line is from rinsed solution of the cuvett wall after two RDX plates have been ablated, whereas the dashed line is from a solution from an ablated RDX plate dissolved in the acetronitrile.

walls, the average 2-5 % of the carbon found in the gas phase by infrared spectroscopy accounts for a significant fraction of the UV laser generated products.

The relative abundances of the species detected by infrared spectroscopy can shed light on the mechanism of UV ablation. HCN is the reservoir of the largest fraction of carbon and nitrogen from the RDX. CO and CO_2 follow HCN in terms of carbon content and NO_2 and N_2O follow HCN in terms of nitrogen content. Under the higher laser fluence (lens-sample-separation distance at175 mm), the oxygen-poor species, CO is the second largest reservoirs of carbon, while at low laser fluence, the oxygen rich CO_2 becomes the second largest reservoir of carbon. The fraction of N_2O increases as the laser is defocused.

Signals of several species previously observed in the thermal decomposition of RDX are not present in our IR spectra. These include H_2CO, HNO_2, and H_2O. Formaldehyde has a strong doublet between 1650-1850 cm^{-1} and strong broad absorbance peak from 2700-3000 cm^{-1}, which are may be present as weak signals in the spectra, see figure 2.7, although unique identification of such weak peaks would be no more than tentative. HNO_2 has a strong doublet at ~1263 cm^{-1} that does not exist in any of the spectra. Consequently, it can be ruled out as a possible product in these experiments. Water is ubiquitous in the experimental environment, existing in measurable quantities in both the laboratory air and on the surfaces of salt window. It has a broad strong absorptions between 3200-3400 cm^{-1} and from 850-600 cm^{-1}, along with a sharp strong absorbance at ~1800 cm^{-1}. The large noise in background water in the environment obscures the observation of the smaller amounts of water formed in the ablation process, hence, although it may be argued that evidence of the formation of water exists, quantification of the amount is not feasible.

Turning to the mechanistic issue, one must consider the photochemical reactions that initiate the formation of the plume and the reactions of the initial products both in the plume and at its surface. HCN is proposed to be the product of the decomposition of a 1,3,5 triazene which results from the photo induced loss of three HONO species. The N_2O is consistent with thermal decomposition through ring fragmentation,[13] and increases sharply as the irradiated surface area is increased. This may indicate that this product may be consumed in further reactions at high laser fluxes.

As would be expected, the relative partial pressures of the more highly oxidized species, CO_2 increases relative to that of CO at all but the lowest laser fluence, which has the lowest laser power to plume volume ratio and presumably the lowest temperature. In fact, there is a clear and constant fractional shortage of nitrogen content in the gases observed from ablation in air. Though no species other than RDX is observed in the acetonitrile rinse of the walls, the possibility exists that an infrared transparent product, such as $N_{2,}$ could be produced, but without direct evidence, that proposition remains speculation. The carbon and nitrogen fractions found in the products of thermal-like processes, HCN and N_2O, are relatively constant in air as a function of laser fluence. This indicates that they are more dependent on laser power than photon density, implying a possible first order process. At this point, no satisfactory explanation exists for the fluence dependence of ablation in air, although the possible contribution of the oxidation of the plume gases can not be ignored. Further studies will be required to clarify these issues.

2.5. Conclusion

The gas phase products resulting from the UV laser ablation of RDX in air have been identified using infrared spectroscopy. HCN and N_2O are identified as direct photochemical products. The HCN is proposed to originate from the thermal decomposition mechanism beginning with the loss of HONO and proceeding with fragmentation of the triazene ring. The observation of N_2O is consistent with the previously proposed thermal mechanism beginning with ring fragmentation. Infrared examination of an acetonitrile rinse of the lower half of the experimental cell following ablation of a standard RDX spot revealed that >83% of the RDX removed in the ablation process ended up adsorbed to the cell walls, and that no significant quantity of non-volatile products was produced.

2.6 References:

---

1 Parr T.; Hanson-Parr D. *Combust. and Flame* **2001**, *127*, 1895.

2 Garrison B. J.; Postawa Z. *Mass Spectrometry Reviews* **2008**, *27*, 289.

3 Zhigilei L.V; Leveugle, E.; Garrison, B.J.; Yingling, Y.G.; Zeifman, M.I. *Chem. Rev.* **2003**, *103*, 321.

4 Dyachenko, A. Thesis of Auburn University, Auburn, AL USA (**2006**).

5 Capellos, C.; Papagiannakopoulos, O.; Liang, Y. L. *Chem. Phys. Lett.* **1989**, 164, 533.

6 Im, H. S.; Bernstein, E.R. *J. Chem. Phys.* **2000**, 113, 7911

7 Guo, Y. Q.; Greenfield, M.; Bernstein, E. R. *J. Chem. Phys.* **2005**, 122, 244310/1.

8 Greenfield, M. Guo, Y. Q. Bernstein, E. R. *Chem. Phys. Lett*. **2006**, 430, 277.

9 Guo, Y. Q.; Greenfield, M.; Bhattacharya, A.; Bernstein, E. R. *J. Chem. Phys*. **2007**, 127, 154301/1.

10 Dickinson, J. T.; Jensen, L. C.; Doering, D. L.; Yee, R. *J. Appl. Phys*. **1990**, 67, 3641.

11 Melius, C. F. in *Chemistry and Physics of Energetic Materials*; Bulusu, S. N., Ed.; Kluwer Academic Press: London, **1990**, pg. 398.

12 Capellos, C.; Lee, S.; Bulusu S.; Gamss, L.A. in *Advances in Chemical Reaction Dynamics*, Rentzepis, P.M.; Capellos, C. Eds., Springer-Verlag, Berlin **1986**, pg. 398.

13 Zhao, X.; Hintsa E. J.; Lee Y.T. *J. Chem. Phys.* **1988**, *88,* 801.

14 Zeman, S. in *Structure and Bonding*, Mingos, D.M.P., Ed.; Springer-Verlag, Berlin **2007**, pg. 195.

15 Chakraborty, D.; Muller R. P.; Dasgupta S.; Goddard, III, W.A. *J. Phys. Chem. A.* **2000**, *104*, 2261.

---

16 Orland, A. S.; Blumenthal, R. *J. Propul. Power* **2005**, 21, 571.

17 Kagann, R. H. *J. Molec. Spectr.* **1982**, 95, 297.

18 Oyumi, Y.; Brill, T. B. *Combust. and Flame* **1985**, *62*, 213.

19 Maki, A. G.; Phhs, *J. Chem. Ref. Data* **1974**, 3, 221

20 LeFloch, A. *Mol. Phys.* **1991**, 133, 72

21 Bormotova, T. A.; Blumenthal, R. *J. Appl. Phys*. **2009**, 105, 034910.

22 Bormotova, T.A.; Blumenthal, R. *Unpublished Results*.

23 Volkov, E.N.; Patetsky, A.A; Korobeinichev, O.P. *Combustion, Explosion and Shock waves*, **2008**, *44*, 43.

24 Karpowicz, R. J.; Brill, T. B. *J. Phys. Chem.* **1984**, 88, 348

25 Grindlay, J. W. *Anal. Chem.* **1972**, 44, 1676

Chapter 3

Study of Products of 266nm UV-Laser Ablation of RDX in Argon

3.1 Introduction

The role of the surrounding atmosphere on ignition and reaction mechanism of explosives has been investigated in several individualstudies.[1,2,3] The difference in gas products and mole fractions under different environmental gases may provide insight into the mechanism of decomposition of explosives. In a thermal explosion study, it was found that the initial temperature for thermal explosion reactions under air is much lower than that under argon[1]. Brill selected a series of a series of secondary explosives (SE), including RDX, and studied their thermal decomposition in air and in an inert Argon atmosphere.[3] The results showed that both the pyrolysis gas products and their mole fractions are dependent on the surrounding atmosphere. Further analysis showed that this effect gets greater with a SE material which has greater vapor pressure.[3] For example, underboth atmospheres of air and Argon, the mole fraction of RDX products showed a greater difference than the one in HMX which has lower vapor pressure than RDX.The explanation for this correlation with vapor pressure is that for a SE with high vapor pressure, gaseous phase reactions dominate,promoting reaction with the environmental gas. For a SE with low vapor pressure, on the other hand, condensed phase reactions dominate and are independent of the surrounding gas. In essence, the authors, Brill et al, believe that the phase of a SE (solid or gaseous)during ignition is the essential reason for the influence of surrounding atmospheres.

Thermal decomposition of SEs is normally achieved through a Temperature-Jump technique, which includes an induction period, during which thermal energy accumulates, eventually allowing the reaction to take place on a large scale. In an experiment with nanosecond UV lasers, several nanoseconds are not long enough to allow for a phase transition to occur. A laser ablation process induced by nanosecond laser pulsescan be considered to consist of two steps. The first one is the generation of a plasma plume, which normally takes place during the laser pulse, in the range of nanosecond. In the second step the plume expands and cools off. It would be reasonable to assume that there is no, or very little, participation of surrounding gas in the first step since it happens very fast and at the very earliest time, whereas for the second step, a active or inert gas may influence the formation of the final products.

To further probe the reaction mechanism of UV-laser ablation of RDX, the gas products generated under an Ar environmentwere analyzed by Fourier Transform Infrared Spectroscopy (FTIR) and compared with the data obtained in the presence of air.The most notable difference between ablation in air and argon was the almost complete absence of NO in the spectra obtained following ablation under air. The mole fraction of each gaseous product showed a difference from ablation in air and in argon and this may be presumed to result from chemical reactions at the interface between the ablation plume and ambient gas, a region known in gas dynamics as the contact surface.

3.2 Experimental

The main experimental elements, including RDX film preparation, instrumentation and gaseous products quantification, used in this chapter are identical to the description in section 2.2. In the previous investigation, samples were immediately ablated after they were loaded into the cuvette cell, showed in figure 2.4. For experiments described in this chapter, an argon environment was created in the cell before the loaded samples are exposed to laser irradiation.

The argon environment was created by inserting a needle long enough to reach through the glass stopcock on top of the cell to its bottom and flowing argon gas into the cell for 15 minutes. The glass stopcock hole is specifically enlarged so that, after accommodating a needle, there is a space for easy outlet of the circulating gas. The input argon was controlled at relatively low velocity (at 40 psi) in order to maintain around one atmosphere pressure inside the cell. The atmosphere pressure is important for 1)the pressure condition tobe similar than the one in air; 2)eliminating the extra factor of pressure that may influence the concentrations of gas products since literature showed that the RDX decomposition products are highly dependent on Argon's pressure.[4]The NO partial pressure has been calculated in the same way as described in section 2.2.3 by equation 2.2. Band strength was using 133 cm^{-2} atm^{-1} as showed in table 2.1.

3.3 Result and Discussion

The IR absorption spectra obtainedduringlaser ablation experiment of a 2.7 mg RDX in an argon atmosphere under the same laser conditions as in air is showed in figure 3.1. All of the peaks previously assigned to HCN, CO_2, CO, N_2O and NO_2 are observed. The most striking new feature in the spectrum of the gas products generated in argon is that double peak centered at 1874cm^{-1} appears. A similar peak has been previously observed and was assigned as the NO molecule.[5] A rotational constant, B_0, of 5.07 x 10^{10} Hz has been calculated based on the spectrum and supports this assignment.[6,7]

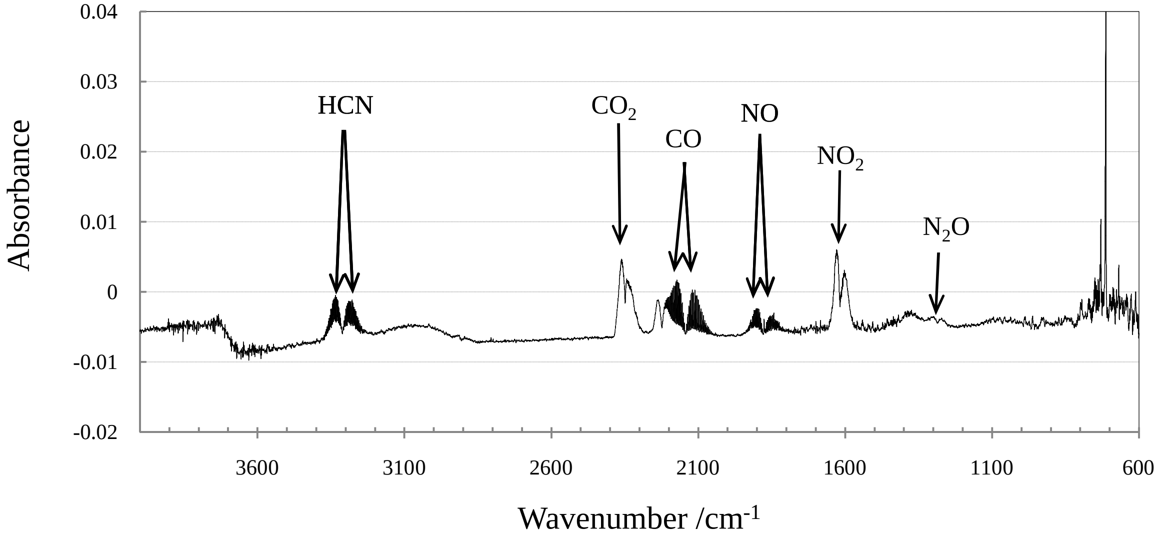

Figure 3.1 -Infared Spectra of gas products after 2.7 mg RDX film was ablated by 266nm UV laser at 168.0mm distance in Argon.

There are several subtle features in this spectrum, which are different than the one obtained from air (fig. 2.7), including a) a double peak centered around 1260 cm^{-1}; b) a small double peak centered around 2880 cm^{-1} and c) less intensity from H_2O band, which appear between 3550cm^{-1} to 4000cm^{-1} and from 1400cm^{-1} to 1800cm^{-1}. The double peak around 1260 cm^{-1} is assigned as the second strongest peak from N_2O,[8] which is easilyobscured by the strong single band around 1350 cm^{-1}, as in the case of figure 2.7. The double peak at around 2880 cm^{-1}has not been identified yet. The little noisy spikes from H_2O which appeared previously in figure 2.7 are greatly induced in this spectrum in argon. This is very helpful in identifying peaks from HONO (1696 cm^{-1})[9] and CH_2O (1744cm^{-1}).[10] Figure 3.1 shows quite clearly that these two possible product species, which are part of the gas products in a thermal pyrolysis of RDX,[8] are not contained in the gaseous products of the current experiment.

Figure 3.2 shows the spectrum of the gas products at three different lens-sample separation distances. It is clear that the same gas species are produced under these three laser fluence, only with different relative abundances. For example, the intensity of CO peak decreases as the sample gets closer to the lens. This same trend has also been observed in the series of spectrum in air, see figure 2.7.

To further examine the dependence of mole fraction of each gas species on the laser fluence, eight lens-sample separation distances from 170 mm to 65 mm with 15mm interval, identical to the air experiments, have been used in the ablation of RDX. Partial pressure of each gas has been calculated by the method described in section 2.2.3 and moles of each gas were deduced by the idea gas equation;

$$n=PV/RT \qquad (3.1)$$

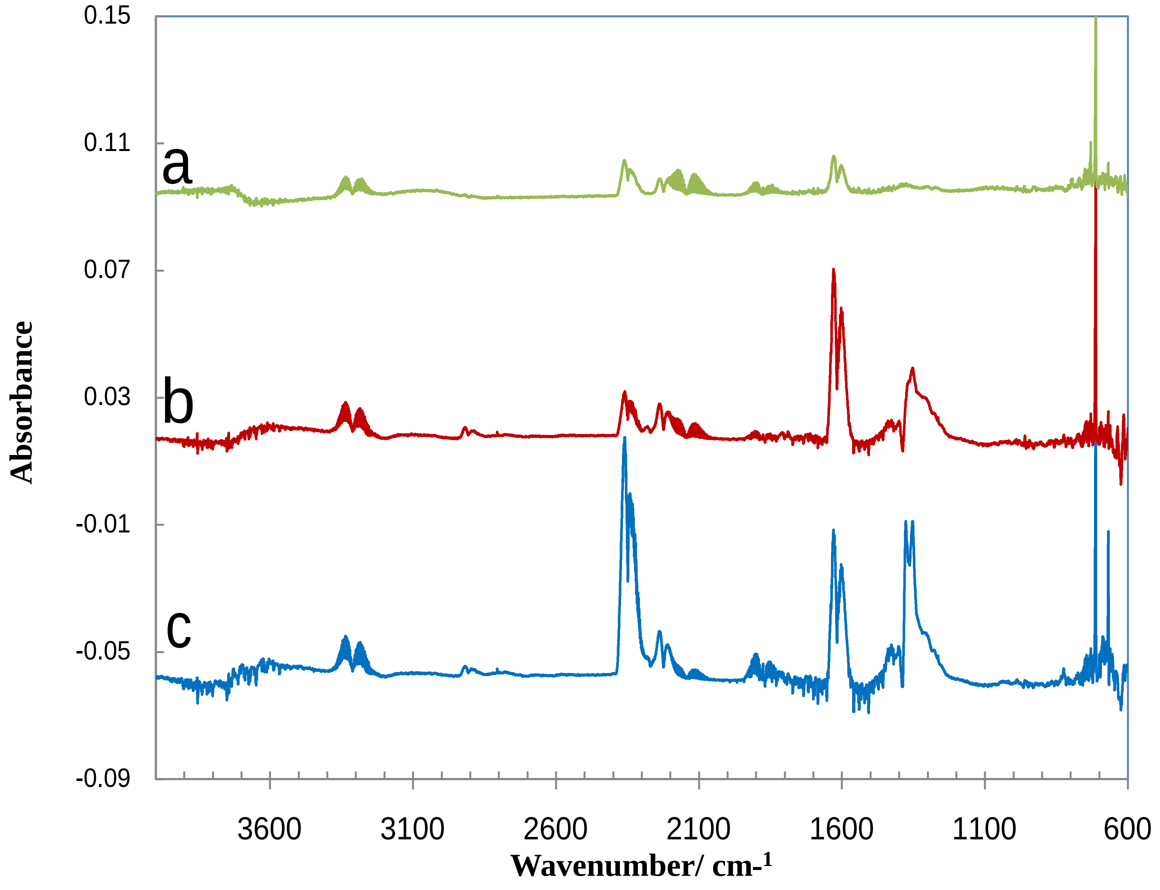

Figure 3.2 : Infared Spectra of gas products after 2.7 mg RDX film ablated by 266nm UV-laser in Argon at laser fluences. of a)168.0mm; b) 148.0mm; and c) 128.0mm

Table 3.1: Fractions of Carbon and Nitrogen following ablation in Argon (percent).

Carbon	170mm	155mm	140mm	125mm	110mm	95mm	80mm	65mm
HCN	6.30	7.26	5.70	3.90	2.78	1.82	1.40	1.69
N_2O	0	0	0	0	0	0	0	0
CO	1.95	1.39	0.68	0.25	0.15	0.10	0.03	0.02
NO	0	0	0	0	0	0	0	0
NO_2	0	0	0	0	0	0	0	0
Sum	6.30	7.26	5.70	3.90	2.78	1.82	1.40	1.69
Nitrogen	170mm	155mm	140mm	125mm	110mm	95mm	80mm	65mm
HCN	3.15	3.63	2.85	1.95	1.39	0.91	0.70	0.84
N_2O	0.72	0.85	0.73	0.58	0.48	0.41	0.36	0.48
CO	0	0	0	0	0	0	0	0
NO	3.56	4.50	3.48	2.92	2.26	1.99	1.85	2.06
NO_2	1.01	0.95	1.22	1.09	1.10	1.12	0.85	1.17
Sum	8.43	9.94	8.28	6.54	5.23	4.42	3.76	4.56

P is the partial pressure calculated, V is the volume of the cell, which is 7.5ml, R is the gas constant, T is the temperature. A room temperature was approximated as the cell temperature, based on the small scale reaction compared to the cell volume and the many minutes between ablation and measurement. The carbon and nitrogen fractions of each gaseous product were calculated and listed in table 3.1. Similar to the results in air, the carbon and nitrogen percent from gas products are less than 10% of the total reactants. A sublimation process, identical to the one suspected in air, is assumed to take place in argon as well.

A relative intensity change of each product over various laser fluences may be observed in figure 3.3. The data has been normalized by the intensity on 170 mm (lens-sample separation distance). A striking feature, compared to the one in air is the NO_2 line, which is more constant over the whole fluence range.The data in air from figure 2.8 is represented here as figure 3.4 for convenience of comparison. This maybe an indication that a direct N-N bond breakage is one of the reacting channels andthe process is a first order photochemical reaction.Capellos et al. also concluded that NO_2 was formed via a one-photon process in a study of 248nm photodecomposition of RDX molecules in gas phase.[11]

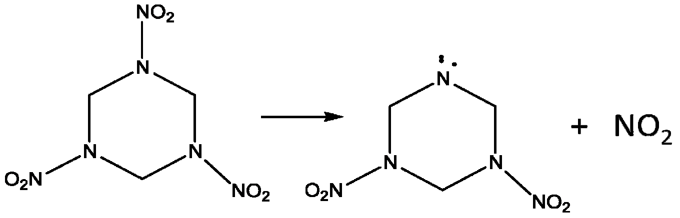

(3. 2)

To understand the dependence of gas species on the laser fluence, the chemical and physical natures of the plume formed during a laser pulse have to be taken into consideration. For a photon pulse of 266 nm and ~ 6 ns, it is reasonable to assume that the plume is formed at a

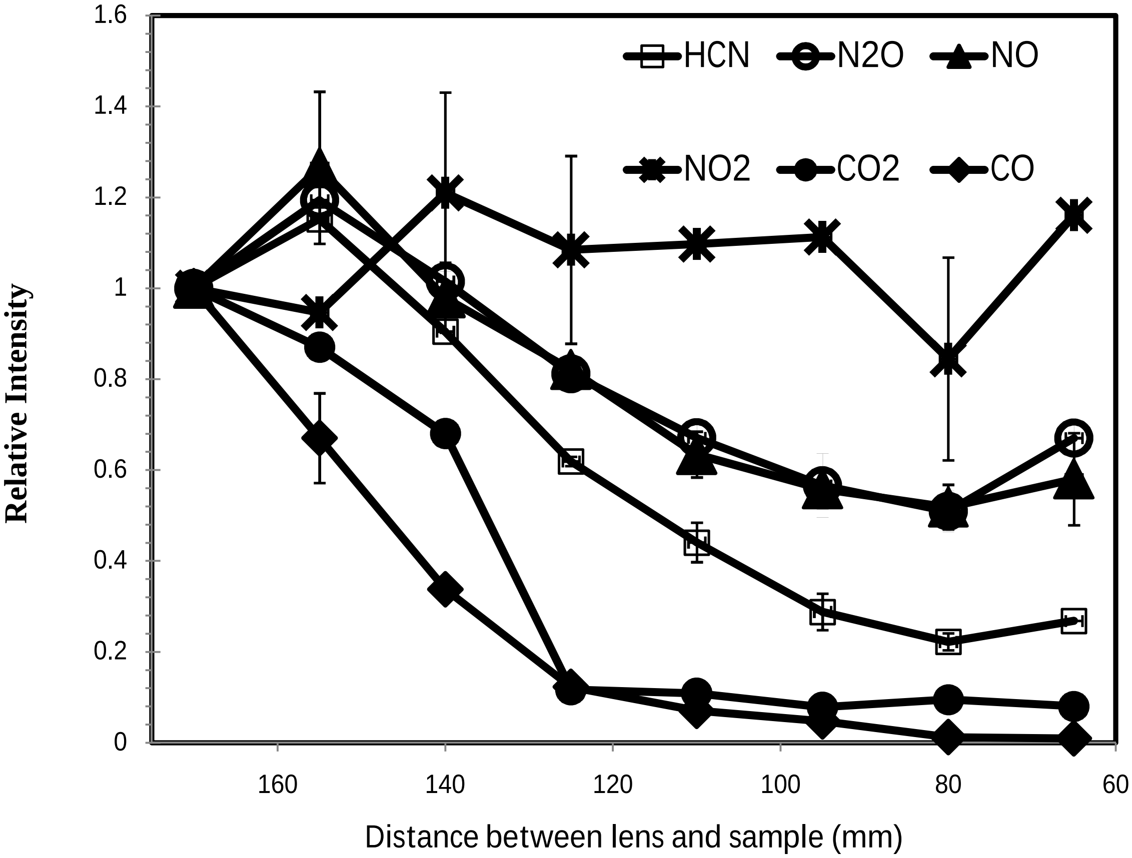

Figure 3.3: The relative intensity of five products: HCN, N_2O, CO, NO_2 and NO from RDX ablation in Argon, at various focal distances. The error bars are calculated from three sets of data and displayed here at some of those points for clarity.

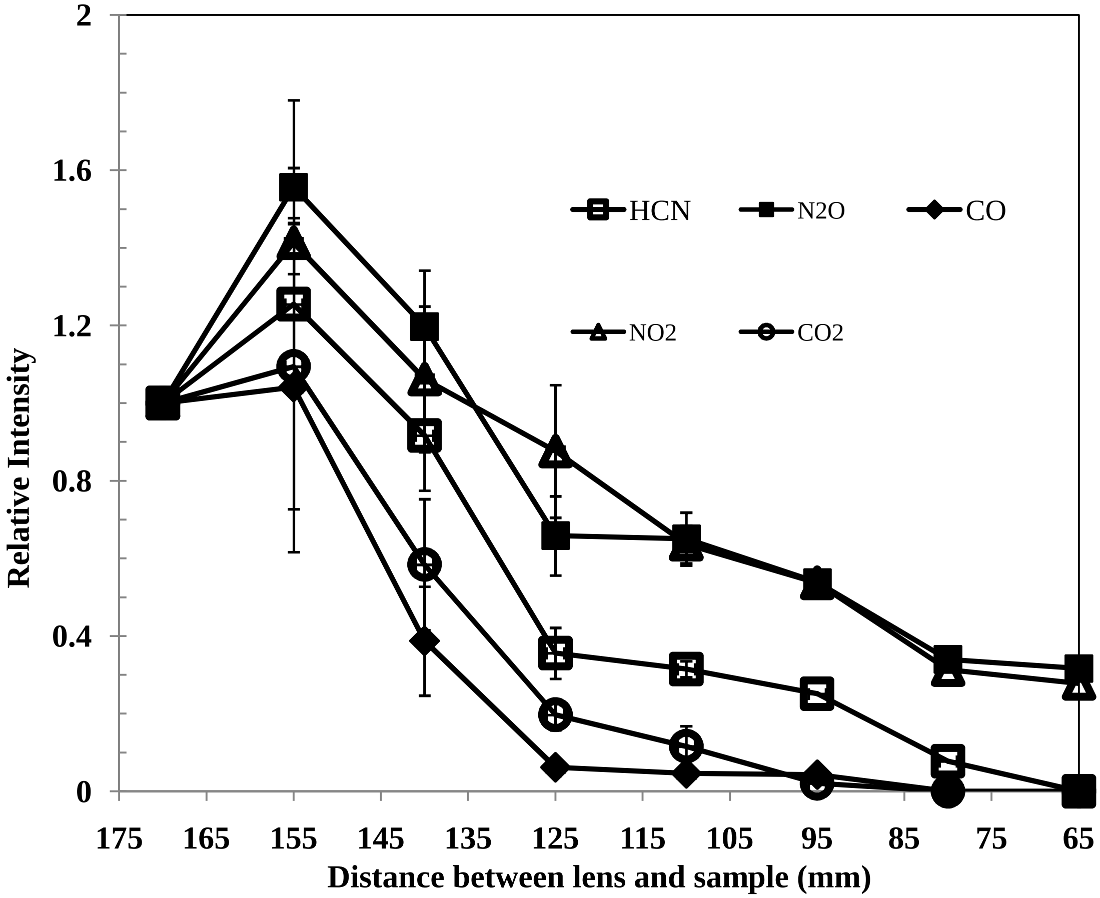

Figure 3.4: The relative intensity of five products: HCN, N_2O, CO, NO_2 and NO from RDX ablation in Air, at various focal distances. The error bars are calculated from three sets of data and displayed here at some of those points for clarity.

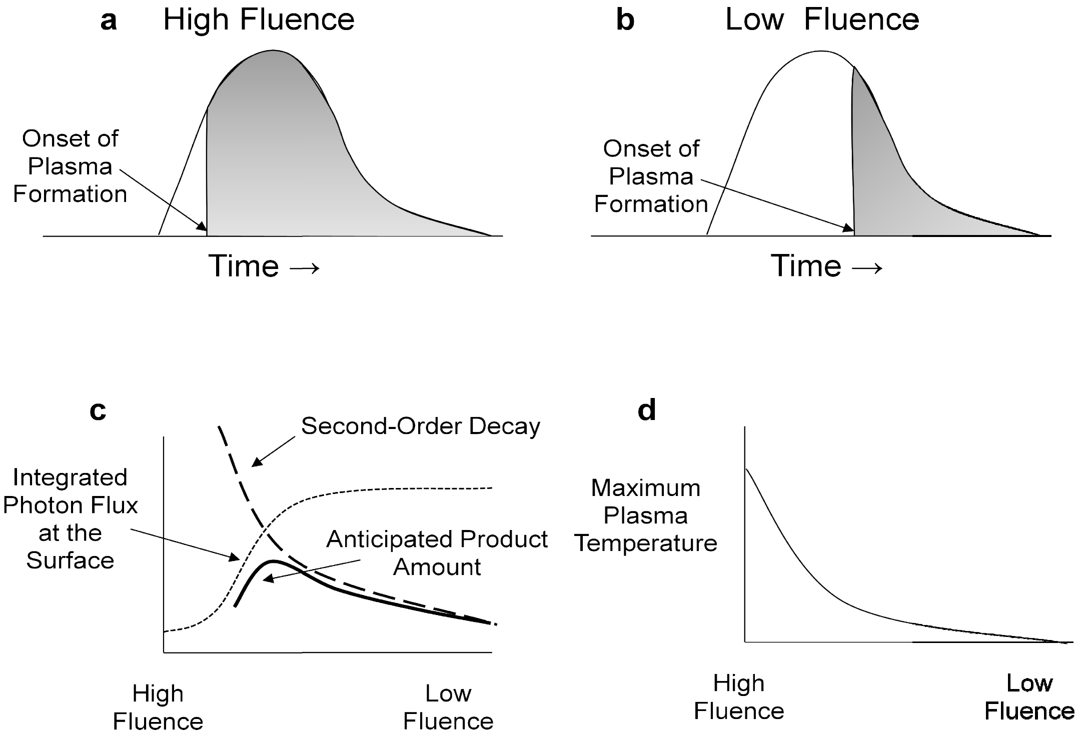

Figure 3.5: Understanding the dependence of gas species amount on laser fluence: a) onset of plasma formation at high laser fluence; and b) onset of plasma formation at low laser fluence; dashed line in c) In second – order process, product amount vs. laser fluence; dotted line in c) Integrated photon flux at the surface vs. fluence; solid line in c) anticipated product amount vs. laser fluence; d) the dependence of maximum plasma temperature on laser fluence.

time onset shorter than the whole life span of a laser pulse. Once the plasma is formed in the early part of a laser pulse, this hot plasma interacts with the remaining photons in two wayssimultaneously: (1) it acts as metal reflecting a fraction of subsequent photons and (2) while absorbing part of the subsequent photons, increasing the temperature of the plasma. The fraction of photons reflected/absorbed is shown as the shadowed areas in (a) and (b).

The time required to form the plasma on sample surface is dependent on the laser fluence, as the formation of plasma will occur sooner at high laser fluence than at low fluence, as shown in figure 3.5 (a) and figure 3.5 (b). This effect of plasma formation on laser fluence is expected to be much more prominent on higher order reaction than on the first order reaction. This can be explained that the number of bonds under photon irradiation are increased as the laser fluence is lower (defocused) simply because of a larger surface area. Therefore in the first order process, the number of photons required to break the number of bonds on an irradiation surface is increased linearly as the fluence is decreased. In the higher order processes, the number of photons required to break the number of bonds on an irradiation surface is increased exponentially as the fluence is decreased. The dotted line in figure 3.5 (c) depicts the photon flux at the sample surface, with lower number of photon flux at high laser fluence and high number at low fluence. A typical second-order kinetics line shape is shown in figure 3.5 (c) as the dashed line, demonstrating the typical dependence of the amount of products on laser fluence for a higher order process. The solid line in figure 3.5 (c) is drawn to show the anticipated product amount vs. laser fluence, determined by both the above-mentioned factors: photon flux at the sample surface and higher order decay. This higher order process is characterized by a maximum at certain fluence.

For a first-order process, the product amount is independent of laser focus or fluence, due to screening by the plasma. The integrated photon flux at the surface will show a trend of lower value at high fluence than at low fluence, as dotted line in figure 3.5 (c), but definitely less prominent than the one in the case of higher order process. The combination of these two determining factors, in the first order process, is expected to yield a relative constant distribution of final products amount over laser fluence.

Another implication provided by the dependence of onset of plasma formation on laser fluence is plasma temperature change over fluence. More remaining photons at high fluence, in figure 3.5 (a) will induce a higher plasma temperature than fewer remaining photons at low fluence, in figure (b). As a result, the maximum plasma temperature will drop from high fluence to low fluence, as shown in figure 3.5 (d). If a product is solely from a thermal process, this product concentration will follow the same trend over laser fluence as the plasma temperature.

The anticipated line shapes of product amount as dependence of laser fluence based on different mechanisms are summarized in figure 3.6. In the case of first order process, as shown in (a), product distribution is anticipated to be lower at higher fluence and rise to a relative constant level over a wide range of lower laser fluence,; In a second-order process, as shown in (b), products amount rises initially at increased laser fluences as screening declines, and then falling as expected for a second-order process, resulting in a maximum peak at certain fluence; finally, a product from just plasma thermal process, as shown in (c), the concentration drops from high fluence to low fluence.

The experimental data of RDX ablation in argon at different fluence, shown in figure 3.3, clearly displays data consistent with each of the these three different characteristic line-shapes: (1) NO, N_2O and HCN have a maximum peak at the second highest laser fluence, resemble the

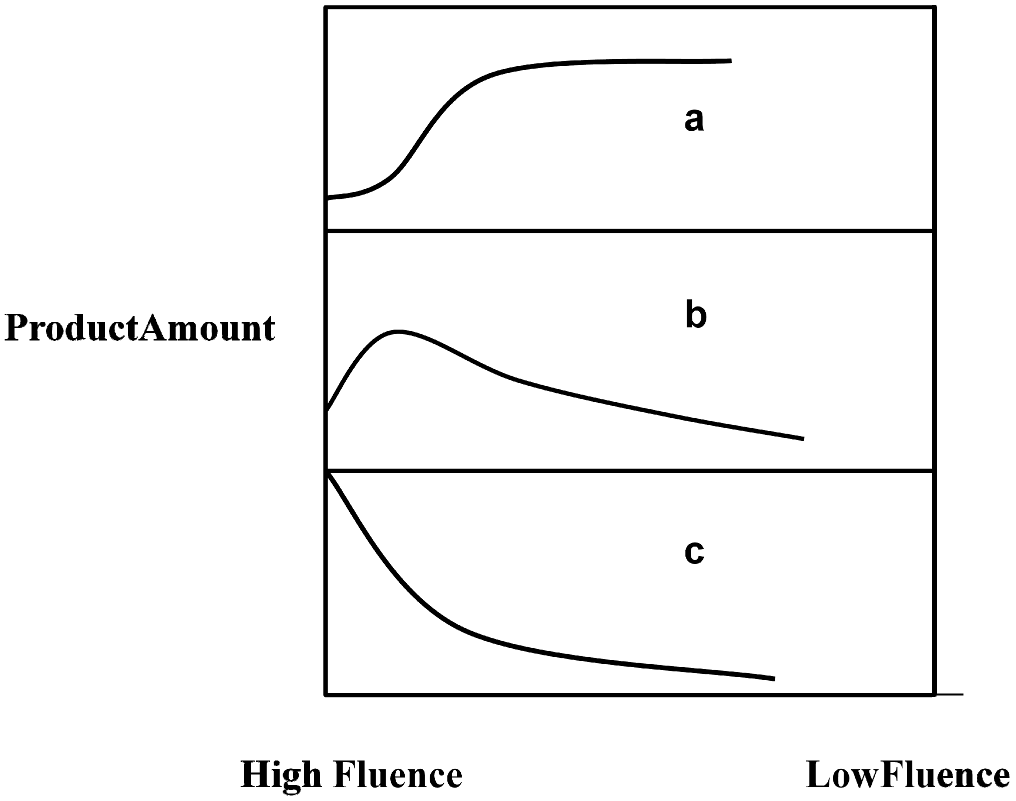

Figure 3.6 Anticipated line shape of products amount over laser fluence based on different mechanisms: a) first order process; b) second order process; c) thermal process of plasma chemistry

l

process; (2) NO_2appears to be from single photon process, since the line shape is relatively constant over a wide range of laser fluence; (3) CO and CO_2, like the line (c) in figure 3.6, follow a drop from high fluence to low fluence, appearing to be products from thermal process.

Comparing this group of data in Argon with the one in Air, figure 3.4, the main difference is that NO_2 amount is not relatively constantly over these fluences in air. This can be from the fact that NO reacts with oxygen in air into NO_2. In another word, the line shape of NO_2 in air environment bears the features of both NO and NO_2 from the original products, therefore, creating a maximum peak as a second order process product. HCN and N_2O line shapes remain similar, indicating the mechanism for the formation of these two products are the same in air as in argon. CO and CO_2also mostlyresemble the thermal process line shape, however there is a higher relative intensity at high fluence, exists at lens-sample separation distance as155 mm. Again, the presence of reactive species, oxygen, in air may result in more CO and CO_2 from the oxidation of HCN, especially at high fluence, since higher temperature is generated at high fluence.

3.4 Conclusions

Products of the 266nm UV-laser ablation of RDX in an Argon environment have been measured as a function of lens-to sample separation distance. All products previously observed in the presence of air, including HCN, NO_2, N_2O, CO, CO_2 are produced in argon experiments as well. A striking new feature in the IR spectrum from Ar is the peak from NO, which has been identified by the peak wavenumber and the rotational constant. Based on the understanding from dependence of plasma formation on laser fluence, three different line shapes of products concentrations have been anticipated for three chemical mechanisms, namely, first order process, second order process and thermal process of plasma chemistry. Comparing experimental data with the predicted line shapes, NO_2 appears to be single photon product, NO, N_2O and HCN appear to be from a multi-photon process, and CO and CO_2 appear to be thermal products in Argon. The presence of reactive species O_2 in air changes the line shape of some species, since the direct product may react with O_2, giving rise to other products. However, the formation of initial products in air seems to follow the same mechanism as in Argon.

3.5 References

---

1 Yang, Ya-Feng; Wang, Hui-Yuan; Wang, Jin-Guo; Zhao, Ru-Yi; Jiang, Qi-Chuan. *J. Alloys and Compounds*, **2009**, 486, 191.

2 Paszula, J.; Trzcinski, W. A. New Trends in Research of Energetic Materials, Proc. 10th, Czech Republic **2007** (Pt.2), 917

3 Hiyoshi, R. I.; Brill, T. B. *Propellants, Explosives, Pyrotechnics,* **2002**, 27, 23

4 Volk, F Ed. Frolov, S. M. Combustion, Detonation, Shock Waves, Proc. Zel'dovich Memorial Conf. Combustion, Moscow, Sept. 12-17, **1994**, 416

5 Alix, J.; Collins, S. *Can. J. Chem.* **1991**, 69, 1535

6 Gallagher, J. J.; Johnson, C. M. *Phys. Rev.***1956**, *103*, 1727.

7 Favero,P.G.; Mirri, A.M. and Gordy,W. *Phys. Rev.***1959**, *114*, 1534.

8 Oyumi, Y.; Brill T. B. *Combustion Flame***1985**, 62, 213

9 Kagann, R. H.; Maki, A. G. *J. Quant. Spectrosc. Radiat. Transfer*.**1983**, 30, 37

10 Nakazawa, T.; Kondo, S.; Saeki, S. J. Chem. Phys.**1982**, 76, 3860

11 Capellos, C. Aapagiannakopoulos, P.; Liang, Y.-L. *Chem. Phys. Lett.***1989**, 164, 533

Chapter 4

Investigations into Laser-Induced-Plasma Initiation of RDX

4.1 Introduction

The main implementation of the plasma-based ignition system is in electrothermal chemical (ETC) guns, where a large capacitor is discharged over plastic materials, generating a high temperature, high pressure plasma that initiate the propellants immediately. With the intent of improving the performance of propellants and gun system, a number of research groups have been studying the physics and chemistry of the plasma-propellant interaction (PPI) process.[1,2,3,4,5] Compared to conventional primary explosive's initiation method, where a sensitive primary explosive (e.g. Lead Azide) reaction is initiated first by a small amount of energy and this reaction further initiates the secondary explosives, plasma initiation has several advantages, such as a short and reproducible delay time and control of the muzzle velocity.[6,7,8] However, the bulky size of the capacitor and power supplies in the ETC gun system greatly limits its practical application.

The interaction of a high-energy pulsed-laser beam with a polymer has experimentally demonstrated to produce a plasma, which resembles the one generated through ETC in many ways.[9,10] The idea of utilizing a laser-induced-plasma (LIP) to initiate propellants promises a reduction of the set-up size from the current ETC guns. Moreover, the highly controllability of laser parameters, such as laser wavelength and power, may offer a precise management of the

ETC gun operation. Finally, an artillery shell requiring a laser system to ignite eliminates the probability of accidental ignitions, improving the safety performance.

The plasma properties are believed to be dependent on the laser wavelength, since different mechanisms are involved in the IR or UV laser radiation. Wang et al. studied plasma formation for several kinds of plastics by a laser ablation at two different wavelength regimes: UV (266 nm) and NIR (1064 nm)[10]. All seven kinds of plastic materials studied in this work showed lower threshold laser energy for plasma formation at 266 nm than at 1064 nm. This is in accordance with the observation by Srinivasan that decreasing wavelength resulted in decreasing threshold laser fluence for polyimide ablation.[11] In both wavelength regimes, UV and IR, the plasma density increases with increasing laser fluence. The electron density in plasma plumes from laser ablation of Si_3N_4 targets shows in the same order of magnitude (10^{25} cm^{-3}) at three wavelength, 1064 nm, 532 nm and 355 nm.[12]

The chemical components of the laser-induced plume have been analyzed in several ways, such as emission spectroscopy[13, 14] and laser-induced fluorescence (LIF).[15,16] Atoms, diatomic molecules, radicals and ions, all likely exist in the plume. As reported by Koren et al. the plume components are dependent on the laser fluence, as shown in the emission of C2, C and CN to predominantly ionic carbon emission as the fluence increases[17]. Small stable gas molecules and small fragments of the polymers have shown to be the final products of UV-ablation of polymers, but these molecules are believed to be generated through recombination of the free radical and ions originally in the plume. For instance, the products of UV laser ablation of poly ethylene terephthalate film have been shown to include toluene and benzaldehyde, which could only be synthesized during cooling of the plasma after initial bond-breaking.[18] Even though there is not much data in term of the plasma density, a high density plasma is expected with a UV-laser ablation of polymer film. One of the reasons is that the quantum yield for bond cleavage upon exposure to UV wavelengths would be relatively high (in the order of 0.1-1.0), depending on the wavelength.[18] Moreover, as suggested by Ortelli etc, the decomposition scheme of polyimide by UV laser (308 nm) irradiation involves more than six free radicals out of one monomer molecule.[19]

The study of the temperature and pressure of laser induced plasma has been carried out both experimentally[20] and theoretically.[21] Simeonsson et al. reported the plasma temperature from laser irradiation on CO and CO_2 gas ranges from 22,000 K to 11,000 K, depending on the delay time from 0.2 μs to 2 μs.[14] This laser induced plasma temperature is nearly identical to the pulsed- plasma temperature measured in the electrothermal capillary source, which shows a temperature between 16,200 K and 23,400 K[22]. Electron densities in the two plasma system are also in the same order of magnitude—10^{17} cm^{-3}. Hence, it is reasonable to expect a laser-induced-plasma to be a miniature replica of the ETC igniter system. The objective of the experiments detailed in this chapter is to perform a preliminary assessment of the possibility and effectiveness of laser-induced-plasma initiation on the propellant, as in this work, RDX, as compared to the ETC system.

4.2 Experimental

4.2.1 Polycarbonate Thin Films

To closely resemble the ETC systems used by U.S. Army Research Laboratories, polyethylene (PE) and polycarbonate (PC) films are studied in this work. A uniform polyethylene film, however, was demonstrated previously to be unattainable with film-making techniques, such as spray and spin-coating technique.[23] Therefore, in this work, polycarbonate films have been prepared and studied as the plasma forming film.

Polycarbonate (PC) films used in this work are of two kinds: (1) commercial films, obtained from McMaster Carr Co (10 mil, 85585K13) and (2) thin films, spin-coated in our lab. The commercial PC films have a thickness of 254 µm and are smooth on both sides. A Laurell WS-400 B spin-coater was used here to prepare polymer thin films. The detail of the spin-coating process has been described previously.[24] In this work, the spin coater was programmed as two-stage operation with: 1) 500 rpm for 5 seconds and 2) 1500 rpm for 45 seconds. The spin-coating solution was made by dissolving commercial polycarbonate film in methylene chloride (UN 1593 Acros). Films of differing thickness were prepared by spin-coating from solutions of various concentrations. The dependence of the film thickness and solution concentration is shown in figure 4.1. The thickness was measured using a profilometer (Tencor Alpha-Step 200). Films of thickness ranging from 0.2 µm to around 4 µm on glass substrates have shown to be smooth, continuous, hydrophobic and pinhole-free. The picture on the left in figure 4.3 shows an example of the spin-coated polycarbonate thin film. The PC film can be peeled-off from the glass substrate easily without changing its appearance. This is important when a free standing film is needed.

A thin polycarbonate film, prepared from spin-coating was measured as a free-standing film on a UV-Vis Spectrometer (Shimadzu UV-3600 UV-Vis near infrared spectrometer). The spectrum, presented in figure 4.2, exhibits a strong absorbance peak at 266 nm, indicates that the polycarbonate is a highly absorbing polymer for 266 nm UV-laser ablation.

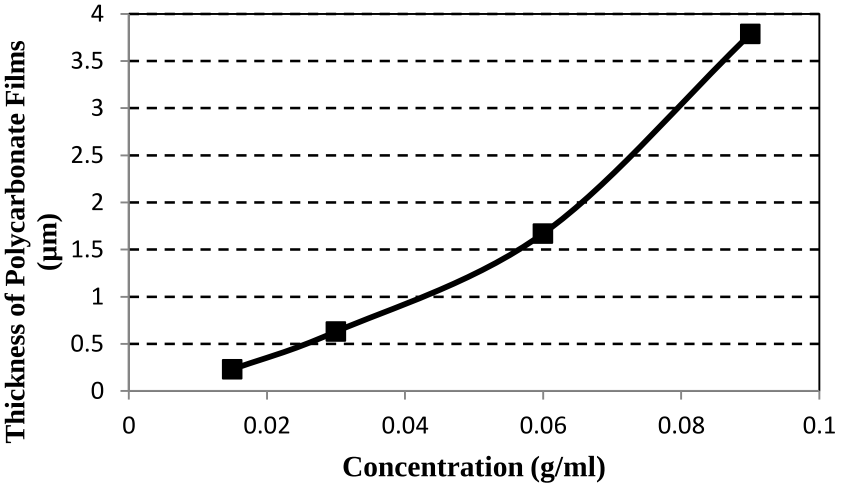

Figure 4.1: Dependence of polycarbonate film thickness on concentration

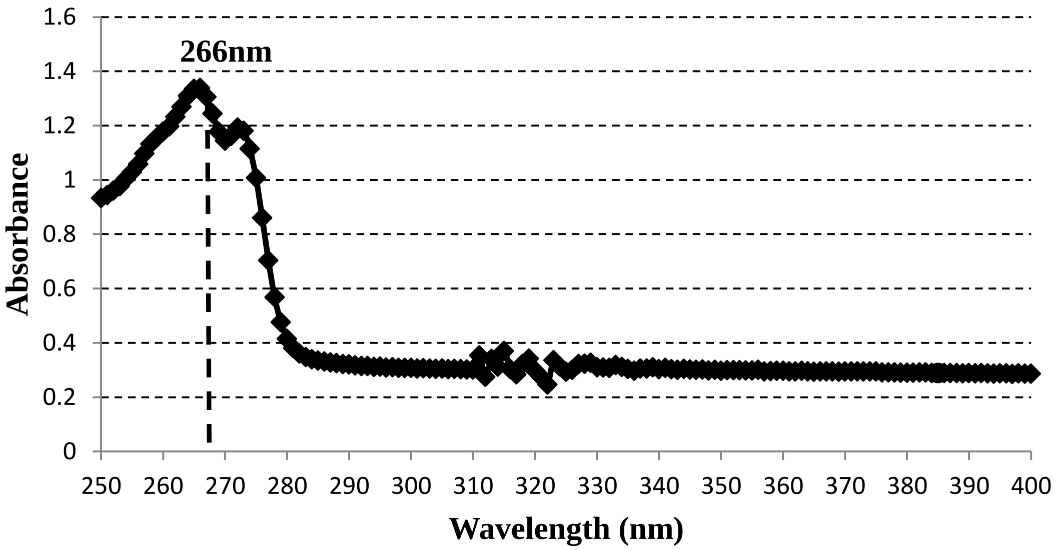

Figure 4.2: UV-Vis Spectrum of a thin PC film, the film (1.7 µm thick) is prepared from polycarbonate solution in methylene chloride with 0.06 g/ml concentration

4.2.2 Polycarbonate Coated RDX film

RDX films were prepared by the same method as described in chapter 2 (2.2.1). It is found that after spin-coating the polycarbonate solution onto a glass slide, where a RDX film had already been deposited, the RDX film appears unchanged. It was also found that the composite film can be peeled off together from the glass slide, as shown in the picture on right in figure 4.3. This feature is of great importance when a freestanding polycarbonate-coated RDX film is needed in the study.

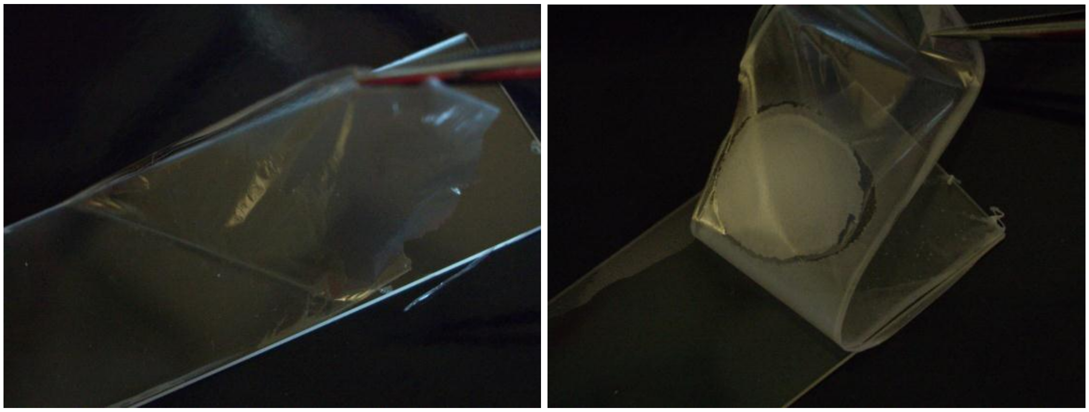

Figure 4.3: A spin-coated polycarbonate thin film peeled off from a glass slide (left), a polycarbonate thin film deposited over an RDX spot and peeled from a glass slide (right)

4.2.3 Instrumentation

A Contimum Inlite Laser (Nd-YAG) was used in the study made in this chapter, with laser parameters as pulse length of 6 ns, wavelength of 266 nm, pulse energy of 50mJ/pulse, a Q-switch delay of 190 μs and 1400V on the flashlamp. Laser fluence at the surface of the polycarbonate film was adjusted by changing the distance between sample and a 200 mm focusing lens.

- Product Pressure Detection Set-up

To detect the pressure of gaseous products generated during laser ablation and laser-induced-plasma initiation, a pressure measurement setup, showed in Figure 4.4, was constructed. A stainless steel chamber with a volume 3.375 cm^3 (calculated from 15 mm diameter) was used as sample and products container. The RDX film or the PC film-covered RDX film had been deposited on glass substrates which then were glued onto the back flange of the chamber. The front of the chamber consists of a quartz window, which allows the UV-laser photons to penetrate. The seal of the chamber was tested by monitoring a pressure level after an extra small amount of gas was introduced.

The chamber is connected to a MKS Baratron pressure gauge which allows detecting any pressure change. The pressure reading as a function of time was collected by Labview 5.1 interface at a rate of 250 points per second. Then a profile of pressure as a function of time will be converted from the one as function of points.

- Witness Board Experiment Set-up

With a sample film deposited on a quartz substrate, at the second when the film is penetrated by laser pulses, the laser light will become visible to register on a board behind the sample, which is termed as witness board. Therefore, by monitoring the light on witness board, one can

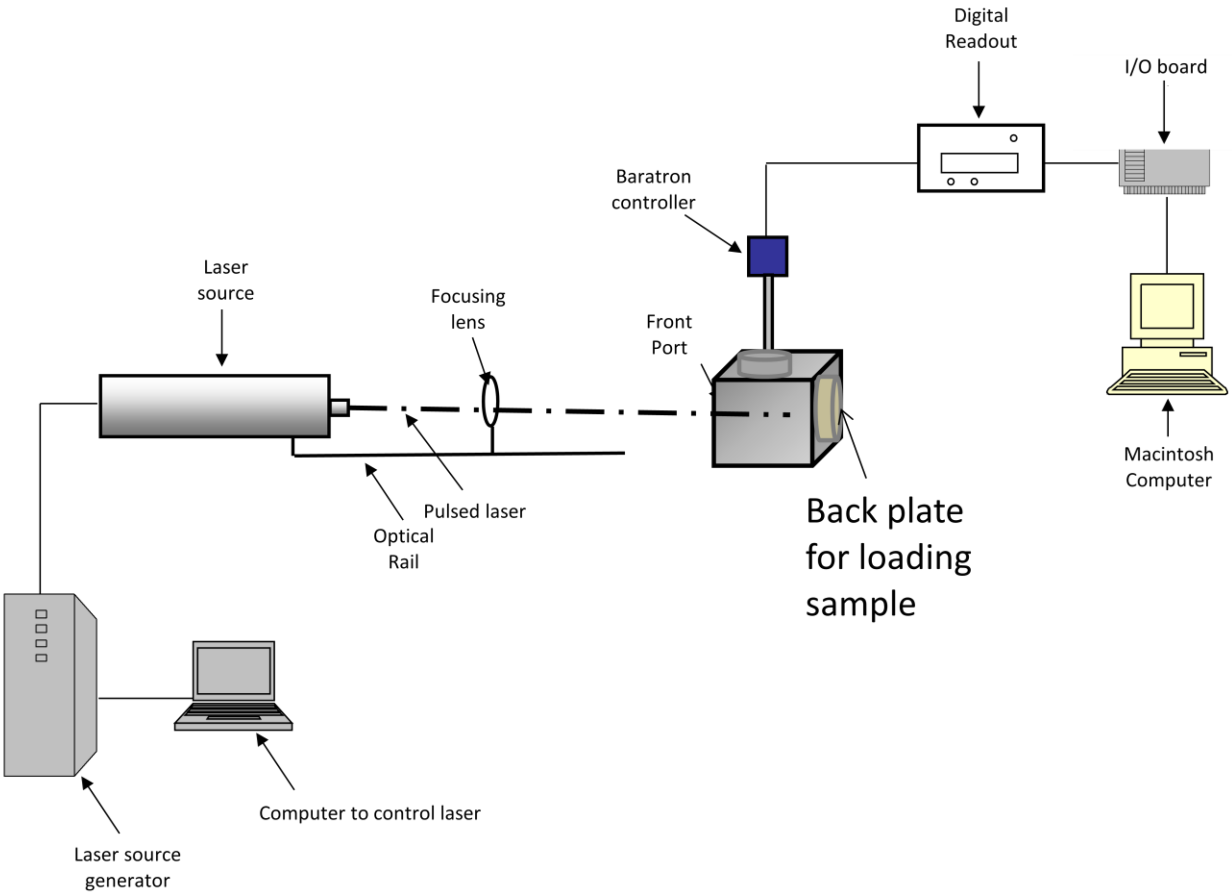

Figure 4. 4 Setup of Pressure Measurement from Laser Ablation Products

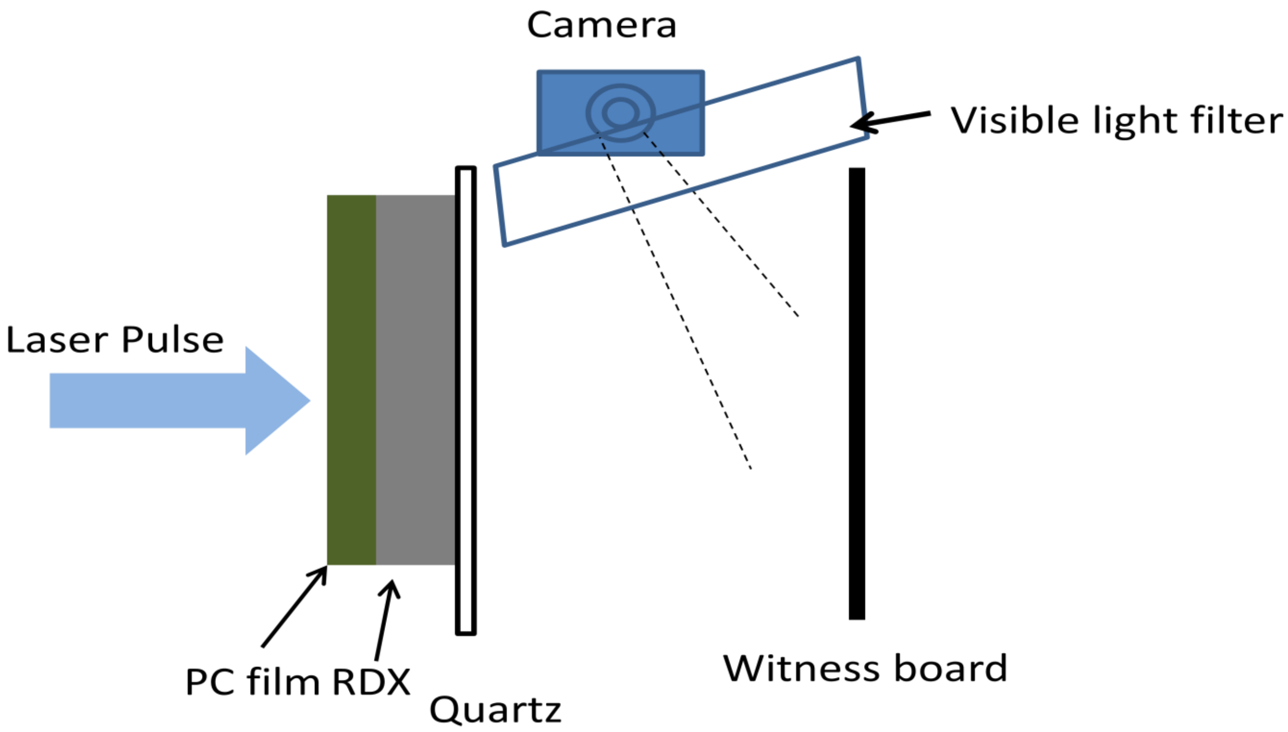

Figure 4.5 An illustration of the experimental set-up in the witness board test of the ignition. A PC/RDX/Quartz sample is used here as an example.

measure the number of pulses necessary to penetrate the sample film. Figure 4.5 shows an illustration of the witness board experimental set-up. A camera with a visible light filter was positioned to monitor the appearance of the UV light on the witness board as soon as the laser pulse penetrates the sample. The lens-sample separation distance is 157.3mm. The reason to choose this low fluence is that more data points will be recorded.

- Dynamic Pressure Measurement set-up

Figure 4.6 shows the dynamic pressure measurement set-up. The miniature dynamic pressure sensor used in this experiment is model 113 B37 (PCB PIEZOTRONICS. INC), which is specifically designed for shock and blast wave measurement. The maximum pressure detection limit is 68 atm. The resonant frequency is approximately as 400 kHz and the rise time is less than 1.5 μs. The output was amplified with a sensor signal conditioner 482A22 and then, a digital oscilloscope (Tektronix TDS 1001 B 40 MHz) was used to record the output signal.

If a static pressure is measured, which means the discharge time constants are sufficiently long, the output signal in voltage can be directly converted to pressure using the calibration curve provided by the manufacturer. For dynamic pressure measurement, it is not that straightforward since a pressure discharge may induce a resonance oscillation from the gauge. A dynamic pressure signal must be deconvoluted from the oscillation.

4.2.4 Photograph Processing

In the reflected light and witness board experiments, a continuous video of laser ablation was recorded by a digital Camera (Pentax optio s5i). The video is collected at 15 frames per second. Laser frequency was purposefully set at 1Hz, 3Hz, 5Hz or 15 Hz in the ablation event, so that when laser and video recording start at the same time, a picture frame with laser light will be recorded at a regular interval and the rest of the frames will be dark. For example, the laser

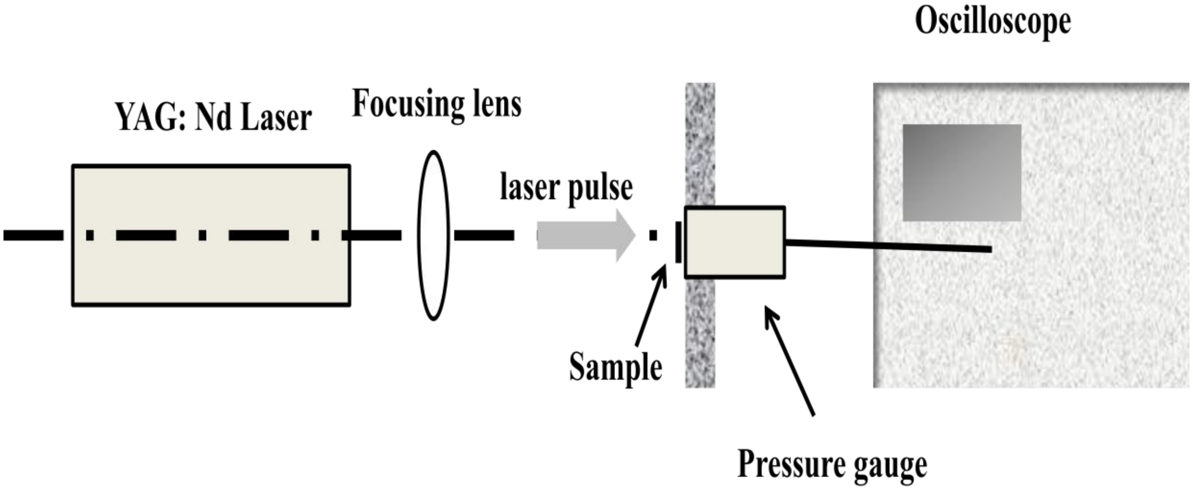

Figure 4.6 Schematic of dynamic pressure measurement set up. The size of all objects in this figure is not in real scale ratio.

frequency was set as 1 Hz frequency in both experiments. Therefore frames showing laser light appearance will be observed in every 15 frames. Fade-To-black AVI Video Editor was used to split the frames in a video. The splitting of red, green, blue (RGB) and the pixel number of each color were processed with ImageJ software.

4.3 Results and Discussions

4.3.1 Primary Calibration of Laser Ablation of a PC Film

It is found that polycarbonate film can be ablated readily over a wide range of laser fluence, adjusted by changing the distance between a focusing lens and the sample. Figure 4.7 shows a picture of the ablation pits on polycarbonate at various lens-sample separation distance ranging from 190 mm (focused) to 100 mm (unfocused). The discoloration observed around the holes, especially the holes obtained at 160 and 150 mm, is soot from the fireball created by the ablation event that can be wiped from the surface with organic solvents, such as methanol. The soot was not shown around the ablation pits from unfocused distances, such as 120 mm to 100 mm. As one would expect, no luminous plume was observed during the ablation at these distances. At very low laser fluence, the laser irradiation may only result in heating of the film. The threshold laser fluence was clearly demonstrated in this group of pictures, as ablation at 100 mm separation distance showed an undistinguishable ablation phenomenon, but little deformation on the film surface.

The size of the ablation pits and the number of laser pulses necessary to penetrate the commercial polycarbonate film (thickness 254 μm) were determined as a function of lens-and-sample separation distance. To improve accuracy in measurement, the soot around ablation pits was washed off with methanol before measurement. Figure 4.8 and figure 4.9 are plots of above two relationships. Clearly, as laser pulse becomes more focused, the size of the ablation pits decreases and it takes fewer laser pulses to break through the film. It is important to note that under more focused conditions, the ablation pits resemble closer an oval shape (190-160 mm), whereas a round circle becomes the characteristic shape when focus is less (e.g.140, 150 mm). This inconsistency may be attributed to the quality of the focusing lens or the laser pulse profile.

Dividing the thickness of the film by the number of pulses taken to penetrate the film, one can obtain an ablation depth per pulse. Having the energy per pulse (50 mJ) divided by the area of the ablation pit, laser fluence was obtained at each lens-sample-separation distance. Figure 4.10 shows a plot of ablation depth per pulses versus laser fluence in logarithmic scale. The satisfying linearity proved Lamber-Beer law governed this process, according to:

$$h = \begin{cases} 0, & if\ F < F_{th} \\ \frac{1}{\alpha} log\left[\frac{F}{F_{th}}\right], & if\ F \geq F_{th} \end{cases} \tag{4.1}$$

here h is the ablation depth per pulse, α is absorption coefficient, F is the laser fluence, and F_{th} is the threshold fluence. An absorption coefficient was calculated to be 2.40 μm^{-1} and Ln(F_{th}) = 6.29. This implies that the threshold fluence is further below than 120 mm separation distance, consistent with the previous result from the ablation picture. Noticed that the data point on the far left side failed to follow the Beer Law, this is possibly due to the heating contribution at this low laser fluence, as discussed previously.

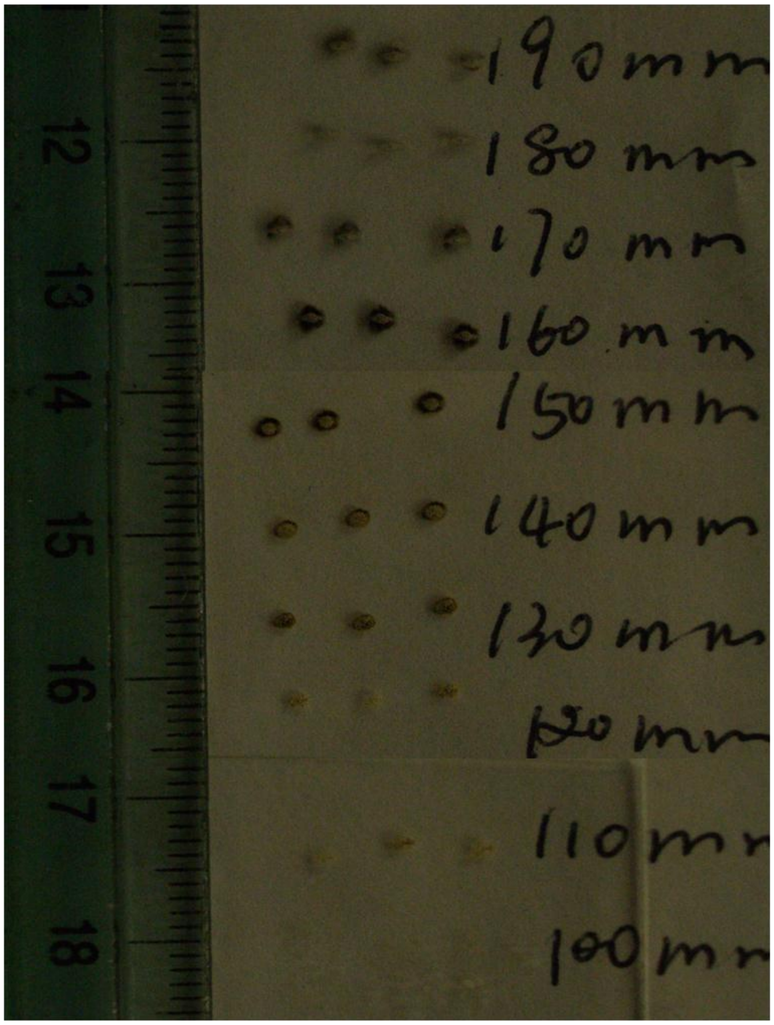

Figure 4.7: Photograph of 266nm laser ablation pits on polycarbonate, the holes on each rows are from the ablation done at different distance from the lens, ranging 190 mm to 100 mm with 10 mm increment from top to bottom. The three pits in each row, which are done at the same distance, are example of the reproducibility of the ablation. Laser frequency: 10 Hz; Laser flash lamp 1400 V.

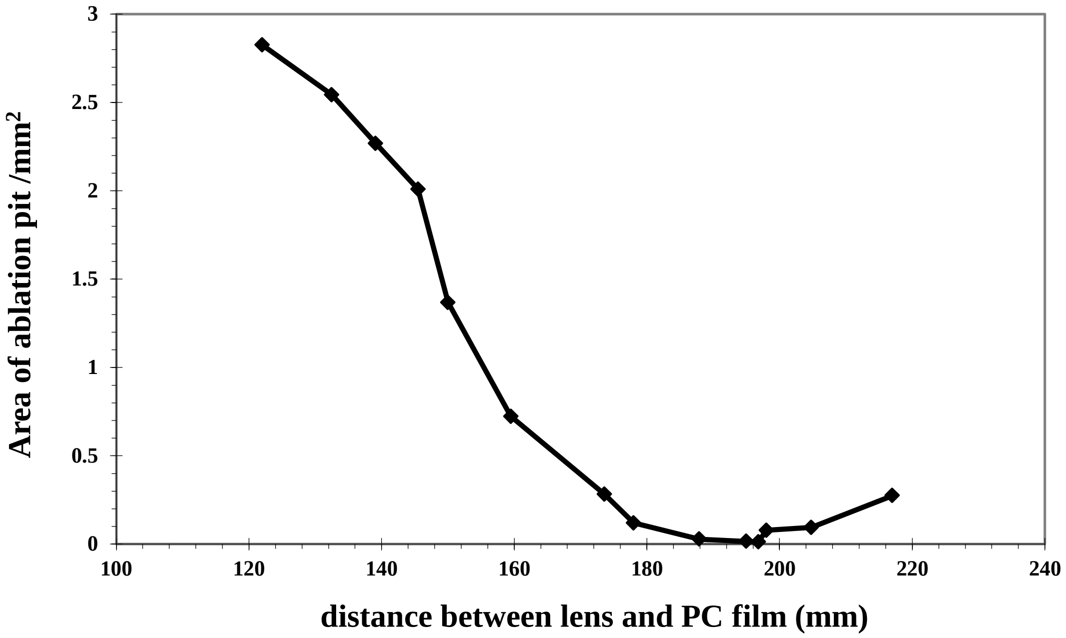

Figure 4.8: The dependence of ablation area on distance between focusing lens and the PC film; laser frequency 10 Hz, Laser flash lamp 1300V

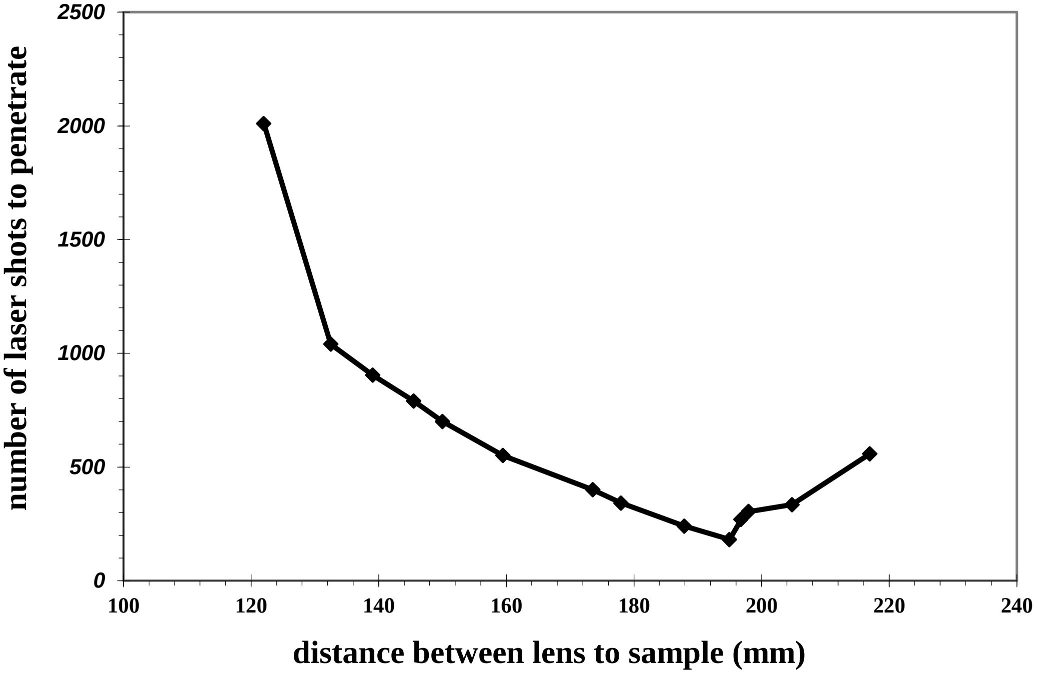

Figure 4.9: Dependence of number of laser pulses required to penetrate the film on the distance between focusing lens and the PC film; Laser frequency 10 Hz, Laser flash lamp 1300 V

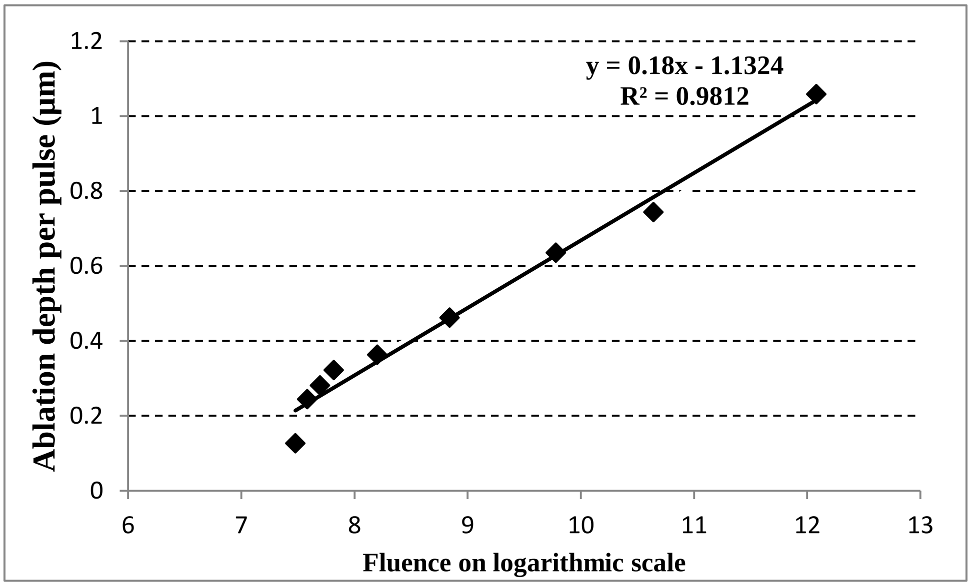

Figure 4.10: Ablation depth per pulse as a function of laser fluence (on logarithmic scale). The data points are taken at lens-sample-separation distance from 120 mm to 190 mm; Laser fluence was in unit of mJ/cm^2

4.3.2 Laser-induced-plasma initiation on RDX

The study of laser-induced-plasma has been approached from several angles: a) products pressure detection; b) observation of reflected light; c) dynamic pressure measurement and d) witness board experiment. Result from each of the following methods will be discussed in the following.

- Products pressure detection

In a sealed small chamber (see figure 4.4 for experimental set-up), upon irradiation of each laser shot, a pressure change from the generated gas products in laser ablation is expected to be detected by a pressure gauge detector. Previous measurements that was done by Dyachenko[23] in a different apparatus showed several interesting results: 1) no detectable pressure rise when a PC film of 27 micron thick was ablated by 40 laser pulses; 2) Three small pressure steps (each pressure ≈0.4 mmHg) were measured with a RDX film ablated with three laser pulses (0.2Hz) and 3) One big pressure jump (1.2 mmHg) was observed when the PC-covered-RDX film was ablated at the 40th laser pulse, shown in figure 4.11. The combustion of polycarbonate takes oxygen in the reactant side and one main product H_2O may condense before pressure gauge can respond (responding time in scale of microsecond). The combination of these two factors may result in a net zero pressure change with polycarbonate ablation. The net pressure yield from gas products may also depend on the predominance of equation 1 over 2 or vice versa.

$$C_{16}H_{14}O_3(s) + 18O_2(g) \rightarrow 16CO_2(g) + 7\ H_2O\ (l) \qquad (1)$$

$$C_{16}H_{14}O_3(s) + 10O_2(g) \rightarrow 16CO(g) + 7\ H_2O\ (l) \qquad (2)$$

The coexistence of these two equations also may result in no pressure change. In fact, both CO and CO_2 were observed in IR spectra of gas products of 266nm laser ablation on commercial PC film[25].

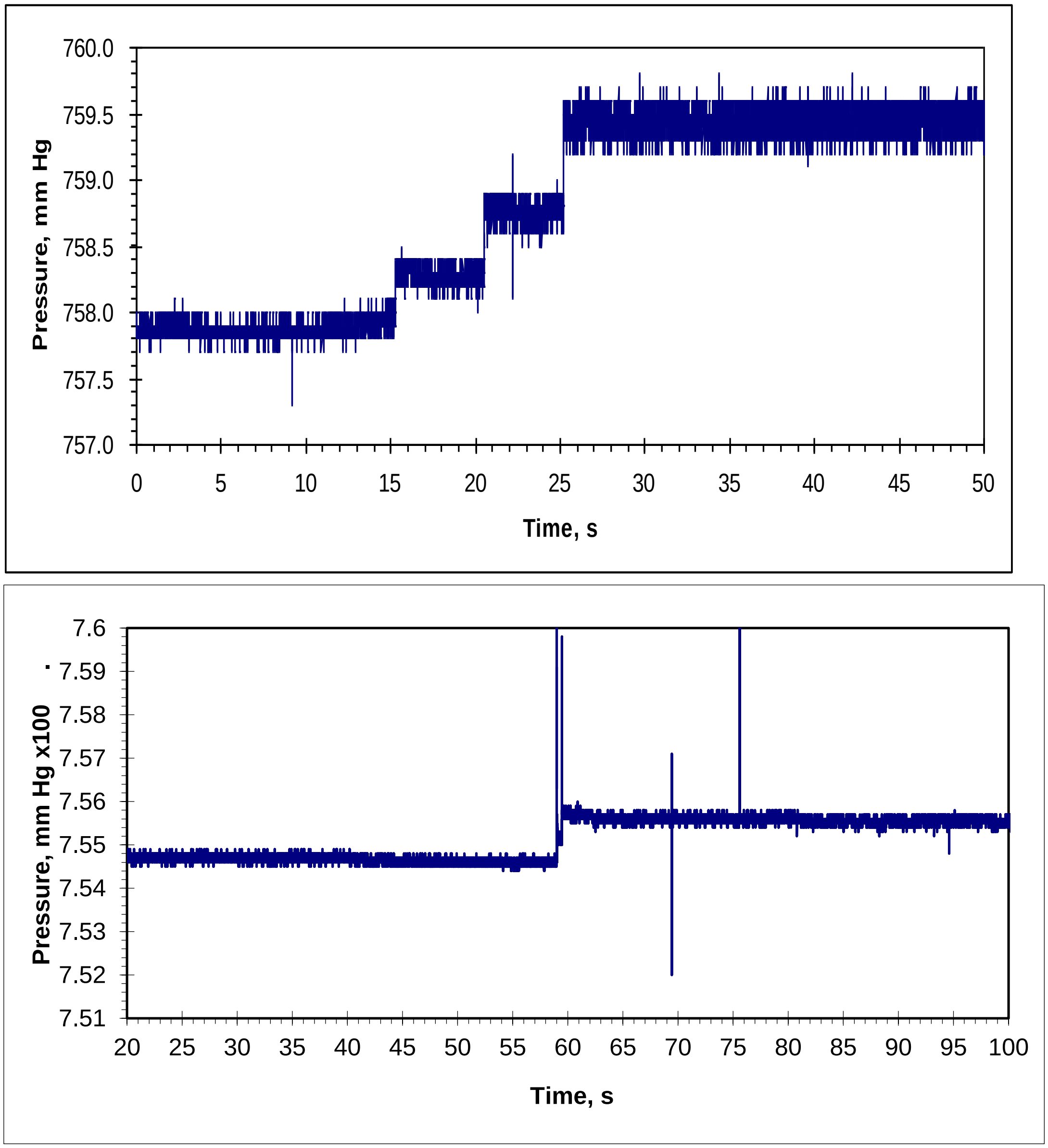

Figure 4.11 Pressure detection of gas products of laser ablation of RDX film (top) and PC/RDX film(bottom) from reference 23

The result on RDX film is understandable since RDX's reaction does not require oxygen and the gas products from each pulse will register a positive pressure change. The measurement with sample PC/film showed a big pressure jump (1.2 mmHg) finished in one single laser pulse (the 40th pulse).This was a very encouraging result since it may indicate that the RDX film was initiated by the plasma from last layer of PC film (after 39 pulses) and the whole RDX film was completed decomposed in one shot.

Encouraged by this group of results, the products pressure detection was revisited. Figure 4.12 showed the measurement of commercial PC film exposed to laser for 100 second at 185 mm focused distance at which approximate120 seconds is the penetration time. Noticed there was a small pressure jump at initial two or three laser pulses and a pressure fell back when the laser stopped irradiation. If this initial pressure rise is from the gas products of PC ablation, the pressure did not continue the rising with the rest of the laser pulses, but kept a relative plateau until the laser stopped. To ensure that no pressure change when laser irradiates light on the empty vessel through the quartz window, a background measurement was conducted and the result is shown in figure 4.13. There was no observable pressure change as laser started and ended showed in this figure. Therefore, the pressure response in figure 4.12 should be a phenomenon from laser ablation on polycarbonate rather than from air. The gas products generated may absorb onto the steel surface inside of the vessel immediately. A measurement was done with laser ablation on RDX sample, as showed in figure 4.14. The RDX film is about 26 μm and was ablated at lens-sample-separation distance 155mm with about 7 pulses. Clearly, the figure did not reveal any pressure change in this event. This is different than the result in figure 4.11. This has been repeated and showed the same result. More measurements were done under more focused distance. Figure 4.15 is one of the results from multiple experiments.

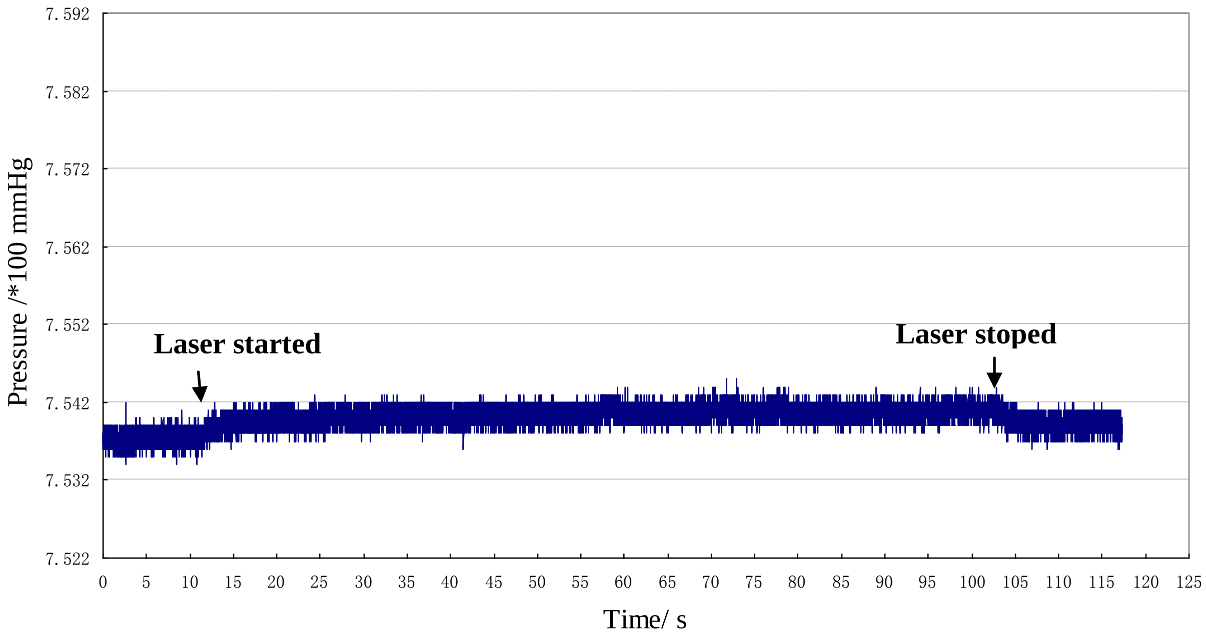

Figuer 4.12 Ablation products pressure measurement of commercial PC film, laser started at 12s and stoped at 103s. Laser works at 10 Hz at maximum fluence.

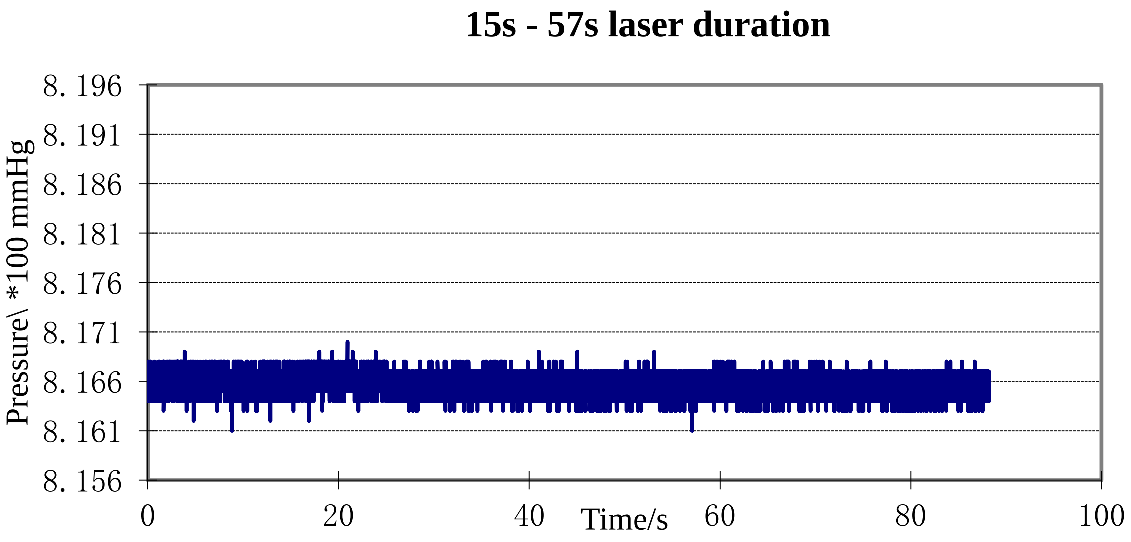

Figure 4.13 Background detection: the empty chamber was exposed to the laser irradiation. Laser started at 15th second and ended at 57th second. Laser works at 10 Hz at maximum fluence

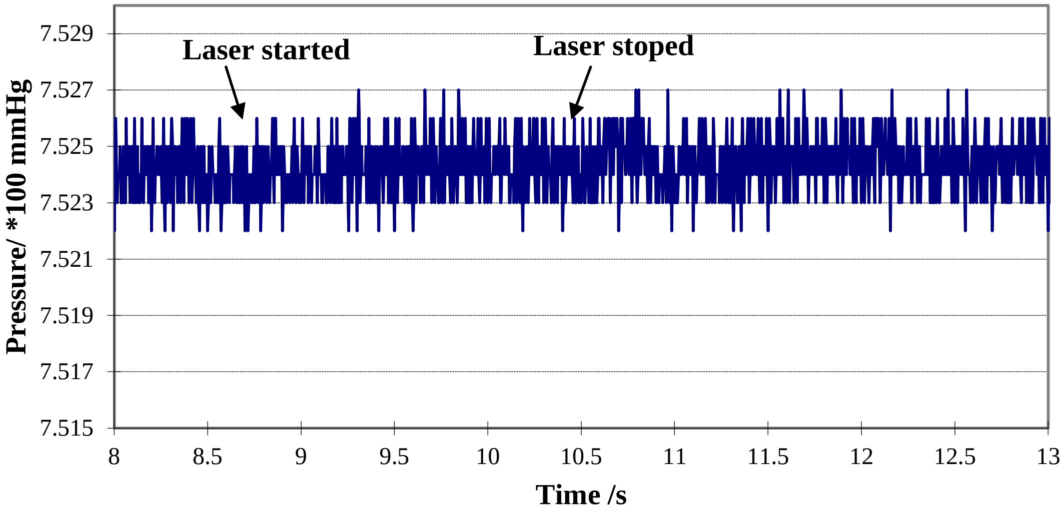

Figure 4. 14 Product pressure measurement of RDX film (26 µm thick) Laser working frequency 0.5Hz, lens and sample separation distance 155mm.

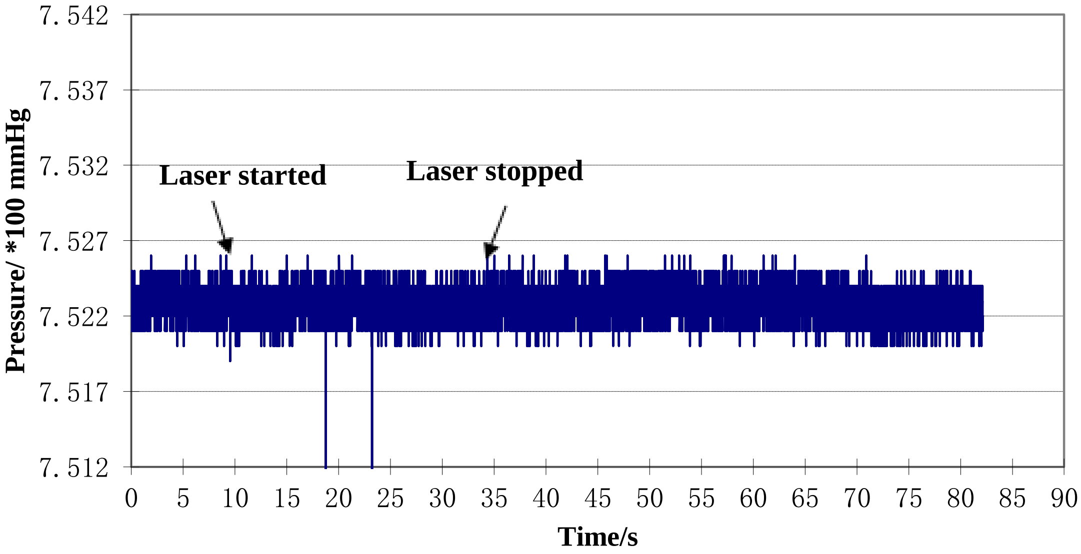

Figure 4.15 Product pressure measurement of RDX film (26 µm thick) at focused distance. Laser working frequency 0.5Hz, lens and sample separation distance 175mm. Laser started and stopped at 11s and 34 respectively.

It can be concluded that no pressure jump was observed from laser ablation on RDX, which is very different than the measurement done previsously. One of the sources creating this difference may be the different vessels used in these two experiments. Not only will the volume of the vessel affect pressure but also the inside surface material. A further investigation may need to be carried out in a smaller vessel and efforts of eliminate gas adsorption onto the walls may be needed as well.

- Reflected light observations

Two groups of samples were exposed to laser light and the reflected light from the sample surface in these two events was recorded in video mode. The pictures of the reflecting light at the first five laser pulses on RDX/glass slide sample and PC/RDX/glass slide are shown in the top and bottom row of figure 4.16 respectively. On both rows, the glass slide is the big green color area, which is from the reflection of the laser light. The small bright dot in the green background is where the laser beam irradiated on the samples. It is clear that on top row of pictures, the bright ablation area is growing through the first and second picture, reaching a final shape on the third picture. This indicates that three laser pulses completed the ablation of the RDX film of 26 μm thick. This correlates well with the pressure results, in figure 4.11, of Dyachenko. Compared to this group, the bottom row pictures showed that there is only one laser pulse taken to finish this process, as the completion of the final shape of the reflecting light from the ablation hole is reached in the second picture. It is important to note that all subsequent frames followed in both videos did not show further change. This result showed good reproducibility. The difference here may be accounted for by the laser-induced-plasma from thin polycarbonate film initiated the RDX ignition.

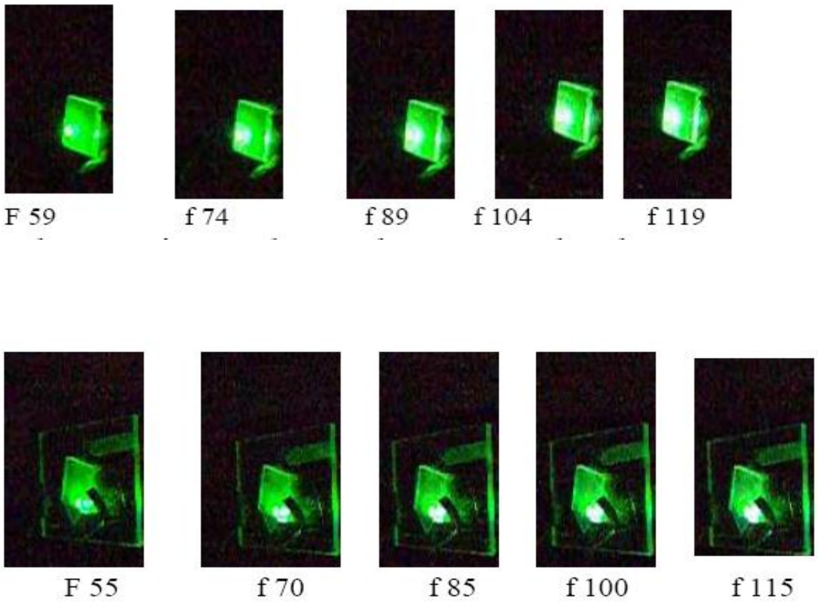

Figure 4.16 Comparison of the photos of reflected light from propellant sample, top rows are from RDX film on glass slide, the bottom row are from PC/RDX/glass slide sample. The f-number denote to the frame number in the video, video recorded at 15 frames per second. The first picture here is the first frame after the laser started. Laser parameters, 1Hz, 50mJ/pulse, 1400V. Lens-sample separation Distance 168mm

- Witness Board Experiment

Figure 4.17 shows a typical result of the light on witness board experiment on two samples: PC/Quartz and PC/RDX/Quartz. The pixel number of the blue color obtained over the frames, described in experimental section, was plotted against the number of laser pulses. With just PC film on Quartz, a flat region in the first 18 laser pulses showed the light intensity is very low, which indicates that the laser did not reach the significant ablation phase in these pulses. The fact that the light intensity in this region is not zero may come from the incomplete filtering of the visible light. After the 18 pulses, the light intensity showed a sharp increase in the next 4 pulses, where laser ablation penetrated the PC film. Finally, a maximum intensity was reached. In comparison, the data in the PC/RDX/Quartz group showed very different features. First, the light intensity starts growing since very early laser pulses and there no longer exists a flat dark region in the beginning pulses. Second, this group of data reaches the maximum intensity sooner than the group from PC/Quartz. It seems a puzzle that with a thick RDX film (26 μm) in the middle of sandwich structure, the laser takes even fewer pulses to penetrate the whole structure.

A laser-induced-plasma from polycarbonate film is expected to impinge on the RDX film on the back and initiate an ignition of the explosive films. A question may be raised as why the light intensity grows gradually to the maximum since an ignition event occurs powerfully enough to remove the whole depth[23]. To explain this, one might have to take into consideration the very roughness of RDX film surface, which is measured by profilometer. When the PC solution was spin-coated onto this surface, an overall structure as showed in figure 4.18 is very likely formed. A relative much smoother PC film surface is expected. Figure 4.18 illustrates the part of sample irradiated by several laser pulses in the wetness board experiment. In this laser fluence, the laser

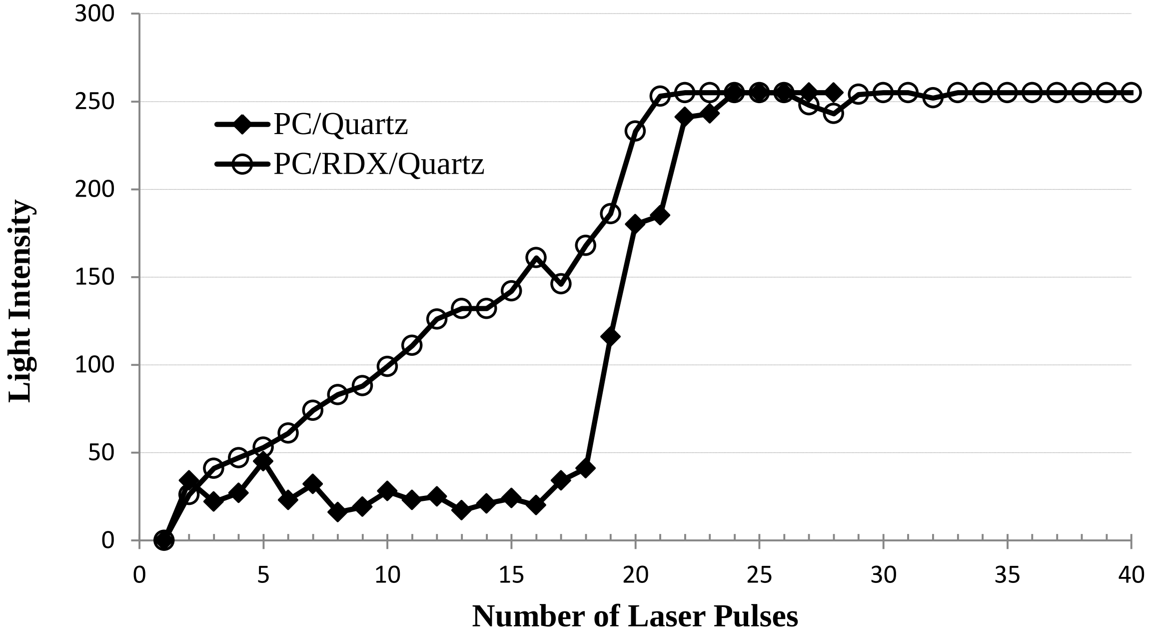

Figure 4.17 The monitor on the light on the witness board on back of two samples: PC film/quartz and PC/RDX/quartz. Laser Ablation Parameters: 1Hz, 1400V, lens-sample separation distance 157.3mm

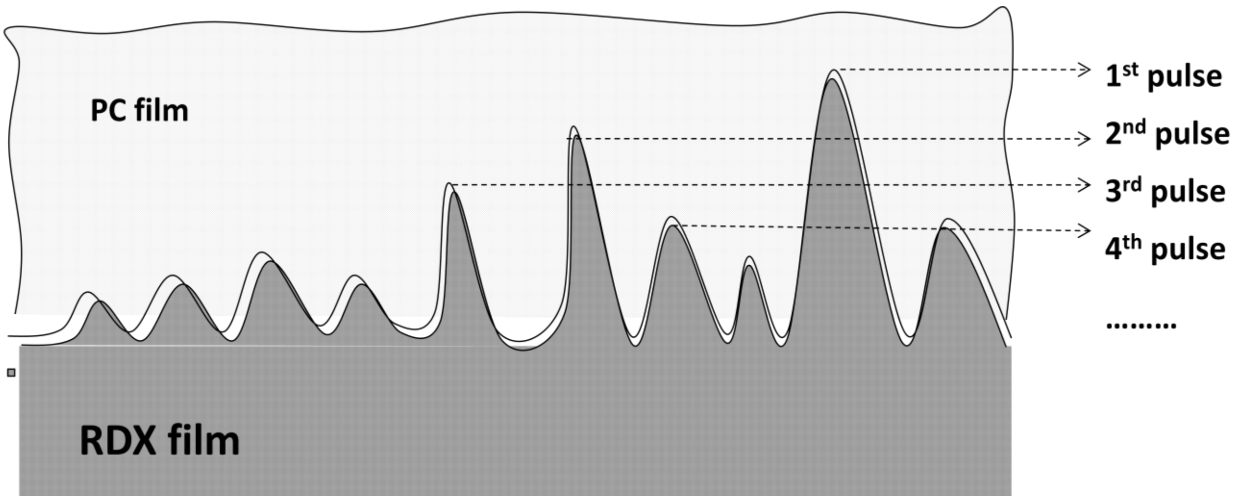

Figure 4.18 A schematic of a PC-covered-RDX film sample in laser ablation. The image represent the small spot on the sample, which is irradiated by laser light. The thickness of the PC film (on the top) and RDX film (on the bottom) are not in ratio to the real structure, which typically has PC film for 1.7 µm and RDX film for 26 µm. The surface roughness of the RDX film is illustrated as the peaks. The first pulse refers to the ablation depth of first laser pulse, which reaches the highest peak on RDX film surface. In the same manner, successive laser pulses reach lower peaks.

pulse only ablate about 1/18 of the PC film which is 1.7 µm. But due to the roughness of the RDX film surface, the PC film layer on top of the highest point of RDX surface is much less than 1.7 µm and is ablated completely in one laser pulse. Therefore, the part of RDX underneath is successively initiated by this local plasma, resulting in a positive light intensity on the witness board. The second pulse may continue to reach the second highest point on the boundary and more RDX will be initiated, resulting in increased light intensity on the witness board. Every successive incoming laser pulse created more penetrated area. Therefore, light intensity on witness board (line with circles in figure 4.17) continues to increase with laser pulses until reaching a maximum.

Comparing this group of data with the result from the reflected light experiment, the difference is that no gradual light increase was seen with reflected light on PC/RDX sample (see figure 4.16). Instead, the progress of the light growing was finished in one laser pulse. This may seem puzzling before understanding the different conditions of these two experiments. The reflected light experiment was done in a much more focused distance than the witness board experiment. At this distance, the laser fluence will be greater, producing greater penetration depth on PC film, 1.7 µm/pulse in this case. Therefore, the PC film inside the laser beam can be ablated with one laser pulse and the resulted plasma initiate the RDX film underneath.

To further investigate this process, a witness board experiment with pure RDX film needs to be done. In addition, it will be helpful to carry out this experiment under different fluences and resulting of light intensity vs. laser pulses at all fluences can be compared. It is expected that the profile of PC/Quartz will rise at earlier pulses and the PC/RDX/Quartz will reach maximum sooner at more focused distance.

- **Dynamic pressure measurement**

In laser ablation, a shock wave is formed as the laser light is absorbed and then it expands outward from the point of laser ablation. As the shock wave expands, the surface of the pressure gauge will be more covered by shock wave and less by ambient air. The measure pressure should change as the factor $s_{coveredSW}$, the shock wave covered area, changes until shock wave cover all pressure gauge and dominated by the following equation:

$$P_{measured} = P_{ambient} \left[1 - \frac{s_{coveredSW}}{S_{PG}}\right] + \frac{\int_{S_{coveredSW}}^{S_{PG}} P_{sw}\, dS_{coveredSW}}{S_{PG}}$$

The dynamic pressure of the shock wave in laser ablation of PC/RDX/PC sandwich structure film is presented in figure 4.19 with the first laser pulse on top and successive laser pulses displayed below. A common feature of all profiles is that the first peak starts within 0.5μs and and a peak pressure reaches at least 1atm, an oscillation appears next, which was explained in section 4.2.3.This indicates that irradiation of every laser pulse produced a shock wave and its pressure is changing rapidly. For the sample structure of PC/RDX/PC, the first two measurements are believed to correspond to the ablation of mere top PC layer of the structure. It is noticed that the first peak in the middle profile is significantly higher, above 9 atm. It is reasonable to suspect that the big pressure rise may be from RDX. However, at this point, it may be tentative to say that a laser-initiated-plasma initiation on RDX has occurred, even though it is very likely. A comparative experiment is considered to be done over just RDX on pressure gauge and observe the pressure signal from simple laser ablation on RDX.

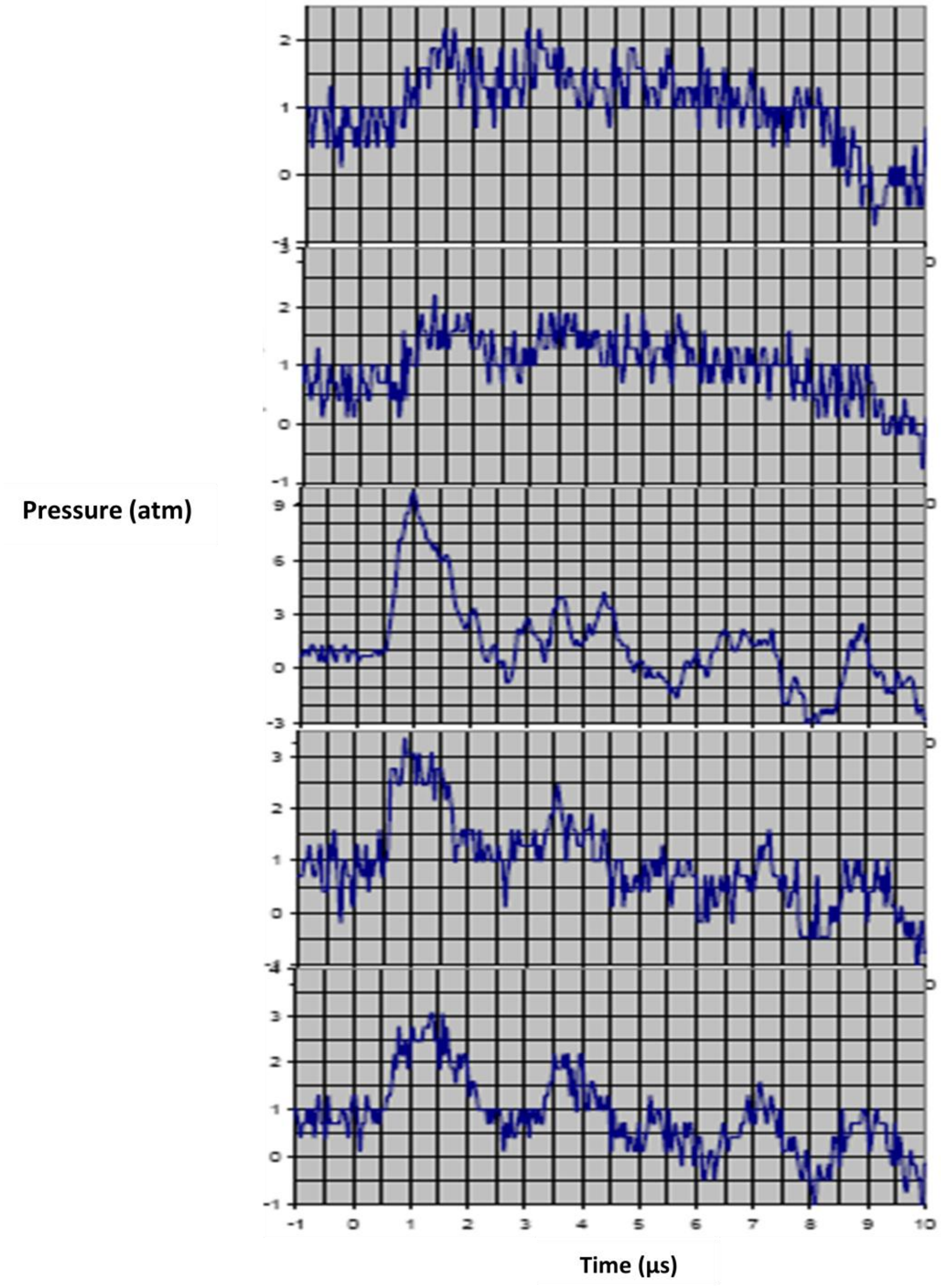

Figure 4. 19 The dynamic pressure measurement of a sample polycarbonate/RDX/polycarbonate in sandwich structure. From top to bottom, the profiles are pressure measurement after first, second, third, fourth and fifth laser pulse respectively. PC film thickness 1.7 µm, RDX film 26µm.

4.4 Conclusion

Preliminary investigations of laser-induced-plasma initiation on RDX were carried out using a variety of experimental techniques and presented in this chapter. A thin polycarbonate (PC) film has been successfully prepared from its solution in methylene chloride using spin-coating technique. The thickness of the thin PC film can be controlled by preparing the solution in different concentrations. Thin PC film was used as the plasma generating source. A sample of PC film spin-coated on top of RDX has been exposed to laser pulse irradiation. The laser-induced plasma initiation has been probed through several approaches, namely, gas products pressure detection, observation of reflected light, witness board experiment and dynamic pressure measurement. All have demonstrated the same evidence of initiation of RDX film by the induced plasma, except the product pressure measurement in the bigger chamber showed different result than the previous result done in smaller apparatus. The inside surface of the apparatus may also play a role since the generated gas product may adsorb onto the surface, changing the pressure result.

4.5 References

---

1 Fifer, R. A., Sagan, S. E., Beyer, R. A. *IEEE Trans Mag.* **2003**, 39, 218

2 Taylor, M. J. *Propellants, Explosives, Pyrotechnics* **2003**, 28, 26

3 Valliere, R.; Blumenthal, R. *J. Appl. Phys.* **2006**, 100, 084904-1

4 Kappen, K., Beyer, R. *Propellants, Explosives, Pyrotechnics* **2003**, 28, 32

5 Del Güercio, M. A. Electrothermal-Chemical (ETC) Closed Chamber Study of Plasma Capillary Materials; ARL-TR-2268;

6 Chaboki, S.; Zelenak, B. Isle. *IEEE Trans. Mag.* **1997**, 33, 284-288

7 Porwitzky, A. J.; Keidar, M.; Boyd, I. D. *IEEE Trans. Mag.* **2009**, 45, 412-416

8 Dyvik, J.; Juleigh, H; Appleton, R.; O'Reilly, J.; Shin, J. *IEEE Trans. Mag*. **2007**, 43, 303,

9 Boueri, M.; Baudelet, M.; Yu, J.; Mao, X.; Mao, S. S.; Russo, R. *Appl. Surf. Sci.* **2009**, 255, 9566

10 Wang, Q., Jander, P., Fricke-Begemann, C., Noll, R. *Spectro. Acta B*, **2008**, 63, 1011.

11 Srinivasan, R. *Science* 1986, 234, 559.

12 Breitling, D.; Schittenhelm, H.; Berger, P.; Dausinger, F.; Hugel, H. *Appl. Phys. A* 69, **1999**, S505.

13 Davis, G. M.; Gower, M. C.; Fotakis, C.; Efthimiopoulos, T.; Argyrakis, P. *Appl. Phys. A* **1985**, 36, 27

14 Simeonsson, J. B.; Miziolek, A. W. *Appl. Phys. B* **1994**, B59, 1.

15 Srinivasan, R.; Braren, B.; Dreyfus, R. W. *J. Appl. Phys.* **1987**, 61, 372

16 Srinivasan, R.; Dreyfus, R. W.*Springer Ser. Opt. Sci.* **1985** 49, 396

17 Koren, G.; Yeh, J. T. C. *J. Appl. Phys.* **1984**, 56, 2120

---

18 Srinivasan, R.; Leigh, W. J. *J. Am. Chem. Soc.* **1982**, 104, 6784

19 Ortelli, E. E.; Geiger, F.; Lippert, T.; Wei, J.; Wokaun, A. *Macromolecules* **1986**, 19, 916

20 Kim, H.; Hambir, S. A.; Dlott, D. D. *Phys. Rev. Lett.* **1999**, 83 (24), 503

21 Zhigilei, L. V.; Garrison, B. *J. Appl. Phys. A* **1999**, 69 (suppl.) S 75

22 Kohel, J. M.; Su, L. K.; Clemens, N. T.; Varghese, P. L. *IEEE Trans. Mag*. **1999**, 35, 201

23 Dyachenko, A. Thesis, Auburn University, Auburn, AL USA (**2006**)

24 Hare, D. E.; Franken, J.; Dlott, D. D. *J. Appl. Phys.* **1995**, 77, 5950

25 Sun. H.; Blumenthal, R. unpublished results

Chapter 5

Summary and Conclusions

Secondary explosives, characteristic of high detonation power and low sensitivity to environmental stimuli, are much more prevalent in military and industrial applications than primary explosives. Chapter 1 has presented a though review of background knowledge around secondary explosives (SE). A great emphasis has been put into initiation methods for SEs, including thermal initiation, shock initiation, optical initiation and plasma initiation.

Studies on optical initiation of SEs have been carried out using two main sources of light, namely a lamp and a laser. The advantage with laser initiation of SEs derives from the very properties of its being versatile, fast acting, immune to accidental firing and powerful to meet the initiation threshold of insensitive SEs. Literatures of laser initiation on SEs have mostly focused on initiation using an IR laser, resulting in a form of thermal initiation at high heating rate. Few reports on laser initiation of SEs in ultraviolet wavelength regime were found. In almost all of these reports, SE molecules existed in an isolated molecular gas phase. In real application however, mostly SEs are used in solid phase. Thereofore, a part of the dissertation in later chapters devoted to the gas products detection of laser initiated decomposition of RDX in solid phase. RDX (Cyclotrimethylenetrinitramine) is selected to be studied since it is one of the most important SEs.

Another initiation method, plasma initiation, has also been discussed intensively in chapter 1, since its importance as an alternate initiation source in Electrothermal-Chemical (ETC) guns. The advantages of this initiation in ETC and the recent advances in investigation of Plasma-Propellant interaction (PPI) have been elaborated. In this dissertation, a laser-induced-plasma initiation method has been proposed to compensate the main drawback of ETC system, which is the bulky size of a capacitor as power supply. In this method, a UV laser is utilized to ablate on a polymer film to produce hot and localized plasma, and then this plasma is impinged on RDX film to initiate the decomposition. Polymer film is used mainly because it is the plasma generating material in ETC by electric charges. Laser ablation in general and laser ablation on polymer film have been introduced and discussed in later part of chapter 1.

In chapter 2, the gas products of 266nm UV laser ablation of solid state RDX in air has been investigated using infrared (IR) spectroscopy. The chemical products observed include HCN, N_2O, CO, CO_2 and NO_2.The partial pressure and number of moles have been calculated based on the peak intensity. The result showed surprisingly that the total carbon and nitrogen content of the gase phase species observed account for less than 10% of the material removed by the ablation process. Taking into consideration that N_2 and H_2 may be the products but cannot be detected by IR spectroscopy, it is still difficult to explain the low carbon content. The detection of washed solution of the container walls after ablation revealed that > 83% of the RDX originally present in the spot ended up as on the walls. This sublimation during laser ablation process may be specific to molecular solids, such as RDX.

The products measurement of this ablation process in Argon environment was carried out and presented in Chapter 3. Gas products in air, HCN, N_2O, CO, CO_2 and NO_2 have also shown in spectra from ablation in Argon. A new feature is the NO peak. The understanding of the dependence of plasma formation on the laser fluence provides insight into the chemical mechanism of each direct gas product. Comparison of the anticipated line shape of gas distribution with the experimental data implies the following possible mechanisms under Argon environment: a) HCN, N_2O and NO are formed via multi-photon process; b) NO_2 may be a single photon product; c) CO and CO_2 are formed via thermal process of plasma chemistry. Further comparison of gas distribution over laser fluence under air and Ar indicates that the above-mentioned direct products may be formed in air following the same mechanism, except the reactive species O_2 in air reacts secondarily with some direct products, such as NO, alternated the line shapes to some degree.

Preliminary investigations of laser-induced-plasma initiation on RDX have been conducted and presented in Chapter 4. A thin polycarbonate (PC) film with varied thickness was successfully generated using spin-coating technique. The laser-induced plasma initiation has been probed through several approaches, namely, gas products pressure detection, observation of reflected light, witness board experiment and dynamic pressure measurement. All experiments have showed that the laser-induced-plasma initiated RDX film underneath. The only exception is that repeated gas products pressure detection experiments showed different results than the one obtained previously. The different size and the inside surface of the chamber may be the cause.